A Chemical Strategy for the Conversion of Lignocellulosic Biomass to Biofuel Precursors and Specialty Chemicals

by

Kristopher Robert Enslow

A dissertation submitted in partial satisfaction of the

requirements for the degree of

Doctor of Philosophy

in

Chemical Engineering

in the

Graduate Division

of the

University of California, Berkeley

Committee in charge:

Professor Alexis T. Bell, Chair
Professor Douglas Clark
Professor T. Don Tilley

Fall 2014

A Chemical Strategy for the Conversion of Lignocellulosic Biomass
to Biofuel Precursors and Specialty Chemicals

by

Kristopher Robert Enslow

Abstract

A Chemical Strategy for the Conversion of Lignocellulosic Biomass
to Biofuel Precursors and Specialty Chemicals

by

Kristopher Robert Enslow

Doctor of Philosophy in Chemical Engineering

University of California, Berkeley

Professor Alexis T. Bell, Chair

The conversion of lignocellulosic biomass to biofuel precursors and specialty chemicals was studied with the intention of developing a chemical understanding of and strategy for selectively converting cellulose, hemicellulose, and lignin to furanic compounds and phenolic monomers.

Beginning work with the cellulosic components, the kinetics of the Brønsted acid-catalyzed hydrolysis of hemicellulose in ionic liquid were studied and compared to those found for similar reactions involving cellulose. In 1-ethyl-3-methylimidazolium chloride ([Emim][Cl]) at 80 ºC, we found that hemicellulose could be hydrolyzed to xylose in a 90% yield after 2 h (with 5 wt% furfural and 4 wt% humins) when water was added in a stepwise fashion. The addition of water was found to be integral in curtailing the conversion of xylose and formation of humins under these conditions. This chemical process presents a viable pathway for producing both xylose and glucose from their respective parent polymers.

The Brønsted acid-catalyzed dehydration of xylose to furfural in water was investigated next. Water was chosen as the reaction solvent given that the strategy for producing xylose previously discussed results in a solution that is higher in water content than in [Emim][Cl]. Reaction temperatures were adjusted to account for the previously observed negligible xylose reactivity at or below 100 ºC in aqueous solutions. At these higher temperatures, xylose dehydration is accompanied by the significant formation of humins *via* complex side processes that ultimately result in a loss in the yield of furfural. The use of biphasic systems has been observed to curtail this loss by extracting furfural as it is produced, with metal halide salts added to the aqueous phase to enhance extraction. While the thermodynamics of using metal halides to improve liquid-liquid extraction are well studied, their impact on the kinetics of xylose dehydration catalyzed by a Brønsted acid are not. The aim of our investigation was to understand how metal halides affect the mechanism and kinetics of xylose dehydration in aqueous solution. We found that the rate of xylose conversion is affected by both the nature of the salt cation and anion, increasing in the order no salt < K^+ < Na^+ < Li^+ and no salt < Cl^- < Br^- < I^-. Furfural selectivity increases similarly with respect to metal cations, but in the order no salt < I^- < Br^- < Cl^- for halide anions. Multinuclear NMR experiments identified that

halide anions principally interact with the hydroxyl groups of xylose, while metal cations interact with both water molecules and xylose hydroxyl groups. These interactions permit halide anions to stabilize critical carbocation intermediates formed during the hydroxyl group removal stage of dehydration. Increasing the strength of halide nucleophilicity was found to promote substitution over elimination reactions at the carbocation site. Therefore, chloride salts were found to be selective to dehydration products, namely furfural, and iodide salts were found to enhance the kinetics of humins formation. The results of these experiments coupled with ^{18}O-labeling experiments indicated that xylose dehydration is initiated by protonation at the C1OH and C2OH sites, with the addition of metal halides increasing the proportion of C1OH initiated dehydrations. Careful selection of a metal halide was found to improve the kinetics of xylose dehydration and selectivity to furfural in water strictly for the Brønsted acid-catalyzed case.

Understanding that the isomers of xylose and glucose dehydrate more readily and selectively to furanics in water than xylose and glucose, we investigated the use of various isomerization catalysts with the strategy to first isomerize xylose and glucose to xylulose and fructose, respectively, and then dehydrate the isomers to furfural and 5-hydroxymethyl furfural (5-HMF), respectively, using a Brønsted acid. A number of Lewis acid catalysts were screened for their effectiveness in converting both xylose and glucose in aqueous media. $SnCl_4$ was identified as the most selective Lewis acid. Under the conditions of use, $SnCl_4$ hydrolyzed to such an extent that the addition of an external Brønsted acid was unnecessary to convert carbohydrates to furanics. $SnCl_4$-catalyzed isomerization/dehydration was performed with xylose and glucose, and found to produce selectivities toward furfural and 5-HMF of up to 58% and 27%, respectively, after 2 h at 140 ºC in water. The addition of a secondary organic layer (*n*-butanol) increased these selectivities to 85% and 69% at the same temperature after 5 h. Minor improvements to these selectivities occurred when small amounts of LiCl were added to the aqueous phase, showing that metal halides have less of an impact on the conversion of carbohydrates to furanics when catalyzed by Lewis acids rather than when strictly catalyzed by Brønsted acids.

The conversion of lignin, the third most abundant biomass component after cellulose and hemicellulose, was also explored. Using the ionic liquid [Emim][Cl] as solvent and a Brønsted acid as catalyst, we investigated the cleavage of β-O-4 ether linkages in both lignin and lignin model compounds. However, in neither case did we observe any evidence of ether bond cleavage. Such an incompatibility between lignin and the ionic liquid solvent was determined to be due to unfavorable solvent-solute interactions. The lack of reactivity of lignin and lignin model compounds in [Emim][Cl] makes this ionic liquid a suitable solvent for the hydrolysis of cellulosic biomass in the presence of and without interference from lignin. Lignin model compounds containing glycerol β-O-4 ether linkages could be hydrolyzed successfully in a variety of organic solvents, most notably a combination of 1,4-dioxane and water. The linkage of the guaiacylglycerol β-guaiacyl ether [G,G] model compound was found to be cleaved *via* a two-step dehydration/hydrolysis leading to guaiacol and Hibbert ketones. The Brønsted acid-catalyzed reactions of an array of lignin model compounds containing glycerol β-O-4 ether linkages revealed that the nature of phenyl group substitution does not influence the rate of ether cleavage.

The results of this study show that Brønsted acids can be used to promote the controlled hydrolysis of the hemicellulose and cellulose fractions of biomass in an ionic liquid such as [Emim][Cl] to their respective sugars, xylose and glucose. On the other hand, the cleavage of glycerol β-O-4 ether linkages in the lignin fraction does not occur due to inhibition of this process by interactions of the cations of the solvent with aromatic groups of the lignin. Dehydration of xylose and glucose dissolved in water can be achieved using a combination of Lewis and Brønsted acids. Notably, $SnCl_4$ is found to effectively catalyze the aldose to ketose isomerization of xylose and glucose, and that the resulting products, xylulose and fructose, can undergo Brønsted acid-catalyzed dehydration to furfural and 5-HMF strictly *via* the Brønsted acidity provided by Sn^{4+} hydrolysis. The desired furanic products, furfural and 5-HMF, can undergo secondary reactions to produce humins and other byproducts, and thus it is necessary to separate the furanics as they are produced. Our work has shown that this can be done effectively using *n*-butanol as an extracting agent. The addition of metal halide salts to the aqueous phase promotes the extraction of furanics into the organic phase by enhancing the thermodynamic activity of these products in the aqueous phase. It is also found that specific interactions of the anions with the hydroxyl groups of xylose enhance the rate of xylose dehydration and that the interactions of metal cations with water enhance the activity of the protons that catalyze the dehydration of xylose.

To my wife, Katherine, and my parents, Robert and Jacqueline.

Table of Contents

List of Schemes

List of Figures

List of Tables

List of Abbreviations and Symbols

[Bmim][Cl]	1-butyl-3-methyl imidazolium chloride
[Bmim][OAc]	1-butyl-3-methyl imidazolium acetate
[Emim][Cl]	1-ethyl-3-methyl imidazolium chloride
[Emim][OAc]	1-ethyl-3-methyl imidazolium acetate
[Emim][MeS]	1-ethyl-3-methyl imidazolium methyl sulfate
[G,P]	guaiacylglycerol β-phenyl ether
[G,G]	guaiacylglycerol β-guaiacyl ether
[G,S]	guaiacylglycerol β-syringyl ether
[P,P]	phenylglycerol β-phenyl ether
[P,G]	phenylglycerol β-guaiacyl ether
[P,S]	phenylglycerol β-syringyl ether
[S,P]	syringylglycerol β-phenyl ether
[S,G]	syringylglycerol β-guaiacyl ether
[S,S]	syringylglycerol β-syringyl ether
5-HMF, HMF	5-hydroxymethyl furfural
A	apparent pre-exponential factor in Arrhenius equation, $k = A \exp(-E_A/(RT))$
ATR	attenuated total reflectance (infrared spectroscopy)
CV	column volumes
DFT	density functional theory
E_A	apparent activation energy given in the Arrhenius equation, $k = k_0 \exp(-E_A/(RT))$
FC	flash chromatography
FID	flame ionization detector
FTIR, IR	Fourier transform infrared spectroscopy
GC	gas chromatography
h	Planck's constant
HPLC	high-performance liquid chromatography
K	partition coefficient
K	equilibrium constant
k_b	Boltzmann's constant
k_i	rate constant for reaction i
N	stoichiometric ratio of xylose molecules to chloride ions
NMR	nuclear magnetic resonance (spectroscopy)
MALDI-TOF	matrix-assisted laser desorption/ionization time-of-flight mass spectrometry
MS	mass spectrometry
MW	molecular weight
ppm	parts per million
R	molar gas constant
R_f	retention factor (thin layer chromatography)
r_i	reaction rate for reaction i

r_0	initial reaction rate
r^2	coefficient of determination
RID	refractive index detector
T	reaction temperature
TLC	thin layer chromatography
UNIFAC	**uni**versal quasichemical **f**unctional-group **a**ctivity **c**oefficients
v/v	volume to volume ratio of two solvents
δ_i	chemical shift of species *i* (ppm)
$\Delta\delta_i$	change in chemical shift of species *i* (ppm)
ΔG_r^o	standard Gibb's free energy of reaction
ΔH_r^o	standard enthalpy of reaction
ΔS_r^o	standard entropy of reaction
$\Delta H^{\ddagger}$	enthalpy of activation
$\Delta S^{\ddagger}$	entropy of activation
γ_i^n	activity coefficient of species *i* in solute *n*

Acknowledgements

As my PhD career approaches completion and I take the time to reflect on my six-year journey, I am overwhelmed with the realization that this has hardly been an individual effort. If it were not for the many people that have contributed to my life before and during my experience at UC Berkeley, I would not be in the position that I am in today. While I wish to take the time to recognize those who have helped to make this dissertation a realization, I recognize that a few sentences can never fully express my gratitude for all of the help and support I have received over the years.

First and foremost, I would like to thank my parents. My mother and father have been a constant source of love, support, and encouragement my entire life. They have worked incredibly hard to provide an existence for me free of want, distraction, and worry, which has allowed me to focus on my education and pursue a future without limitation. My father's tireless work ethic in providing for our family has taught me the value of hard work and the importance of making my own way in life. My mother's calm disposition and humility have instilled within me the same qualities and have made me a responsible, thoughtful individual. I am lucky to have them both in my life and am a better person because of it.

My journey to Berkeley officially began while earning my Bachelors in Chemical Engineering at the University of Southern California (go Trojans!). Our department at USC was small, and thus permitted a lot of student-faculty interaction that helped to truly give me a deep understanding of and appreciation for chemistry and engineering. Without being specific, I am thankful to the entire faculty for helping to shape my thinking as an engineer and for giving me the solid fundamental background that I rely upon daily. Until my final semester, I was almost certain that my higher education would terminate with a Bachelors degree and a job at Chevron. However, something always bothered me about the prospect of that decision, as it seemed too limiting. I had just scratched the surface of chemical engineering and knew that I wanted to do more with my career than just apply the principles I had learned – I wanted to contribute to the advancement of the field. Discussions with friends Sevag Sislian and Matt MacDonald helped me to conclude that the best outlet for this desire was to pursue my doctorate, and with their encouragement, I submitted my application to attend Berkeley.

While at Berkeley, I have had the opportunity to meet many different people who have not only helped shape the way I conduct research, but also the person that I have become since entering the program. Chief amongst them has been my research advisor, Professor Alexis Bell. I am incredibly grateful to have had the opportunity to work with Alex in his catalysis group. He has had a major role in developing the way I consider and perform rigorous scientific work, and has vastly improved my ability to communicate technically, whether through manuscript writing or giving oral presentations. His guidance throughout the years has provided a balanced PhD experience that has permitted me to explore a multitude of ideas and to grow as a technical researcher and presenter.

Within the Bell research group, I have had the pleasure of working with and learning from a number of exceptional graduate students and post docs. When I first joined, I was fortunate enough to have excellent guidance from Sean Dee, Chidambaram (Chidam) Mandan, and Sasisanker (Sasi) Padmanabhan, all of whom were instrumental in helping me get quickly set up and acclimated to biomass research. I especially want to

thank Sean and Sasi for showing me the ins and outs of working with ionic liquids and cellulosic biomass. Bean Getsoian and Will Vining were invaluable in mentoring me during preparation for my preliminary and qualifying exams, and I owe my passing of both to their depth of knowledge and patience. In addition to these lab mates, I also need to thank Anton Mlinar, Eric Sacia, Balakrishnan (Balki) Madhesan, Lin Louie, and Alex Wang. Whether it was discussing research, playing a game of softball/round of golf, or just chatting about random topics, they have all helped to make my time at Berkeley more fun.

While working on the biomass conversion project, I have had the opportunity to mentor several outstanding visiting scholars and undergraduate students: Tom Hamilton, Terry Kim, Sherry Xin, Frederike Carstensen, David Doan, and Daniel Tjandra. A fair amount of work in this dissertation was accomplished due to their effort and dedication, and I thank them not only for their research assistance but also their thoughtful probing and challenging ideas which worked to further the research.

Outside of the Bell research group, I am indebted to post docs Jason Nichols and Jerome Volkman of the Bergman group for improving my working knowledge of organic and inorganic chemistry, teaching me how to successfully synthesize organic compounds, and for commiserating with me during some early struggles with the lignin phase of my research project. I also want to thank post docs Cedric Chung, Oz Gazit, and Alexandré Charmout of the Katz group for fruitful discussions on the application of catalysis in biomass deconstruction. At the Energy Biosciences Institute, where my project called home, Stefan Bauer, Mara Bryan, Adam Cohen, Zack Phillips, and Crystal Chan were instrumental in ensuring that the laboratory functioned at the highest levels without allowing for any research interference. Also, Chris Canlas at the College of Chemistry NMR facility was a gigantic resource during stages of my research project requiring NMR experiments with various isotopes.

Last, but certainly not least, I want to thank my wife, Katherine, for her overwhelming love and patience as I worked to complete my dissertation. I have to thank her for the numerous visits from Southern California before we were married, her companionship during some late night NMR runs, and most of all for being the voice inside my head over the years pushing me along and chanting “you’re almost there, keep going.”

Well, Katherine, I finally made it here, and I cannot wait to embrace what the future holds for us.

Thank you everyone.

Chapter 1

Introduction

Despite projected growths in crude oil production supported by developments in tight oil and shale, demand for cleaner, renewable transportation fuels is driving a global shift away from petroleum dependency. Such a demand has led the United States and the European Union to establish mandates requiring the integration of biofuels into the transportation sector, with 5% and 10% of transportation fuels required to be biomass-derived in the US and the EU, respectively, by the year 2020 [1]. Without an overhaul of the current transportation infrastructure, viable biofuels must be compatible with existing gasoline and diesel engines. They must also be sourced from low-cost feedstocks and produced efficiently in order to compete economically with petroleum-based liquid fuels. For the advancement of the renewable fuels economy, it is vital that efficient processing technologies be developed for the conversion of inexpensive biomass into materials that can be combined with gasoline/diesel/jet or be used as stand-alone fuels.

Perennial grasses, such as *Miscanthus x giganteus*, have been identified as attractive feedstocks for biofuel production on the basis that they make efficient use of land, have low moisture and mineral content, do not require irrigation, and have high energy to mass ratios [2]. As shown in Figure 1.1, this type of biomass consists of three main components: cellulose (25-50%), hemicellulose (20-40%), and lignin (10-30%) [3]. Cellulose is a linear crystalline polymer comprised of glucose monomers linked together by β-1,4 glycosidic bonds. Interchain hydrogen bonding permits cellulose to form microfibrils, which hydrogen bond to a coating of hemicellulose. Hemicellulose is a complex amorphous polymer consisting of a backbone of xylose monomers (also bound together *via* β-1,4 glycosidic bonds), which is branched with arabinose, glucose, galactose, and mannose monomers. The hemicellulose is esterically linked to lignin, a highly branched/substituted polyaromatic compound composed of guaiacyl, syringyl, and *p*-hydroxyphenol phenylpropanoids.

A number of pathways have been explored to deconstruct these three components of biomass to a variety of potential fuels and specialty chemicals. However, it has been noted that routes beginning with the acid-catalyzed hydrolysis of biomass can potentially lead to products that retain the greatest proportion of thermal energy when compared to the starting lignocellulosic material (up to 95%) [3]. This route holds the potential to be the most efficient use of biomass to produce biofuels, even more so than the enzymatic hydrolysis/fermentation of biomass to produce the currently leading biofuel, ethanol (which only retains 50% of its thermal energy potential).

The acid-catalyzed hydrolysis of hemicellulose produces C5 and C6 carbohydrates, namely xylose, while that of cellulose strictly produces glucose. Dehydrating either xylose or glucose yields furfural or 5-hydroxymethyl furfural (5-HMF), respectively. These furanics are high value chemicals that can be used as platform molecules in the production of a wide range of commodity chemicals [3-5] and fuels [3, 6-9]. Traditionally, furfural has been used in the chemicals industry as a source of furanic derivatives used to synthesize polyethers for textiles, and resins used in the production of plastics and paints [4]. In the 1940s, furfural began to gain attention as a platform

molecule for the production of methyl-tetrahydrofuran, a fuel additive for gasoline with an octane rating of 74 [6]. More recently, both furfural and 5-HMF have garnered traction as fuel precursors in various condensation and esterification/etherification reactions that have been proposed as viable routes for converting these furanics to a range of jet and diesel fuels [7]. For example, condensation of furfural with 2-methylfuran (a furfural derivative [5]) can produce tri-furanyl molecules in the diesel range [8], while aldol condensation of furfural with carboanion-forming species (i.e. acetone) can create C8-C14 alkanes in the jet fuel range [9]. Although furfural and 5-HMF can be used to make fuels, they cannot be used as standalone fuels due to polymerization reactions that occur readily to form resins unsuitable for combustion [5].

The acid-catalyzed deconstruction of lignin is less specific than its cellulosic counterparts given its complexity and lack of general structure. As a result, lignin is mainly used to generate process heat for cellulosic conversion processes or is converted to bio-oils or syn-gas [3]. However, in principal, lignin can be used as a source for a number of phenolic- and BTX-based aromatic molecules that can be used as specialty chemicals or upgraded for use as fuel oxygenates. The production of gasoline oxygenates from lignin is likely the highest value use of the biomass, and can be combined with fuels derived from cellulosic furanics to aid in the reduction of CO emissions and increase fuel octane/energy density [10].

The conversion process for producing fuels and fuel additives from biomass should be as environmentally friendly as the products themselves. Ionic liquids have drawn recent attention for their use as "green" solvents due to their extremely low vapor pressure, inflammability, chemical inertness, and recyclability [11]. Early work has shown their ability to dissolve cellulose to an appreciable extent [12], and has since been expanded to include hemicellulose and lignin [13]. As a result, ionic liquids are attractive solvents for use as environmentally friendly media in the hydrolysis of cellulose/hemicellulose and the deconstruction of lignin.

Overall, the objective of this study was to investigate and establish viable chemical pathways for deconstructing cellulose, hemicellulose, and lignin to their constituent monomers, and further upgrade them to useful platform molecules for use in biofuel, additive, and specialty chemical production. Chapter 2 begins the investigation by examining the mechanism and kinetics of the Brønsted acid-catalyzed hydrolysis of hemicellulose (and to a lesser extent, cellulose) in the ionic liquid 1-ethyl-3-methyl imidazolium chloride ([Emim][Cl]), as well as those of the dehydration of xylose to furfural in the same solvent. The ability of water to suppress the kinetics of xylose dehydration and subsequent degradation reactions to form undesired products called humins are also studied, with a multi-stage water addition method developed to allow for the strict hydrolysis of hemicellulose without significant product loss. Chapter 3 more closely examines the chemistry of the Brønsted acid-catalyzed dehydration of xylose in water. The role of metal halide addition in affecting xylose conversion and humins formation rates is discussed, with complementary multinuclear NMR performed to probe the explicit interactions between dissolved ions, xylose, and water. Isotopic labeling experiments reveal that the dehydration of xylose to furfural can proceed *via* C1OH- or C2OH-initiated dehydration, with the addition of metal halides influencing the likelihood of either pathway. The results of these investigations lead to a mechanistic understanding of the means by which metal halides alter the kinetics of Brønsted acid-catalyzed

dehydration of xylose in aqueous solution as well as the influence metal halides have on the formation of humins. Chapter 4 investigates a number of Lewis acid catalysts and evaluates their ability to selectively dehydrate both xylose and glucose to their corresponding furanics, furfural and 5-HMF, in water at moderate temperatures. Such studies reveal that $SnCl_4$ most selectively produces both furanics, and subsequent biphasic reactions with the Lewis acid show that the addition of an extracting agent can significantly boost product selectivities to previously unattained levels. Attention is also paid to the hydrolysis of Sn^{4+} in water, with specific focus on the dual nature of $SnCl_4$ as a provider of Lewis and Brønsted acidity. Comparisons are drawn to the work in the previous chapter to explain the benefits of utilizing a combination of Lewis and Brønsted acids in xylose/glucose dehydration reactions.

Having discussed methods of selectively converting cellulosic materials to furanic platform molecules, Chapter 5 shifts focus to the remaining biopolymer, lignin. The Brønsted acid-catalyzed deconstruction/hydrolysis of high molecular weight lignin is studied in both [Emim][Cl] and various organic solvents. Additionally, lignin model compounds are used to establish the chemical pathway for the hydrolysis of the most abundant linkage within lignin, the arylglycerol-β-aryl ether. The production of Hibbert ketones provides evidence of a dehydration/hydrolysis pathway that prevails in the cleavage of lignin model compounds. Organic solvents are discussed as being more effective than [Emim][Cl] as media for cleavage reactions, and ionic liquid is proposed as a beneficial solvent for the co-processing of cellulose, hemicellulose, and lignin at moderate temperatures without concern that lignin might interfere with the chemistry of cellulosic hydrolysis.

Figure 1.1 A representative depiction of biomass from the cellular level downward, showing the three major components cellulose, hemicellulose, and lignin. Adapted from Ref. [14].

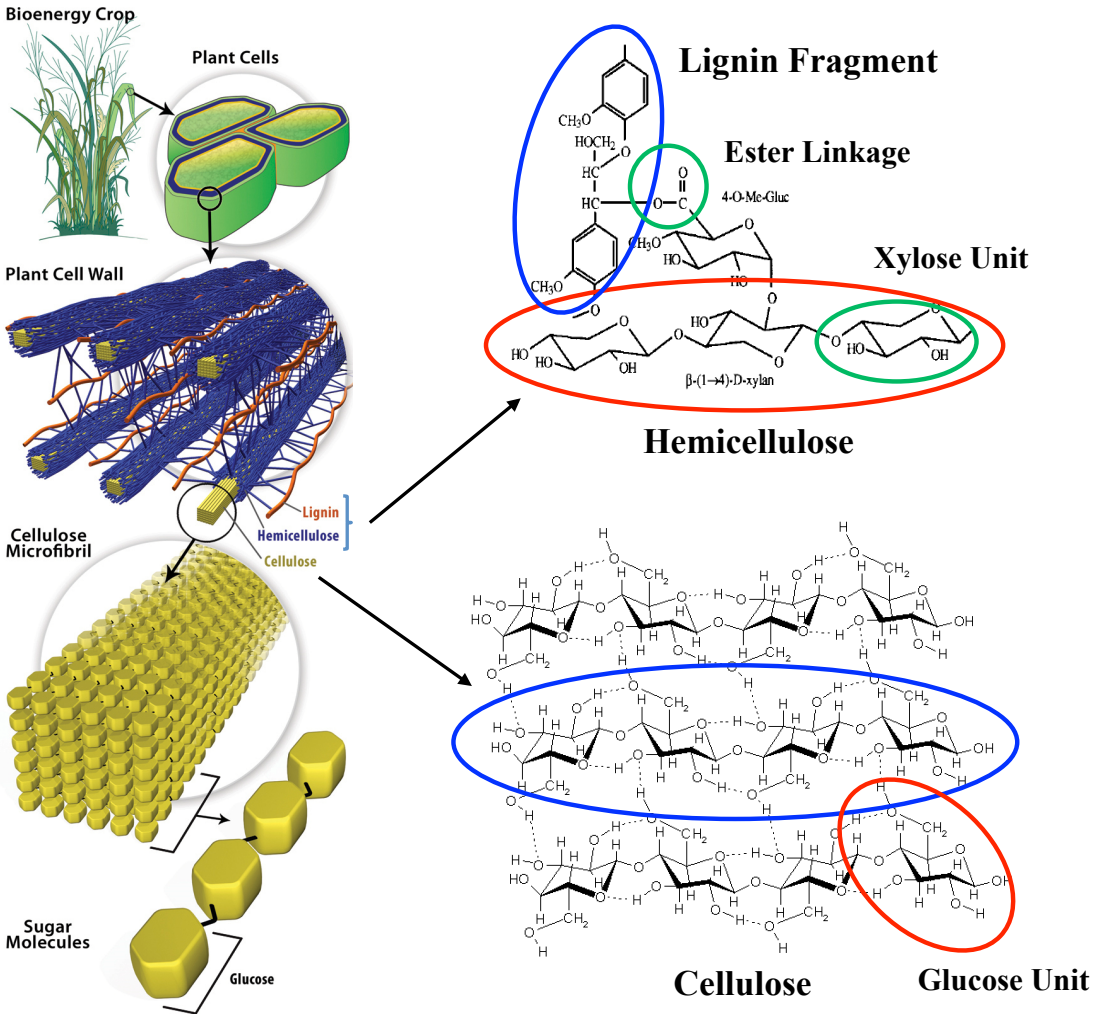

References:

[1] J. J. Conti, P. D. Holtberg, J. R. Diefenderfer, S. A. Napolitano, A. M. Schaal, J. T. Turnure, L. D. Westfall, Report No. DOE/EIA-0383(2014), *Annual Energy Outlook 2014 with Projections to 2040*, US Energy Information Administration, Washington, DC, **2014**. < http://www.eia.gov/forecasts/aeo/>.
[2] M. B. Jones, M. Walsh, *Miscanthus for Energy and Fibre*, James & James, London, **2001**, pp. 109-154.
[3] G. W. Huber, S. Iborra, A. Corma, *Chem. Rev.* **2006**, *106*(9), 4044.
[4] T. Werpy, G. Petersen, A. Aden, J. Bozell, J. Holladay, J. White, A. Manheim, Report No. NREL/TP-510– 35523, *Top Value Added Chemicals from Biomass: Vol. 1—Results of Screening for Potential Candidates from Sugars and Synthesis Gas*, National Renewable Energy Laboratory, Golden, CO, **2004**.
[5] K. J. Zeitsch, *Sugar Ser*. **2000**, *13*, 1-353.
[6] S. Bayan, E. Beati, *Chim. Ind. (Milan, Italy)* **1941**, *23*, 432.
[7] a) J. N. Chheda, G. W. Huber, J. A. Dumesic, *Angew. Chem. Int. Ed.* **2007**, *46*(38), 7164; b) G.A. Tompsett, N. Li, G. W. Huber, *Thermochemical Processing of Biomass: Conversion into Fuels, Chemicals and Power* (Ed.: Robert C. Brown), John Wiley & Sons, Chichester, **2011**, pp. 223-279.
[8] B. Madhesan, E. R. Sacia, A. T. Bell, *ChemSusChem* **2014**, *7*, 1078.
[9] a) G. W. Huber, J. N. Chheda, C. J. Barrett, J. A. Dumesic, *Science* **2005**, *300*, 2075; b) G. W. Huber, J. A. Dumesic, *Catal. Today* **2006**, *111*, 119.
[10] J. E. Holladay, J. F. White, J. J. Bozell, D. Johnson, Report No. PNNL-16983, *Top Value-Added Chemicals from Biomass-Volume II—Results of Screening for Potential Candidates from Biorefinery Lignin*, Pacific Northwest National Laboratory, Richland, WA, **2007**.
[11] O. A. El Seoud, A. Koschella, L. C. Fidale, S. Dorn, T. Heinze, *Biomacromolecules* **2007**, *8*(9), 2629.
[12] R. Swatloski, S. Spear, J. Holbrey, R. Rogers, *J. Am. Chem. Soc.* **2002**, *124*, 4974.
[13] H. Olivier-Bourbigou, L. Magna, D. Morvan, *Applied Catalysis A: General* **2010**, *373*, 1.
[14] S. K. Ritter, *Chem. Eng. News* **2008**, *46*, 15.

Chapter 2

The Kinetics of Brønsted Acid-Catalyzed Hydrolysis of Hemicellulose Dissolved in 1-Ethyl-3-Methyl Imidazolium Chloride

Abstract

Conversion of plant biomass provides a sustainable pathway toward renewable fuels. Hemicellulose, a readily available form of biomass, can be catalytically converted to provide a range of fuel molecules, from furanics and sugar alcohols to alkanes and aromatics. Using ionic liquids as solvent and Brønsted acid catalysts for biomass deconstruction, we investigated the kinetics of hemicellulose (xylan) hydrolysis and subsequent dehydration/degradation reactions. These findings were compared to those found for similar reactions involving cellulose. In 1-ethyl-3-methylimidazolium chloride ([Emim][Cl]) at 80 ºC, we report that hemicellulose could be hydrolyzed to xylose in a 90% yield after 2 h, with 5 wt% dehydration products and 4 wt% humins, when water was added stepwise. This chemical process presents a viable pathway for producing sugars capable of being chemically (*via* dehydration/hydrogenation) or biologically (*via* fermentation) upgraded to potential fuel molecules.

2.1 Introduction

Lignocellulosic biomass is an attractive feedstock for the production of fuels and chemicals in a sustainable manner [1-3]. The challenge is to deconstruct biomass (such as *Miscanthus x giganteus*) into its component parts – cellulose (25-50 wt%), hemicellulose (shown in Scheme 2.1, 20-40 wt%), and lignin (10-30 wt%) [4] – so that they can then be converted into final products by either biochemical [5-7] or chemical means [6-11]. Recent studies have shown that ionic liquids, salts with melting points below 100 ºC, are capable of complete biomass dissolution [12], thereby facilitating the further processing of the components [13, 14]. It has also been shown that once dissolved in ionic liquids, cellulose and hemicellulose can be hydrolyzed to their component sugars using acid catalysts [14-17]. The hydrolysis of both cellulosic components is, however, accompanied by the dehydration of the released sugars to form furanics, such as 5-hydroxymethyl furfural (HMF) and furfural, and by the condensation of the furanic products with sugars to form humic substances or humins [16-18]. For these reasons there is an interest in understanding the kinetics of acid-catalyzed cellulose and hemicellulose hydrolysis occurring in ionic liquids, so that reaction conditions can be chosen to minimize the loss of organic matter to humins and to furfural and its derivatives. Investigations of cellulose hydrolysis in ionic liquids has shown that the rate is first order in the concentrations of β-1,4 glycosidic bonds and acid, but zero order in the concentration of water [16]. It has also been demonstrated that the progressive addition of water during the course of cellulose hydrolysis reduces the dehydration of glucose to HMF and the formation of humins [9, 18]. By contrast, the kinetics of hemicellulose dissolution under comparable conditions have not been investigated and, hence, are a subject of interest.

The focus of the present study is on understanding the mechanism and kinetics of hemicellulose hydrolysis to xylose (and other monomeric sugars) occurring in ionic liquids with minimal formation of side products such as furfural and humins. The results of this investigation are compared to similar kinetics for cellulose hydrolysis and glucose dehydration. The ability of water to suppress the kinetics of sugar dehydration was also explored.

2.2 Methods

2.2.1 Materials

The ionic liquid 1-ethyl-3-methyl imidazolium chloride ([Emim][Cl], 95%), xylan (from Birchwood, ≥90% xylose residues by HPAE), D-xylose (99%), microcrystalline cellulose (avicel ph-101), L-arabinose (99%), 2-furaldehyde (furfural, 99%), 5-hydroxymethal furfural (5-HMF, 99%), sulfuric acid (H_2SO_4, 98%), methanesulfonic acid (CH_3SO_3H, 99%), trifluoroacetic acid (CF_3COOH, 99%), phosphoric acid (H_3PO_4, 99%), acetic acid (CH_3COOH, glacial), and 1,4-dioxane (anhydrous, 99.8%) were purchased from Sigma-Aldrich. Hydrochloric acid (HCl, 37%) was purchased from Fischer Scientific. Xylobiose (XB, >95%), xylotriose (XTr, >95%), and xylotetraose (XTe, >95%) were purchased from MegaZyme. All ionic liquids were vacuum dried at 100 ºC for 24 h prior to use to ensure minimal water content (measured *via* Karl-Fischer titration to be approximately 2 wt%). All other materials were used as purchased, without further purification or modification.

2.2.2 Experimental Approach

All experiments were performed using a Symx core module deck to maintain constant reaction temperature and stirring rate. A representative procedure for xylan hydrolysis: xylan (27 mg, 200 μmol sugar residues) is allowed to dissolve in [Emim][Cl] (500 mg, 480 μl) in a 5 ml threaded cap vial at 80 ºC and a 200 rpm stirring rate for 2 h, or until a clear solution is formed. De-ionized water (1 mmol) and H_2SO_4 (100 μmol) are then added and the reactor vial is sealed. Upon completion of the reaction, the sample is removed and quenched in an ice bath. An internal standard (1 ml of 10 mg/ml 1,6-hexanediol in water) is added and the sample is centrifuged to remove all water insoluble particulates. A portion of the reaction mixture (500 μl) is removed and mixed with H^+/OH^- ion exchange resin to remove the bulk of [Emim][Cl], after which 200 μl is taken for analysis. For reactions involving an additional organic phase, 1,4-dioxane (500 μl) is added prior to the addition of H_2SO_4, and is removed *via* centrifuging prior to addition of the internal standard. A different internal standard (1 ml of 5 mg/ml guaiacol in 1,4-dioxane) is added to this organic phase prior to analysis.

2.2.3 Catalyst Screening

A range of Brønsted acids were screened for effectiveness in hydrolyzing xylan. Consistent with a similar study on cellobiose hydrolysis [17] and correlations between pKa values of acids in water and acids in ionic liquid [15], the relative order of acid strengths in [Emim][Cl] is the same as that in water. The curve generated from this experiment (Figure 2.1) closely resembles the extent of acid dissociation in water and is similar to what is seen for the acid hydrolysis of cellulose in ionic liquids [18]. Weak

acids (pKa, aqueous >2.1, specific catalysis region) showed virtually no reactivity, medium strength acids (-2< pKa, aqueous <2.1) showed moderate reactivity, and strong acids (pKa, aqueous < -2, general catalysis region) showed the greatest reaction rates. Strong acid reactivity was uniform in acids of aqueous pKa less than -2.

2.2.4 Product Analysis

A Shimadzu HPLC equipped with a Biorad Aminex HPX-87H column (300 x 7.8 mm; 0.01 N H_2SO_4; 0.6 ml/min; 50 ºC) and a refractive index detector (RID) was used to analyze all aqueous/ionic liquid-phase samples. Product quantities were determined by converting integrated HPLC peak areas into concentrations using a 7-point calibration curve generated from purchased standards.

A Varian CP-3800 Gas Chromatograph equipped with a FactorFour Capillary Column (UF-5ms 30 m, 0.25 mm, 0.25 μm, P/N CP8944) connected to a Varian quadrupole-mass spectrometer (MS) and flame ionization detector (FID) was used to analyze all organic phase samples. After product identification by mass spectrometer, product concentrations were determined from integrated FID peak areas using a 6-point calibration curve generated from purchased standards.

Insoluble particulates were quantified by weighing after washing and drying. Upon separation of insoluble particulates from the liquid phase(s), the solids were washed three times with de-ionized water and dried under a $1.3x10^{-5}$ Pa vacuum for 24 h before being weighed.

Xylan was used on a wet basis. Before each use, the xylan was first tested for water content (Karl-Fischer), and then that water content was subtracted from the xylan mass to determine the true xylan mass. The water content for xylan was typically 8 wt%. Product yields were determined on a molar basis relative to the number of product residues present in xylan. For example, xylose yield was calculated by dividing the moles of xylose produced by the initial number of moles of xylose residues present in xylan. The initial moles of xylose residues in xylan were calculated by dividing 90% of the weighed xylan (the xylose residue containing portion of xylan as determined by the HPAE analysis of xylan performed by Sigma-Aldrich) by the molecular weight of a xylose residue (150 g/mol). Humins yields are reported as the mass of recovered humins over the total mass of initial xylan after correction for water content. All reported yields were typically reproducible to within a +/- 5% relative error (based upon the calculation of one standard deviation).

2.3 Results and Discussion

2.3.1 Xylan Hydrolysis and Xylose Dehydration

The temporal evolution of products formed during H_2SO_4-catalyzed hydrolysis of 5 wt% xylan dissolved in [Emim][Cl] is shown in Figure 2.2 (the overall reaction pathway can be seen in Scheme 2.2). Over the course of the first 20 min, xylobiose and xylose were observed as the primary products. Both product yields increased until xylobiose reached its maximum at 14 wt% after 30 min and xylose reached its maximum at 47 wt% after 60 min. Furfural was produced from the dehydration of xylose after 20 min and reached a level of 18 wt% after 180 min. Glucose and arabinose were also identified by HPLC analysis; however, their yields were relatively small and never

exceeded 4 wt% each. The yields of these sugars were consistent with the makeup of xylan, which contains approximately 10 wt% arabinose and glucose residues. The dehydration product of glucose, 5-HMF, was seen at long reaction times, but never in quantities greater than 1 wt%. After 45 min, a black precipitate (humins) began to form and continued to accumulate throughout the duration of the experiment, reaching a level of 10 wt% at the end of the reaction (180 min). Recent work has suggested that this humins material is formed from the coupling loss reaction between xylose and furfural [17, 18]. Oligomers larger than xylobiose (xylotriose and xylotetraose) were not detected, which is consistent with work done under similar conditions in water [19]. This would suggest that the hydrolysis of β-1,4 bonds near the xylan chain ends is preferential to inner bond scission. After 60 min, at which point xylose yields were maximal, all xylan had completely reacted. This was evidenced by the observation that with excessive water dilution of for the reaction mixture after 60 min, xylan did not precipitate. In total, seven major products were identified in this reaction. Additional soluble products, most likely resulting from the condensation of xylose and furfural or the degradation of these products, accounted for 40 wt% of the original mass of the dissolved xylan. The presence of these unidentified degradation products was indicated by the change in solution color over the course of the reaction, from clear yellow to dark amber.

Figure 2.3 shows the H_2SO_4-catalyzed reaction of xylose dissolved in [Emim][Cl]. In the presence of H_2SO_4 after 90 min, 80% of the starting xylose is converted. Furfural is produced *via* the dehydration of xylose at a yield of 20%, while the other 60% of reacted xylose is converted into unidentified degradation products, both soluble and insoluble (humins, 20 wt%). This reaction illustrates that the rate of xylose degradation is greater than that of xylose dehydration.

2.3.2 Kinetics of Xylan Hydrolysis

The kinetics for the initial rate of xylan hydrolysis can be represented by the following expression:

$$r_0 = k_{app}[H_2O]^{\alpha}[H^+]^{\beta}[\beta-1,4]^{\gamma} \quad (1)$$

where r_o is the initial rate of hydrolysis, k_{app} is the apparent rate coefficient, $[H_2O]$ is the concentration of water, [β-1,4] is the concentration of β-1,4 glycosidic linkages in xylan, $[H^+]$ is the concentration of free protons (assuming that the acid catalyst is fully dissociated), and α, β, and γ are the orders in H_2O, H^+, and β-1,4 glycosidic linkages, respectively. It was determined (see Figure 2.4) by independently varying water, free proton, and β-1,4 glycosidic linkage concentrations that the initial rate dependence is zero-order with respect to water, and first-order with respect to the concentrations of both free protons and β-1,4 glycosidic linkages, yielding the following modified initial rate expression:

$$r_0 = k_{app}[H^+][\beta-1,4] \quad (2)$$

The form of this equation can be rationalized on the basis of the mechanism presented in Scheme 2.3. It is envisioned that the first step in the sequence is reversible protonation of

β-1,4 glycosidic linkages, which is then followed by rapid formation of an oxonium cation. The latter species undergoes rapid hydration to form xylose. It should be noted that since this step follows the rate-limiting step, it is kinetically irrelevant, and for this reason the concentration of water does not influence the initial rate of xylan hydrolysis. From Scheme 2.3, it can be concluded that k_{app} can be presented as:

$$k_{app} = K_1^{\ddagger} k_2^{\ddagger} \tag{3}$$

where $K^{\ddagger}_1$ is the equilibrium constant for protonation of β-1,4 glycosidic linkages (reaction 1), and $k^{\ddagger}_2$ is the rate coefficient for the formation of the oxonium cation (reaction 2).

The apparent rate coefficient k_{app} can be further represented in its Arrhenius form as $k_{app} = A\exp(-E_a/RT)$, where A is the apparent pre-exponential factor, E_a is the apparent activation energy, and T is the temperature. The apparent activation energy was found by performing the hydrolysis of xylan at temperatures ranging from 353 K to 373 K. To avoid the effects of secondary processes, all measurements were made for xylan conversion of less than 10 wt%. Figure 2.5 shows an Arrhenius plot of the initial rate of xylan hydrolysis versus the inverse temperature. The apparent activation energy calculated from this plot is 60 kJ/mol. This apparent activation energy is considerably lower than that found specifically from the H_2SO_4-catalyzed hydrolysis of xylan (from Birchwood) in water (127 kJ/mol over the range 100-130 ºC) [7]. Similarly, the activation energy of xylose degradation was calculated to be 72 kJ/mol and that of furfural formation from the dehydration of xylose was found to be 114 kJ/mol.

2.3.3 Comparison of the Kinetics of Xylan and Cellulose Hydrolyses

The form of equation 2 is identical to that recently reported for the hydrolysis of cellulose (Avicel) in [Bmim][Cl] [18], and can also be rationalized on the basis of the mechanism presented in Scheme 2.3. Values of A, E_a, and k_{app} evaluated at 353, 363, and 373 K are presented in Table 2.1 for the hydrolysis of xylan and are compared with values of these parameters determined for the initial hydrolysis of cellulose (Avicel) under identical conditions. The data presented in Table 2.1 show that the activation energy for the hydrolysis of xylan is considerably smaller than that for cellulose hydrolysis, 60 kJ/mol versus 96 kJ/mol. Although the pre-exponential factor for xylan hydrolysis is much lower than that for the hydrolysis of cellulose, 5.71×10^2 mL/μmol-s versus 1.31×10^7 mL/μmol-s, the apparent rate coefficient for xylan hydrolysis is about an order of magnitude higher than that for the hydrolysis of cellulose.

The significant differences in the rate parameters for the hydrolysis of xylan and Avicel can be attributed to the differences in the structures of the two carbohydrates. Glucose, being a hexose sugar, has an additional CH_2OH group that extends equatorially from the C5 position in the sugar, a feature not present in xylose. This hydroxymethyl group terminates in a primary alcohol that can act as a protecting group in cellulose. The rearrangement of this group (shown in Scheme 2.4) can result in intramolecular hydrogen bonding between the primary hydrogen of the CH_2OH group and the oxygen of the β-1,4 glycosidic bond [20]. This interaction would form a low energy, stable chair conformation that could hinder reaction at the β-1,4 oxygen in a couple of ways. Firstly, the chair conformation would sterically limit the approach space within which the proton

can maneuver before it is able to react at a glycosidic bond site. Electronically, the hydrogen bonding of the methoxy group to the glycosidic bond oxygen would effectively reduce the number of available electron donor sites at the β-1,4 glycosidic bond for proton attack. Both these steric and electronic hindrances are expected to raise the energy barrier for hydrolysis, providing a potential explanation for the higher observed activation energy for cellulose hydrolysis over that of hemicellulose hydrolysis.

The observed initial rate constant of xylan hydrolysis is approximately 8 times higher on average than that of cellulose under similar reaction conditions over the explored temperature range of 353-373 K. Again, the presence of the additional hydroxymethyl groups within cellulose likely contributed to a lowered initial rate. Unlike the secondary alcohols present in glucose and xylose, the primary alcohol in the methoxy group of glucose has the ability to abstract catalytic protons from solution through an equilibrium protonation/deprotonation reaction [20], lowering the concentration of catalyst available for hydrolyzing the β-1,4 ether bond in cellulose (see Scheme 2.5). Thus at the same initial catalyst loadings, fewer catalytic protons are available for cellulose hydrolysis, resulting in a lower initial rate when compared with hemicellulose hydrolysis.

Comparing the pre-exponential factor of hemicellulose and cellulose hydrolyses shows that the factor for cellulose is four orders of magnitude larger than that for hemicellulose. This can be interpreted entropically by applying transition state theory to our system using the Erying equation (modified to include E_a):

$$k = \frac{k_B T}{h} e^{(\Delta S^{\ddagger}/R)} e^{(-E_a/RT)} \tag{4}$$

where the preexponential factor is now defined as:

$$A = \frac{k_B T}{h} e^{(\Delta S^{\ddagger}/R)} \tag{5}$$

Solving for $\Delta S^{\ddagger}$ for both cellulose and hemicellulose shows that the change in entropy for cellulose hydrolysis is approximately 2.8 times higher than for hemicellulose hydrolysis.

2.3.4 Kinetics of Xylose Dehydration and Degradation Reactions

Two principal mechanisms have been proposed for the mechanism of xylose dehydration to furfural [21-25]. The first pathway (see Scheme 2.6) envisions that xylose undergoes a ring transformation in which the C2 hydroxyl group is protonated and leaves the ring as water. The resulting carbocation forms a bond with the ring oxygen, thereby breaking the bond between the ring oxygen and the anomeric carbon. The reactive intermediate, 2,5-anhydroxylose, then further dehydrates to form furfural. Quantum mechanical studies have shown that protonation of the C2 hydroxyl exhibits the lowest energy barrier for initiating the dehydration of xylose to furfural compared to all other protonation sites [21]. Similar results were found for initiation of glucose dehydration to 5-HMF [22]. The second proposed pathway (see Scheme 2.7) begins with xylose isomerization to its acyclic form and subsequent enolization [23] or direct conversion to xylulose through hydride transfer. Recent NMR labeling studies have shown the hydride

transfer mechanism to be the correct one for xylose dehydration occurring in ionic liquids [24].

Although the dehydration of xylose to furfural is the most easily characterized reaction stemming from xylose disappearance in an acidic medium, other side reactions are known to occur. As seen from Figure 2.3, approximately 60 wt% of the original xylose is converted to soluble and insoluble products (humins). These degradation products can be attributed to the following reactions: (1) xylose coupling with xylose-to-furfural intermediates; (2) furfural resinification (self-coupling); (3) reaction between furfural and either xylose or xylose-to-furfural intermediates [25]. This set of xylose-derived reactions is shown in Scheme 2.8 and can be modeled using the following ordinary differential equations:

$$\frac{d[X]}{dt} = -(k_1 + k_2[F] + k_3[X])[X][H^+] \quad (6)$$

$$\frac{d[I]}{dt} = (k_1[X] - k_4[I])[H^+] \quad (7)$$

$$\frac{d[F]}{dt} = (k_4[I] - k_2[X][F] - k_5[F]^2)[H^+] \quad (8)$$

$$\frac{d[H]}{dt} = k_2[X][F][H^+] \quad (9)$$

$$\frac{d[D]}{dt} = k_3[X]^2[H^+] \quad (10)$$

$$\frac{d[R]}{dt} = k_5[F]^2[H^+] \quad (11)$$

where [X], [I], [F], [H], [D], and [R] are the xylose, intermediate product, furfural, humins, degradation product, and resinification product concentrations, respectively. These equations can be simplified by considering experimental results. Xylose-to-furfural intermediates were not observed in the present study during product analysis, nor have they been clearly identified in the literature. Thus, the steady-state assumption can be invoked in the modeling of the intermediates such that $d[I]/dt = k_1[X] - k_4[I] \approx 0$, and hence $k_1[X] \approx k_4[I]$. Furthermore, we can assume that resinification does not occur to a significant extent based on the recent observation that furfural dissolved in [Bmim][Cl] is relatively stable in the presence of an acid catalyst and in the absence of xylose [21]. These assumptions lead to a modified differential equation representing change in furfural concentration with respect to time:

$$\frac{d[F]}{dt} = (k_1 - k_2[F])[X][H^+] \quad (12)$$

Values for k_1, k_2, and k_3 were determined by least squares minimization of the residuals

between the predicted concentrations of X, H, D, and F, obtained by solving eqns. 6, 9, 10, and 12, and the experimental data shown in Figure 2.3. A good fit to the data could be obtained with the rate coefficients listed in Table 2.2, with r^2 fit values of 0.98 and 0.99 for xylose and furfural, respectively (Figure 2.6 shows this kinetic model fit to experimental data). These rate coefficients reveal that degradation products are formed 20% faster than humins.

Similarly, the rate coefficients for the parent reactions involved in the hydrolysis of xylan to xylobiose and xylose (shown in Scheme 2.9) were found using the previously determined constants (k_1, k_2 and k_3) and the following set of equations:

$$\frac{d[\beta-1,4]}{dt} = -(k_{x1} + k_{xb})[\beta-1,4][H^+] \tag{13}$$

$$\frac{d[XB]}{dt} = (k_{xb}[\beta-1,4] - k_{x2}[XB])[H^+] \tag{14}$$

$$\frac{d[X]}{dt} = k_{x1}[\beta-1,4][H^+] + k_{x2}[XB][H^+] - (k_1 - k_2[F] + k_3[X])[X][H^+] \tag{15}$$

where [β-1,4] is the concentration of β-1,4 glycosidic linkages in xylan and [XB] is the xylobiose concentration. A satisfactory fit to the data presented in Figure 2.2 could be obtained with these rate coefficients (listed in Table 2.2), with r^2 fit values of 0.91, 0.93 and 0.94 for xylobiose, xylose, and furfural, respectively (Figure 2.7 shows this kinetic model fit to experimental data). These rate constants show that xylan hydrolysis to xylose is 28% faster than xylan hydrolysis to xylobiose, while xylobiose hydrolysis is an order of magnitude faster than xylan hydrolysis. These trends are consistent with those found for the hydrolysis of xylan in water [7]. We also find that xylose dehydrates to furfural 13% faster than xylan hydrolyzes to xylose. Finally, it is observed that the sum of k_{x1} and k_{x2} approximates the value of k_{app} reported in Table 2.1.

2.3.5 Role of Water in Xylose Dehydration and Degradation Reactions

While the initial rate of xylan hydrolysis was found to have a zero-order dependence on water, the reactions that occur beyond hydrolysis have an observable dependence on the concentration of water. Figure 2.8 shows the temporal evolution of xylose from xylan for a range of starting from 400 mM (1 mole of water per mole of β-1,4 glycosidic bonds) to 6M (15 moles of water per mole of β-1,4 glycosidic bonds). As expected, at short reaction times the concentration of water has virtually no effect on xylose yield, as hydrolysis is the principal reaction. However, over longer periods of time, higher water concentrations enhance the production of xylose, increasing maximum yields from 37% with 400 mM of water to 57% with 6M of water. Over this range of water concentrations, the yields of furfural (not shown) decreased from 15% to 8%, and the formation of humins decreased (as judged by the visual appearance of the reaction solutions) with increasing initial water concentration.

Various hypotheses have been offered to explain the ability of water to inhibit the extent of xylose dehydration and degradation reactions. It has been suggested that Le Chatelier's Principle can explain the shift in equilibrium away from dehydration products

in favor of xylose in the presence of higher concentrations of water [9]. However, this seems unlikely, as it has been reported that starting with excess furfural and performing the xylose dehydration reaction does not impede the complete conversion of xylose [17]. Other authors have suggested that water is a stronger base than any of the hydroxyl groups of xylose, and thus would be preferentially protonated [21]. In support of this suggestion is an *ab initio* molecular dynamics study that examined the affinity of free protons for xylose in the presence of differing numbers of water molecules [26]. The authors of this work show that water molecules compete with the hydroxyl groups on xylose for available protons, and that, in the presence of enough water molecules, solvent protonation is preferred over xylose protonation, resulting in the termination of the xylose dehydration pathway. Our observations of an inverse relationship between initial water concentration and furfural/humins yields are consistent with these findings.

The results of these experiments do not, however, suggest that xylan hydrolysis experiments should be initiated with a high concentration of water in order to achieve optimal yields of xylose. Xylan, like cellulose, is not water-soluble and will precipitate completely from an ionic liquid-water solution containing >20M water, resulting in the quenching of xylose hydrolysis. Recent studies have addressed this issue by employing a multistage water addition strategy to maximize glucose yields in the depolymerization of cellulose in ionic liquid [9, 18]. In this strategy, water was added at varying time intervals such that as the hydrolysis of cellulose proceeded, shorter polymer chains with higher water tolerances would evolve. Building on these results, we tested various intervals and quantities of water addition to develop an optimal water addition strategy for xylan hydrolysis in [Emim][Cl]. Table 2.3 details these results. Using the method that provided the best overall xylose yield, we found that we could double the xylose yields obtained when water was only introduced at the start of reaction. Gradually introducing water from an initial 9 wt% to 48 wt% over 60 min (entry 5 of Table 2.3), the xylose yield increased from 45% to 90%, while furfural yields were reduced to 5% from 15% over the course of 120 min. Additionally, humins content was measured to be only 4% at reaction termination. To compare under similar conditions where an optimized water addition strategy was used, one study found that cellulose (Avicel) could be hydrolyzed to 76 wt% glucose, 10 wt% 5-HMF, and 0 wt% humins after 90 min at 105 ºC [18].

2.4 Conclusions

We have found that hemicellulose (xylan) can be easily hydrolyzed in [Emim][Cl] to its primary sugar, xylose, in high yields with minimal dehydration and degradation products (furfural and humins). Desirable product yields showed marked increases when a multi-stage water addition strategy was employed. A kinetic model defining all essential reactions involved in, and stemming from, xylan hydrolysis was developed and discussed. Xylan hydrolysis was found to exhibit faster initial reaction rates than cellulose hydrolysis under similar conditions in ionic liquid. Both xylan hydrolysis and xylose degradation showed lower activation energies over cellulose hydrolysis and glucose degradation, respectively. These observations were attributed to the inherent structural differences between xylan and cellulose.

2.5 Supplemental Information

2.5.1 Effect of H_2SO_4 Concentration on Xylan Hydrolysis to Xylose

The effect of varying the concentration of H_2SO_4 on the Brønsted acid-catalyzed hydrolysis of xylan to xylose at 80 ºC in [Emim][Cl] was studied, with the results shown in Figure 2.9. As the acid concentration is increased from 40 mM to 1000 mM, the rate of xylose formation increases, with maximum yields of >40% achieved within 2 h when >100 mM H_2SO_4 was used. The disappearance of xylose beyond these maximums at high catalyst concentrations shows that lower catalyst loadings are necessary to mitigate product loss under these conditions. These results are consistent with the previous determination of first-order dependency of xylan hydrolysis on proton concentration.

2.5.2 Effect of H_2SO_4 Concentration on Xylose Dehydration to Furfural

The effect of varying the concentration of H_2SO_4 on the Brønsted acid-catalyzed dehydration of xylose to furfural at 80 ºC in [Emim][Cl] was studied, with the results shown in Figure 2.10. As the acid concentration is increased from 40 mM to 1000 mM, the rate of furfural formation increases, with maximum yields of >14% achieved within 2 h when >200 mM H_2SO_4 was used. The disappearance of furfural beyond these maximums at high catalyst concentrations demonstrates the instability of furfural at high catalyst loadings in ionic liquids. These results are consistent with the previous determination of first-order dependency of xylose dehydration on proton concentration.

2.5.3 Effect of Using 1,4-Dioxane on the Formation of Humins

The effect of using 1,4-dioxane as an extracting agent on the formation of humins during the Brønsted acid-catalyzed hydrolysis of xylan at 80 ºC was investigated. Table 2.4 details these results. When extractions using 1,4-dioxane were employed over a 1.5 h period, xylobiose and xylose yields improved slightly while furfural yields were reduced by ~50% and humins were eliminated. The frequency of extraction was found to have a minimal impact on improving yields, however. This experiment demonstrates that using an effective extracting agent can be a competitive alternative to the multi-stage water addition strategy in mitigating product loss during the hydrolysis of xylan.

Scheme 2.1 A representative hemicellulose fragment displaying the characteristic xylose backbone (highlighted in **blue**) branched with various C5 and C6 sugars including arabinose and glucose. Adapted from Ref. [4].

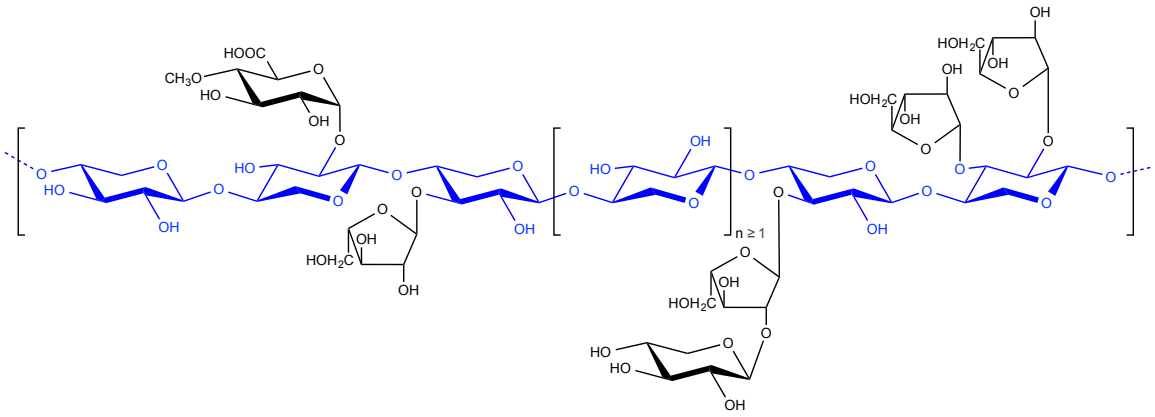

Scheme 2.2 A representative hydrolysis reaction pathway of a hemicellulose, homoxylan. Major products shown include xylobiose and xylose from the hydrolysis of hemicellulose, furfural from the dehydration of xylose, degradation products from xylose, and humins from the reaction between xylose and furfural.

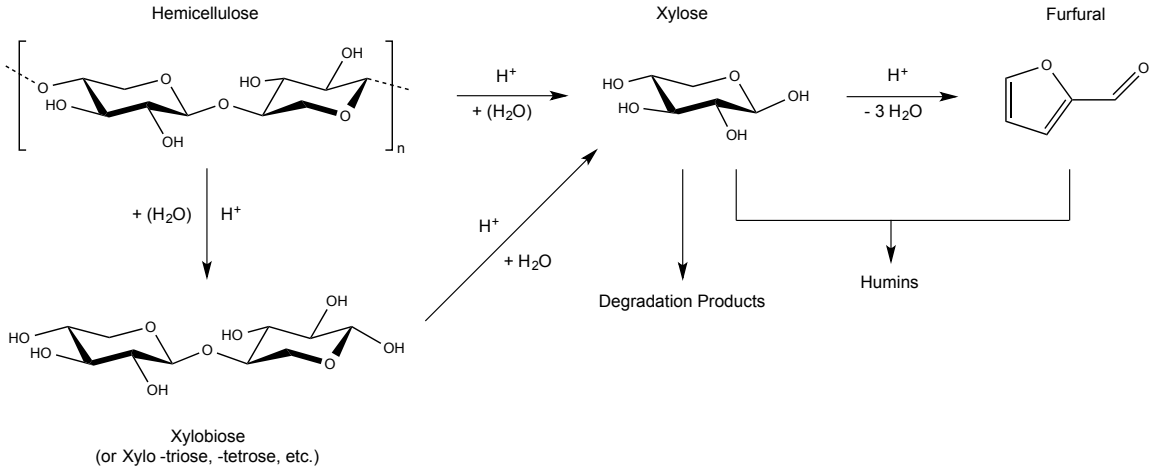

Scheme 2.3 Proposed mechanism for the hydrolysis of xylan, initiated by the reversible protonation of a β-1,4 glycosidic linkage (where $K^{\ddagger}_{1}$ is the associated equilibrium constant), followed by the rapid formation of an oxonium cation (with rate constant $k^{\ddagger}_{2}$) and subsequent rapid hydration to xylose.

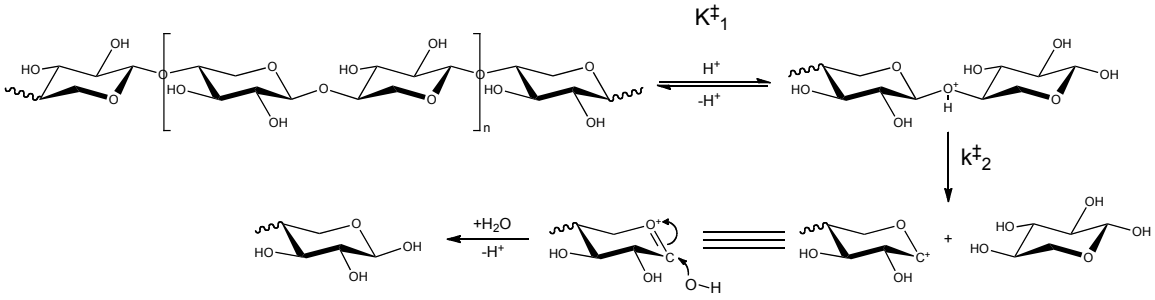

Scheme 2.4 Rearrangement chemistry of the C5 hydroxymethyl group of cellulose, showing the potential van der Waals interaction between the active hydrogen of a hydroxymethyl group with a β-1,4 glycosidic bond.

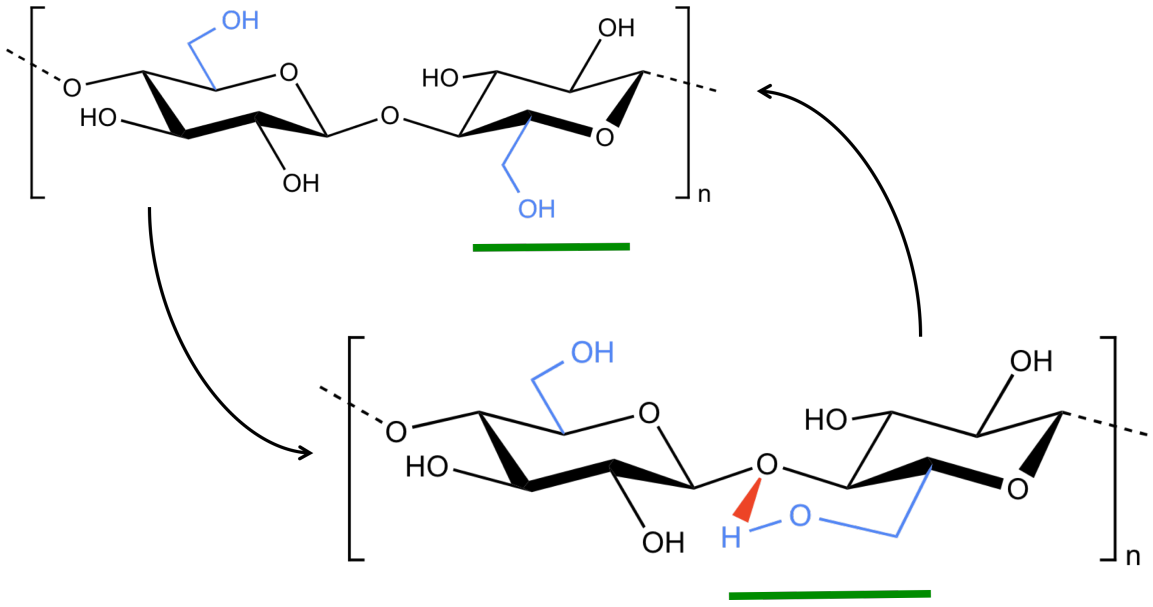

Scheme 2.5 Equilibrium protonation reaction of the C5 hydroxymethyl oxygen of cellulose in the presence of a strong acid.

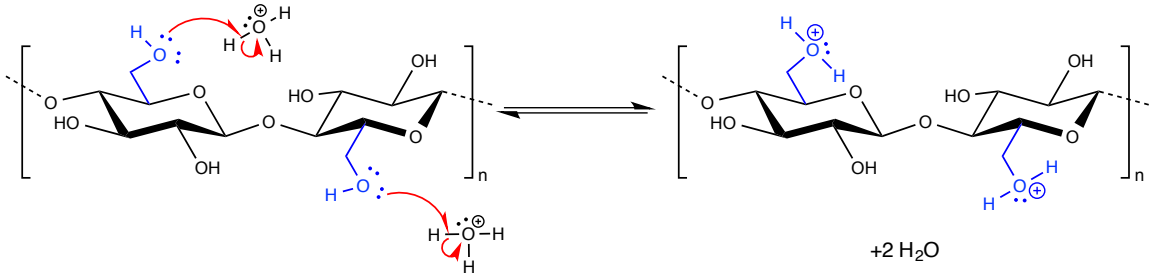

Scheme 2.6 Proposed reaction pathway for the dehydration of xylose to furfural, initiated by the dehydration of xylose at the C2 position.

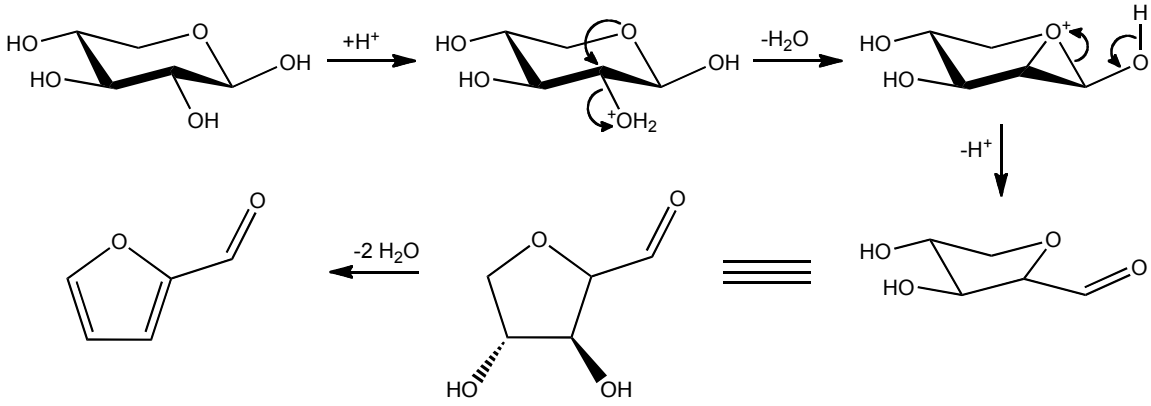

Scheme 2.7 Proposed reaction pathway for the dehydration of xylose to furfural *via* an acyclic pathway that features xylulose as a reactive intermediate.

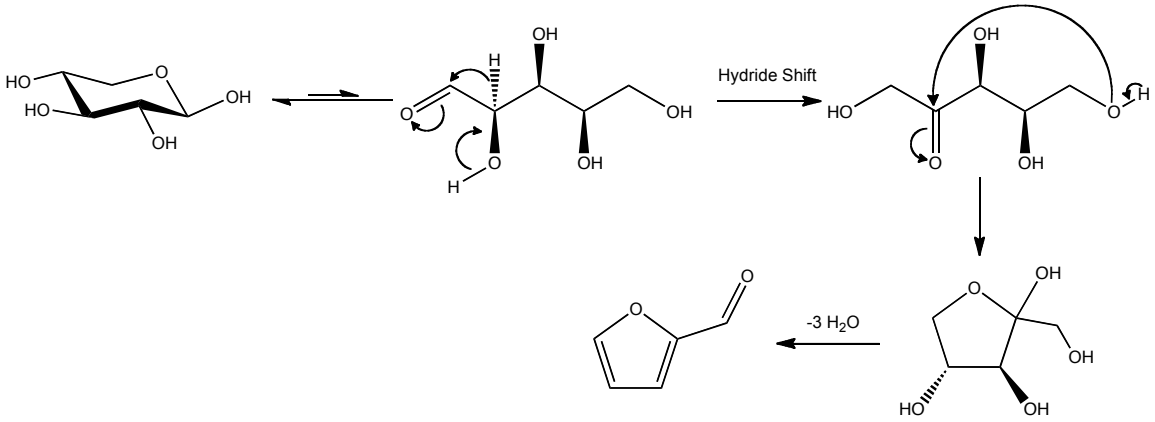

Scheme 2.8 Proposed xylose dehydration/degradation pathways (including secondary reactions) used in kinetic modeling.

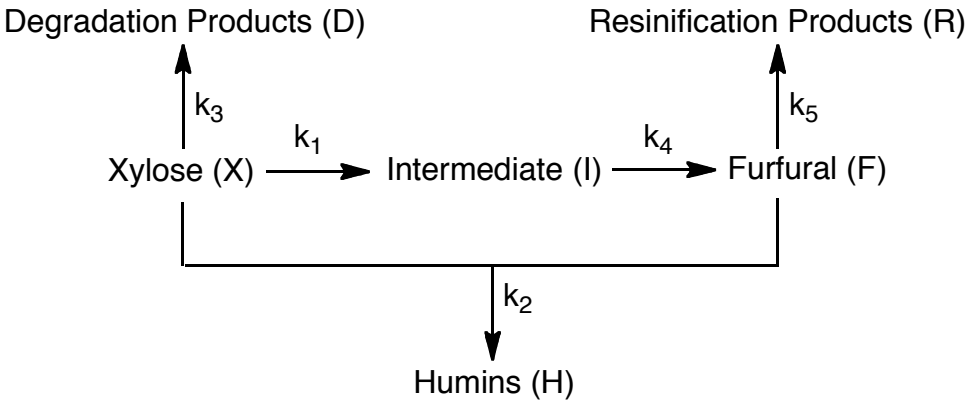

Scheme 2.9 Proposed xylan hydrolysis pathways used in kinetic modeling.

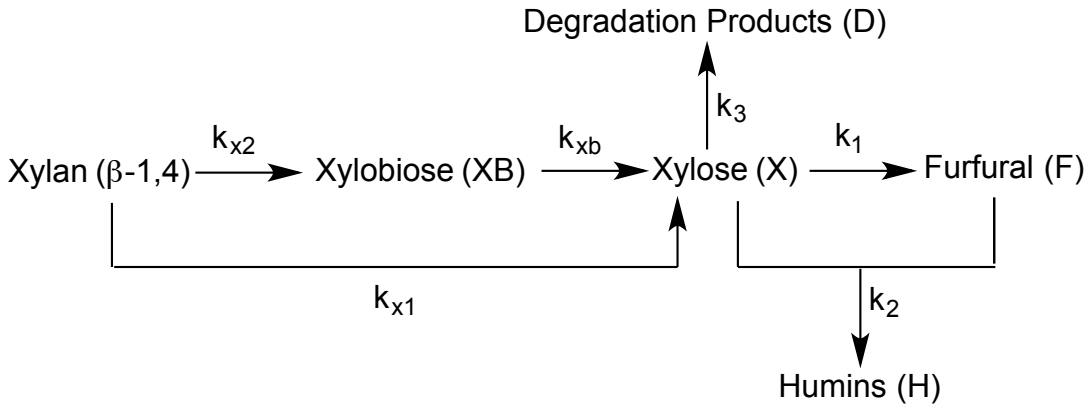

Figure 2.1 Initial rates of xylan hydrolysis at 80 ºC in [Emim][Cl] catalyzed by various Brønsted acids (200 mM) with 1.8M water. Acids used: HCl (pKa = -8), H_2SO_4 (pKa = -3), CH_3SO_3H (pKa = -2), CF_3COOH (pKa = 1), H_3PO_4 (pKa = 2.1), CH_3COOH (pKa = 4.75), and water (pKa = 15.4).

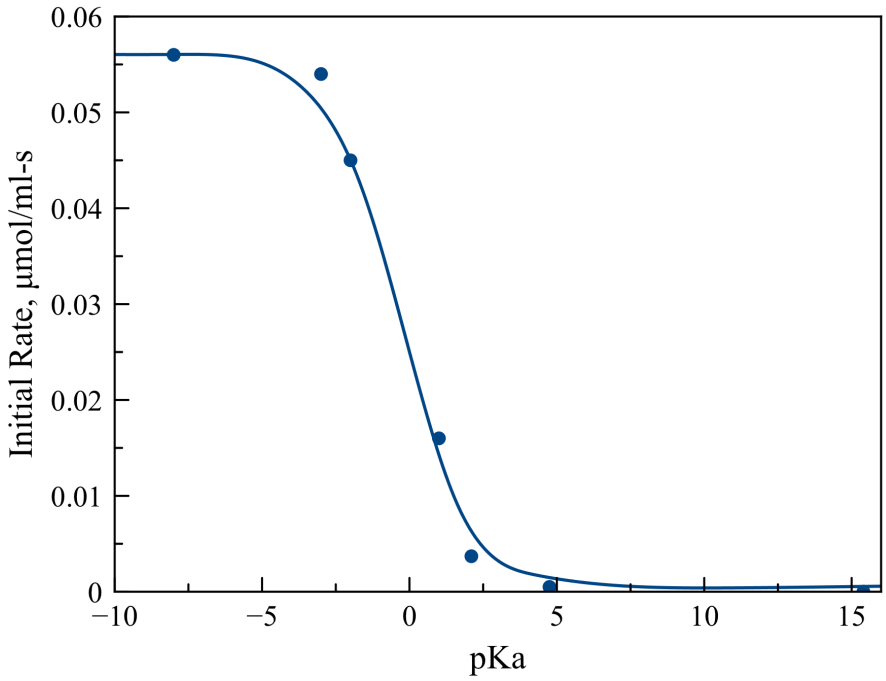

Figure 2.2 Hydrolysis of xylan at 80 ºC catalyzed by H_2SO_4 (200 mM) with water (1.8M). 27 mg xylan in 500 µl [Emim][Cl].

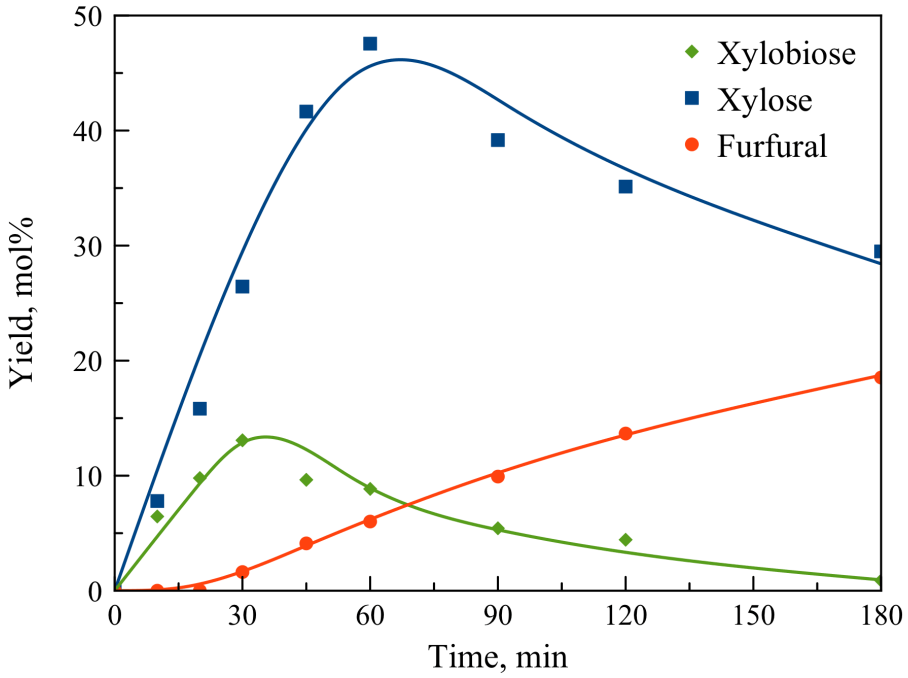

Figure 2.3 Dehydration/degradation of xylose at 80 ºC catalyzed by H_2SO_4 (200 mM) with water (1.8M). 27 mg xylose in 500 µl [Emim][Cl].

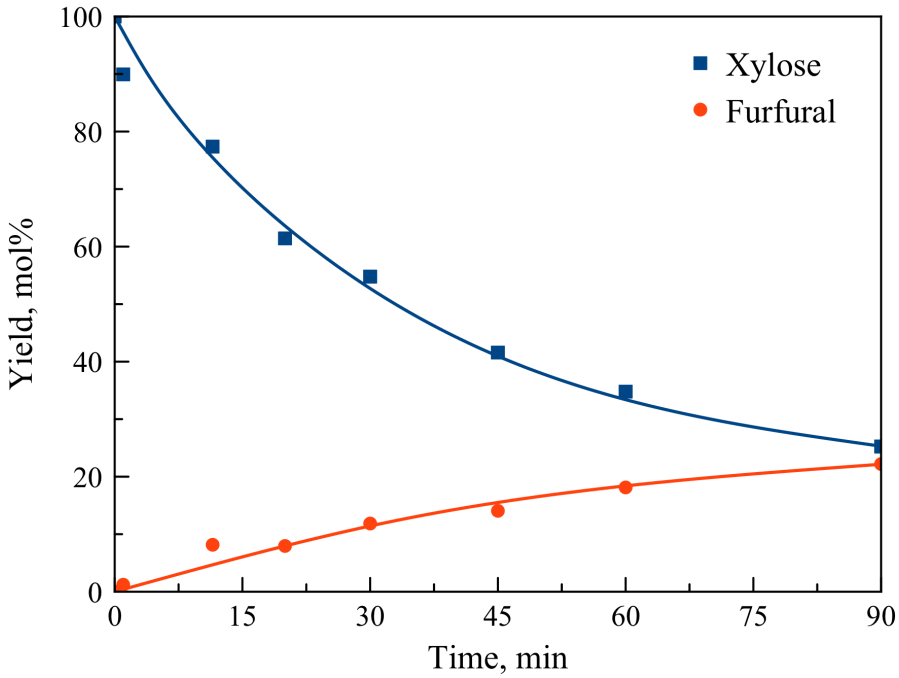

Figure 2.4 Rate law data for xylan hydrolysis: $r_0 = k*[H_2O]^x[H^+]^y[\beta\text{-}1,4\ \text{linkage}]^z$, where reaction orders were found from the ln-ln plot to be $x = 0.011$, $y = 0.944$, and $z = 1.0062$. Reaction conditions: 353 K, 1.8M water, 200 mM H_2SO_4, and 400 mM xylan in [Emim][Cl] unless otherwise varied to obtain the respective order of magnitude (water was varied from 400 to 5700 mM, H_2SO_4 was varied from 100 to 1000 mM, and the concentration of β-1,4 linkages were varied from 75 to 570 mM).

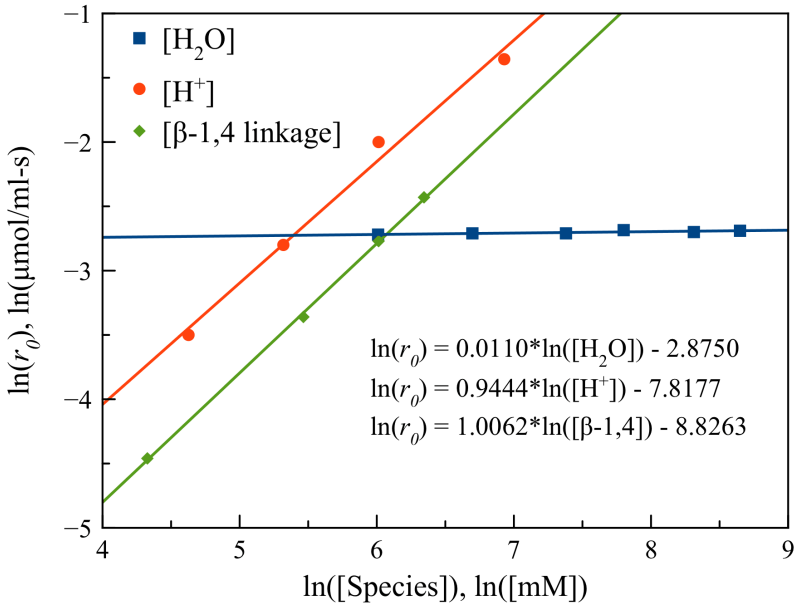

Figure 2.5 Arrhenius plots for xylan hydrolysis (●, E_a = 60 kJ/mol; $\ln(r_o) = -7245.9*T^{-1} + 17.739$), xylose degradation (■, E_a = 72 kJ/mol; $\ln(r_o) = -8823.3*T^{-1} + 22.845$), and the dehydration of xylose to furfural (◆, E_a = 114 kJ/mol; $\ln(r_o) = -13670*T^{-1} + 33.819$) in [Emim][Cl].

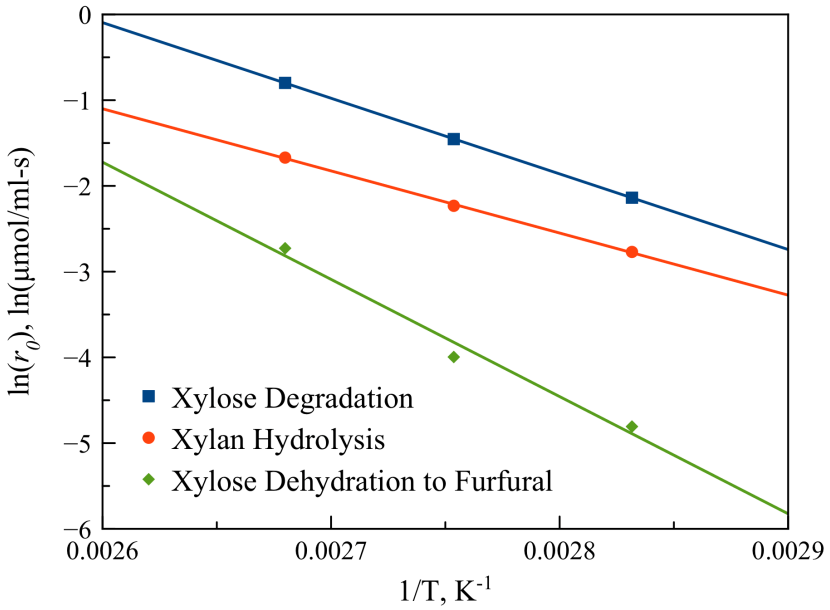

Figure 2.6 Kinetic model fit to the experimental data presented in Figure 2.3 (for xylose dehydration), determined by least squares minimization of residuals using the lsqcurvefit and ode45 routines within MATLAB (R2010b). Figure shows the predicted xylose conversion and yields of furfural, degradation products, and humins over time.

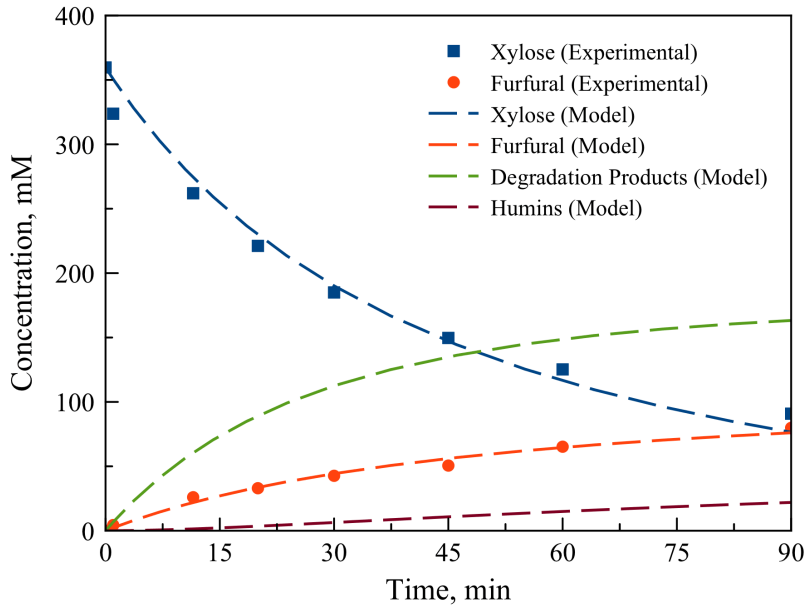

Figure 2.7 Kinetic model fit to the experimental data presented in Figure 2.2 (for xylan hydrolysis), determined by least squares minimization of residuals using the lsqcurvefit and ode45 routines within MATLAB (R2010b). Figure shows the predicted yields of xylobiose, xylose, and furfural from the hydrolysis of xylan over time.

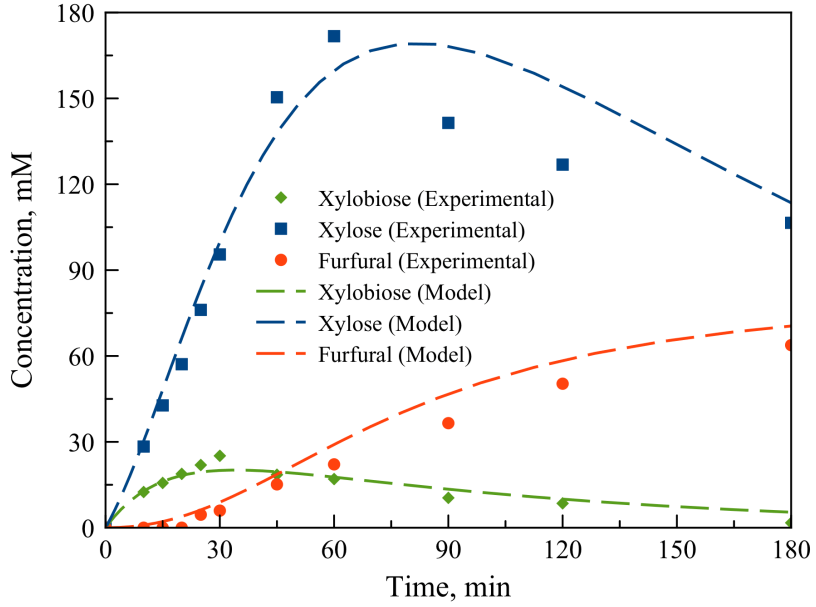

Figure 2.8 Effect of starting water concentration on the yield of xylose from the hydrolysis of xylan at 80 ºC in [Emim][Cl] catalyzed by H_2SO_4 (200 mM).

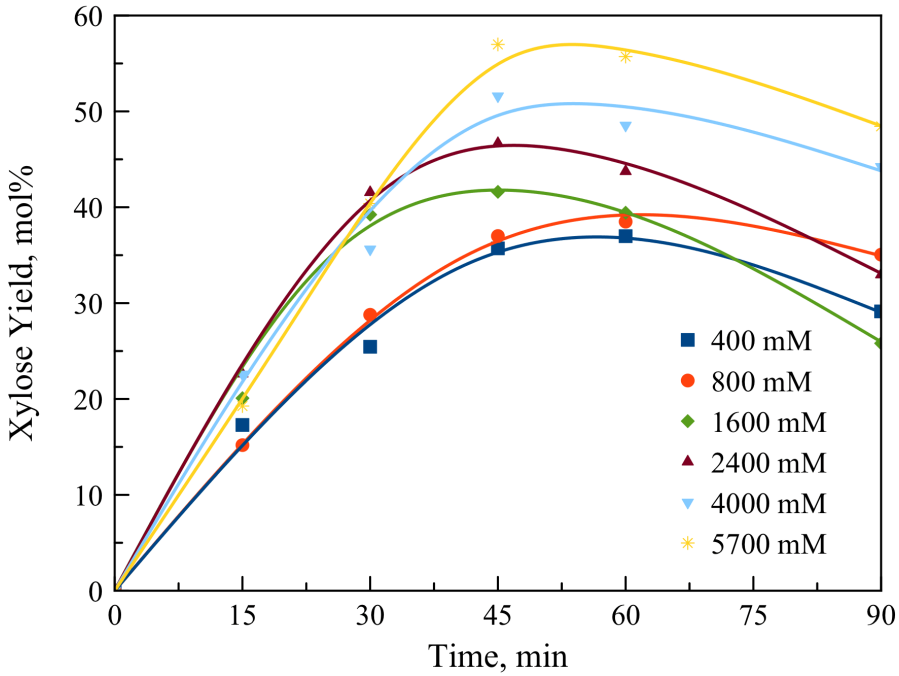

Figure 2.9 Effect of H_2SO_4 concentration on the yield of xylose from the hydrolysis of xylan at 80 ºC in [Emim][Cl].

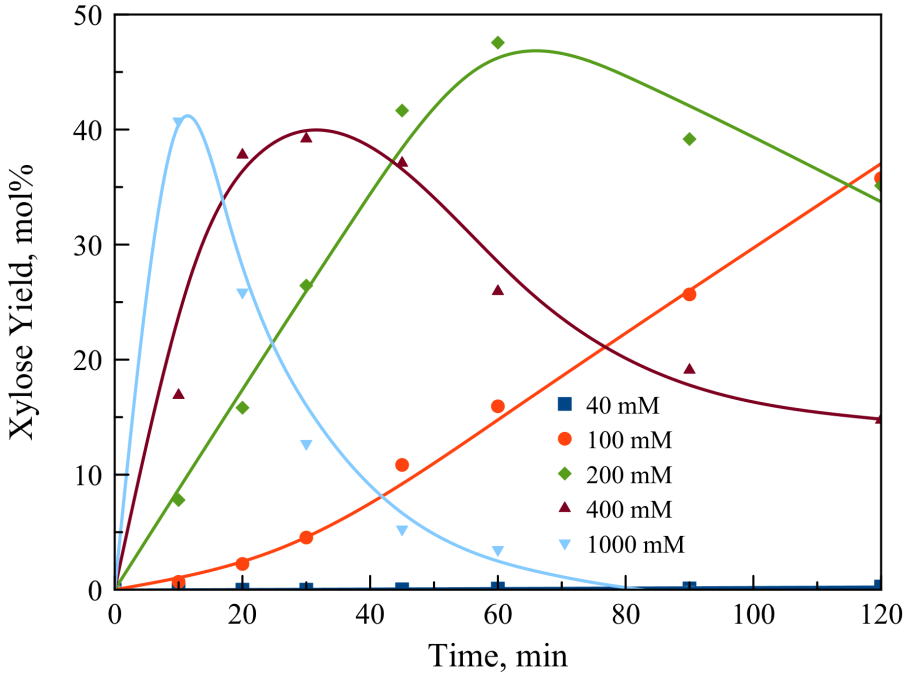

Figure 2.10 Effect of H_2SO_4 concentration on the yield of furfural from the dehydration of xylose at 80 ºC in [Emim][Cl].

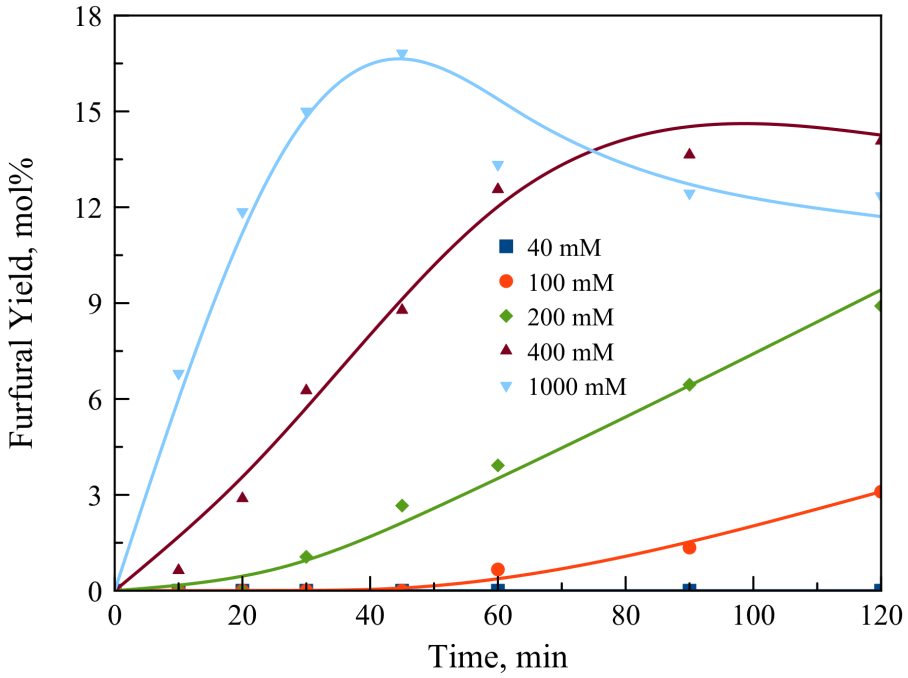

Table 2.1 Comparison of the initial rates and kinetic parameters of hemicellulose and cellulose hydrolyses at 353, 363, and 373 K. Both hydrolyses were performed in [Emim][Cl] with initial reactant and H_2SO_4 concentrations of 400 mM and 200mM, respectively.

	Xylan (from Birchwood)			Cellulose (Avicel)		
E_a, kJ/mol	60			93		
Temperature, K	353	363	373	353	363	373
r_0, μmol/mL-s	6.21×10^{-2}	1.09×10^{-1}	1.87×10^{-1}	1.84×10^{-2}	3.75×10^{-2}	8.53×10^{-2}
A, mL/μmol-s	5.70×10^{2}	5.71×10^{2}	5.72×10^{2}	1.12×10^{7}	1.12×10^{7}	1.11×10^{7}
k, mL/μmol-s	7.60×10^{-7}	1.34×10^{-6}	2.28×10^{-6}	2.31×10^{-7}	4.70×10^{-7}	1.07×10^{-6}

Table 2.2 Reaction rate constants determined *via* least squares minimization of residuals between predictions by kinetic models and the experimental data from Figure 2.3 (for xylose dehydration) and Figure 2.2 (for xylan hydrolysis) using the lsqcurvefit and ode45 routines within MATLAB (R2010b).

Xylose Dehydration		
$k_1/10^{-4}$, L mol^{-1}s^{-1}	$k_2/10^{-3}$, L^2 mol^{-2}s^{-1}	$k_3/10^{-3}$, L^2 mol^{-2}s^{-1}
5.38	3.18	4.40

Xylan Hydrolysis		
$k_{x1}/10^{-4}$, L mol^{-1}s^{-1}	$k_{x2}/10^{-4}$, L mol^{-1}s^{-1}	$k_{xb}/10^{-3}$, L mol^{-1}s^{-1}
4.76	3.73	5.34

Table 2.3 Effect of multistage water addition on the hydrolysis of xylan at 80 ºC catalyzed by H_2SO_4 (200 mM). 27 mg xylan in 500 ul [Emim][Cl]. [a]Represents total water present in weight percent at the given time.

	Water Content, wt%[a]						
Entry	0 min	15 min	30 min	60 min	Time, min	Xylose Yield, mol%	Furfural Yield, mol%
1	3	-	-	-	15	23	2
					30	42	5
					60	44	11
					90	33	16
2	7	-	-	-	15	23	2
					30	36	3
					60	49	9
					90	44	14
3	9	-	-	-	15	19	0
					30	40	3
					60	56	7
					90	48	12
4	7	12	26	39	15	19	0
					30	33	0
					60	61	0
					90	68	6
					120	60	10
5	9	17	34	48	15	15	0
					30	35	0
					60	57	0
					90	79	0
					120	90	4
6	9	20	40	58	15	13	0
					30	28	0
					60	57	0
					90	56	0
					120	61	0

Table 2.4 Effect of using 1,4-dioxane as an extracting agent on the formation of humins during the hydrolysis of xylan at 80 ºC catalyzed by H_2SO_4 (200 mM) with water (1.8M) after 90 min. 27 mg xylan in 500 µl [Emim][Cl]. [a]500 µl 1,4-dioxane used. [b]500 µl 1,4-dioxane used, extracted and replaced at 30 min intervals (3 total extractions). [c]500 µl 1,4-dioxane used, extracted and replaced at 15 min intervals (6 total extractions). [d]Furfural yield represents the sum of furfural detected in the [Emim][Cl] phase and all 1,4-dioxane phases.

	Xylobiose, mol%	Xylose, mol%	Furfural,[d] mol%	Humins, mol%
No Dioxane	3	38	13	10
1:1 v/v Dioxane/IL[a]	4	42	7	0
30 min Extractions[b]	4	43	6	0
15 min Extractions[c]	5	44	5	0

References

[1] G. W. Huber, S. Iborra, A. Corma, A. *Chem. Rev.* **2006**, *106*(9), 4044.
[2] a) M. Kleinert, T. Berth, *Energy Fuels* **2008**, *22*(2), 1371; b) D. S. Argyropoulos, S. Menachem, *Adv. Biochem. Eng. Biotech*. **1997**, *57*, 127.
[3] a) T. Werpy, G. Petersen, A. Aden, J. Bozell, J. Holladay, J. White, A. Manheim, Report No. NREL/TP-510– 35523, *Top Value Added Chemicals from Biomass: Vol. 1—Results of Screening for Potential Candidates from Sugars and Synthesis Gas*, National Renewable Energy Laboratory, Golden, CO, **2004**; b) J. E. Holladay, J. F. White, J. J. Bozell, D. Johnson, Report No. PNNL-16983, *Top Value-Added Chemicals from Biomass-Volume II—Results of Screening for Potential Candidates from Biorefinery Lignin*, Pacific Northwest National Laboratory, Richland, WA, **2007**.
[4] M. B. Jones, M. Walsh, *Miscanthus for Energy and Fibre*, James & James, London, **2001**, pp. 109-154.
[5] B. C. Saha, *J. Ind. Microbiol. Biotechnol*. **2003**, *30*(5), 279.
[6] a) C. E. Wyman, S. R. Decker, M. E. Himmel, J. W. Brady, C. E. Skopec, L. Viikari, *Polysaccharides: Structural Diversity and Functional Versatility 2nd ed* (Ed.: Severian Dumitriu), Marcel Dekker, New York, **2005**, pp. 995-1034; b) S. E. Jacobsen, C. E. Wyman, *Appl. Biochem. Biotechnol*. **2000**, *84–86*, 81.
[7] P. Maki-Arvela, T. Salmi, B. Holmbom, S. Willfor, D. Y. Murzin, *Chem. Rev*. **2011**, *111*(9), 5638.
[8] B. P. Lavarackm, G. J. Griffin, D. Rodman, *Biomass Bioenergy* **2002**, *23*, 367.
[9] J. B. Binder, R. T. Raines, *Proc. Natl. Acad. Sci. U. S. A*. **2010**, *107*(10), 4516.
[10] a) J. B. Binder, R. T. Raines, *J. Am. Chem. Soc*. **2009**, *131*(5), 1979; b) J. B. Binder, M. Gray, J. White, Z. Zhang, *Biomass Bioenergy* **2009**, *33*, 1122.
[11] J. N. Chheda, Y. Roman-Leshkov, J. A. Dumesic, *Green Chem*. **2007**, *9*(4), 342.
[12] R. Swatloski, S. Spear, J. Holbrey, R. Rogers, *J. Am. Chem. Soc*. **2002**, *124*, 4974.
[13] O. A. El Seoud, A. Koschella, L. C. Fidale, S. Dorn, T. Heinze, *Biomacromolecules* **2007**, *8*(9), 2629.
[14] H. Olivier-Bourbigou, L. Magna, D. Morvan, *Applied Catalysis A: General* **2010**, *373*, 1.
[15] D. MacFarlane, S. Forsyth, *Ionic Liquids as Green Solvents: Progress and Prospects* (Eds.: R. D. Rogers and K. R. Seddon), ACS Symposium Series 856, Oxford University Press, Washington, DC, **2003**, pp. 264–276.
[16] L. Vanoye, M. Fanselow, J. D. Holbrey, M. P. Atkins, K. R. Seddon, *Green Chem*. **2009**, *11*(3), 390.
[17] C. Sievers, I. Musin, T. Marzialetti, M. B. Valenzuela-Olarte, P. K. Agrawal, C. W. Jones, *ChemSusChem* **2009**, *2*(7), 665.
[18] S. J. Dee, A. T. Bell, *ChemSusChem* **2011**, *4*(8), 1166.
[19] O. Akpinar, K. Erdogan, U. Bakir, L. Yilmaz, *LWT–Food Sci. Technol*. **2010**, *43*, 119.
[20] T. W. G. Solomons, C. B. Fryhle, *Organic Chemistry 8th ed.*, John Wiley & Sons, Hoboken, NJ, **2004**.
[21] M. R. Nimlos, X. Qian, M. Davis, M. E. Himmel, D. K. Johnson, *J. Phys. Chem. A* **2006**, *110*, 11824.

[22] X. H. Qian, M. R. Nimlos, M. Davis, D. K. Johnson, M. E. Himmel, *Carbohydr. Res.* **2005**, *340*, 2319.
[23] K. J. Zeitsch, *Sugar Ser*. 2000, *13*, 1-353.
[24] J. B. Binder, J. J. Blank, A. V. Cefali, R. T. Raines, *ChemSusChem* **2010**, *3*(11), 1268.
[25] G. Marcotullio, W. de Jong, *Carbohydr. Res*. **2011**, *346*(11), 1291.
[26] X. H. Qian, M. R. Nimlos, D. K. Johnson, M. E. Himmel, *Appl. Biochem. Biotechnol*. **2005**, *124*, 989.

Chapter 3

The Role of Metal Halides in Enhancing the Dehydration of Xylose to Furfural

Abstract

The dehydration of xylose yields furfural, a product of considerable value as both a commodity chemical and a platform for producing a variety of fuels. When xylose is dehydrated in aqueous solution in the presence of a Brønsted acid catalyst, humins are formed *via* complex side processes that ultimately result in a loss in the yield of furfural. Such degradative processes can be minimized *via* the *in situ* extraction of furfural into an organic solvent. The partitioning of furfural from water into a given extracting solvent can be enhanced by the addition of salt to the aqueous phase, a process that increases the thermodynamic activity of furfural in water. While the thermodynamics of using salts to improve liquid-liquid extraction are well studied, their impact on the kinetics of xylose dehydration catalyzed by a Brønsted acid are not. The aim of the present study was to understand how metal halide salts affect the mechanism and kinetics of xylose dehydration in aqueous solution. We found that the rate of xylose consumption is affected by both the nature of the salt cation and anion, increasing in the order no salt < K^+ < Na^+ < Li^+ and no salt < Cl^- < Br^- < I^-. Furfural selectivity increases similarly with respect to metal cations, but in the order no salt < I^- < Br^- < Cl^- for halide anions. Multinuclear NMR was used to identify the interactions of cations and anions with xylose and to develop a model for explaining xylose-metal halide and water-metal halide interactions. The results of these experiments coupled with ^{18}O-labeling experiments indicate that xylose dehydration is initiated by protonation at the C1OH and C2OH sites, with halide anions acting to stabilize critical intermediates. The means by which metal halides affect the formation of humins was also investigated, and the role of cations and anions in affecting the selectivity to humins is discussed.

3.1 Introduction

Furfural is a high value chemical that can be used to produce a wide range of commodity chemicals [1,2] and fuels [3-6]. At present, the industrial production of furfural is accomplished through the Brønsted acid-catalyzed hydrolysis of agricultural waste, a process that has a product selectivity of less than 60% [2, 7]. Furfural can also be sourced from any biomass material containing hemicellulose, a biopolymer which can be hydrolyzed to its principle component, xylose [8]. The subsequent dehydration of xylose produces furfural, however, this reaction is accompanied by complex side reactions leading to humins, intractable condensation products that can greatly reduce furfural selectivity. One approach for minimizing the loss of furfural is *in situ* extraction. Recent studies have shown that furfural selectivities in excess of 85% can be achieved by extracting the furfural formed by Brønsted acid-catalyzed dehydration of xylose using a biphasic system consisting of water and MIBK [9] or water:DMSO (1:1 v/v) and MIBK:2-butanol (7:3 v/v) [10]. The increased furfural selectivity is attributed to the

removal of furfural from the aqueous phase, thereby minimizing the possibility for furfural to undergo self-resinification or react with xylose to form humins. It has also been reported that the addition of salt, such as a metal halides, to the aqueous phase enhances the extraction of furfural from the aqueous phase into the organic phase as a consequence of the salt lowering the activity coefficient of water, consequently increasing the activity coefficient of the furfural [11].

A question not addressed in previous studies is whether dissolved salt affects the rate of xylose dehydration and/or the rate of humin formation in an aqueous phase. To the best of our knowledge, this subject has received very little attention. What is known is that dissolved metal halides enhance the yield of furfural obtained *via* the aqueous phase dehydration of xylose [12]. It should be noted, though, that this work was carried out with low substrate concentrations and high temperature (35 mM xylose, 200 ºC), conditions for which entropic effects are expected to diminish condensation reactions that lead to the formation of humins [2]. The only explanation given for the observed effect of salt addition is that it enhances the formation of 1,2-enediol, an intermediate in the mechanism of xylose dehydration [12]. Thus, the effects of dissolved salts on the rates of xylose dehydration and humins formation are little understood.

The present study was undertaken with the aim of developing a more thorough understanding of the role of metal halides in the dehydration of xylose to furfural in aqueous solution. Multinuclear NMR spectroscopy was used to probe both the interactions of metal cations and halide anions with water and xylose. These studies were complemented by experiments utilizing ^{13}C labeling of the xylose anomeric carbon to probe isomeric distributions and ^{18}O labeling of the xylose ring oxygen to identify reaction pathway populations. The results of these investigations have led to a mechanistic understanding of the means by which metal halides alter the kinetics of Brønsted acid-catalyzed dehydration of xylose in aqueous solution as well as the influence metal halides have on the formation of humins.

3.2 Methods

3.2.1 Materials

D-xylose (99%, Sigma-Aldrich), D-[5-^{18}O]-xylose (90 atom% ^{18}O, Omicron Biochemicals, Inc.), and 2-furaldehyde (furfural, 99%, Sigma-Aldrich) were used as reagents and standards (for quantification). D-xylose-1-^{13}C (99 atom% ^{13}C, Sigma-Aldrich) was used in ^{1}H- and ^{13}C-NMR studies.

Lithium chloride (LiCl, BioXtra, ≥99.0% (titration)), lithium bromide (LiBr, anhydrous, Redi-Dri, ReagentPlus, ≥99%), lithium iodide (LiI, 99.9% (trace metals basis)), sodium bromide (NaBr, puriss., 99-100.5%), sodium iodide (NaI, anhydrous, Redi-Dri, ACS reagent, ≥99.5%), potassium chloride (KCl, approx. 99%), potassium bromide (KBr, BioXtra, ≥99.0%), potassium iodide (KI, puriss., ≥99.5%), magnesium chloride ($MgCl_2$, anhydrous, ≥98%), and calcium chloride ($CaCl_2$, anhydrous, Redi-Dri, ≥97%) were purchased from Sigma-Aldrich; sodium chloride (NaCl, ≥99.0%) was purchased from Fisher Scientific. Sulfuric acid (H_2SO_4, 98%, Sigma-Aldrich) and hydrochloric acid (HCl, 37% v/v, Fisher Scientific) were used as Brønsted acid catalysts. All materials were used as purchased, without further purification or modification.

3.2.2 Experimental Approach

All experiments were performed in 10 ml glass vials (from Sigma-Aldrich *via* supplier Supelco) sealed with 20 mm aluminum-crimped PTFE septa and heated using a silicon oil bath to maintain constant reaction temperature and stirring rate. In a representative xylose dehydration experiment, xylose was dissolved in 5M brine (i.e. 5M NaCl in nanopure water), to which HCl was added to create a solution (750 mM xylose, 50 mM H^+). A 4 ml aliquot of this solution was sealed into a 10 ml glass vial. The vial was then placed in a silicone oil bath heated to 140 ºC and stirred at 600 rpm. Upon completion of the reaction, the sample was removed and quenched in an ice bath. An internal standard (1 ml of 75 mg/ml 1,6-hexanediol in water) was added and the sample centrifuged to remove all water insoluble particulates. A portion of the reaction mixture (500 µl) was diluted in a 1:1 ratio with nanopure water and taken for HPLC analysis. For reactions involving an additional organic phase, the aqueous phase volume was reduced to 1 ml and toluene (4 ml) was added prior to sealing the reaction vial. At reaction end, the organic phase was separated *via* centrifuging. The aqueous phase was treated as above and analyzed *via* HPLC while a different internal standard (1 ml of 5 mg/ml guaiacol in toluene) was added to the organic phase prior to GC/MS analysis.

The influence of metal halides on the dehydration of xylose and the formation of furfural was carried out using a 5M solution of the metal halide. The choice of this concentration was based on preliminary experiments (see Figure 3.1) carried out with NaCl solutions ranging in concentration from 0 to 5M. The natural log of the initial reaction rate versus the salt concentration revealed three distinct regimes: (1) at low concentrations (500 mM and under), rate of xylose dehydration was roughly zero-order, (2) at intermediate concentrations (500 mM to 3.5M), the rate was roughly first-order, and (3) at high concentrations (3.5M to 5M), the rate was roughly zero-order. To maximize initial xylose conversion/furfural production rates, the highest salt concentration that could be achieved for all salts with respect to room-temperature solubility limits was found to be 5M. Only salts containing Cl^-, Br^-, and I^- were used. Fluoride (F^-) salts were purposely excluded in order to avoid a reduction in the pH of the reaction solution due to the reaction of proton (from the hydrochloric acid Brønsted acid catalyst, pKa = -8) with the more basic flouride anions. Consequently, only halides of equal or lesser basicity than Cl^- were explored.

3.2.3 Product Analysis

A Shimadzu HPLC equipped with a Phenomenex Rezex RFQ-Fast Acid H+ column (100 x 7.8 mm; 0.01 N H_2SO_4; 1.0 ml/min; 55 ºC) and a refractive index detector (RID) was used to analyze all aqueous samples. Product quantities were determined by converting integrated HPLC peak areas into concentrations using a 7-point calibration curve generated from purchased standards.

A Varian CP-3800 Gas Chromatograph equipped with a FactorFour Capillary Column (UF-5ms 30 m, 0.25 mm, 0.25 µm, P/N CP8944) connected to a Varian quadrupole-mass spectrometer (MS) and flame ionization detector (FID) was used to analyze all organic phase samples. After product identification by mass spectrometer, product concentrations were determined from integrated FID peak areas using a 6-point calibration curve generated from purchased standards.

A Bruker AVQ-400 console with a Bruker 9.39 T magnet was used to perform all ^{1}H and ^{13}C nuclear magnetic resonance (NMR) experiments. A Bruker AVB-400 console with a Bruker 9.39 T magnet was used to perform all ^{35}Cl-NMR experiments.

Reagent and product yields are reported as molar percentages relative to initial molar concentrations of xylose (i.e. furfural yields = moles furfural/initial moles xylose). All reported yields were typically reproducible to within a +/- 5% relative error (based upon the calculation of one standard deviation).

3.3 Results and Discussion

3.3.1 Xylose Dehydration in Water

Figure 3.2 shows the temporal evolution of products formed during HCl-catalyzed dehydration of xylose in water at 140 ºC. Over the course of the reaction, furfural is observed as the primary identifiable product. The difference between the consumption of xylose and the formation of furfural is attributed to the formation of humins – a combination of soluble (but not identifiable) products contributing to the discoloration of the reacting solution and a dark brown-to-black precipitate. During 600 min of reaction 92% of the xylose is consumed. The furfural yield increases initially, reaches a maximum of 30% after 200 min, and then slowly declines. By contrast, the yield of humins increases monotonically, and after 600 min constitutes the principal product of xylose dehydration.

At early reaction times (<10 min), xylose is consumed at a rate that exceeds the rate of furfural formation, suggesting the loss of xylose due to self-condensation or reaction with anhydro-xylose intermediates. The decline in furfural yield for reaction times longer than that needed to reach the maximum yield suggests that furfural undergoes secondary reaction in the presence of a Brønsted acid. This hypothesis was confirmed by observing the reaction of an aqueous solution of furfural, containing 375 mM of furfural and 200 mM HCl, at 140 ºC. After 2 h of reaction, the concentration of furfural decreased by 24% due to resinification (self-coupling), a process reported to occur readily at temperatures below 200 ºC [2]. Furfural can also undergo condensation with anhydro-xylose intermediates *via* dioxolane-like bridging structures. Consistent with this proposal, it was observed (see Figure 3.3) that the addition of furfural at the start of xylose dehydration reduces the furfural produced from xylose (from 26 mol% to 9 mol%). However, direct condensation of furfural with xylose is unlikely, since the rate at which xylose is consumed is unchanged by the initial furfural concentration. These two observations indicate that a reaction occurs between furfural and an intermediate along the pathway from xylose to furfural. Scheme 3.1 shows a proposed pathway for the dehydration of xylose to furfural and for the loss of xylose and furfural *via* condensation reactions. The mechanisms by which the latter two processes might occur are given in Schemes 3.2 and 3.3.

The kinetics of xylose consumption and furfural and humins formation can be described by the following set of ordinary differential equations, which are based on Scheme 3.1:

$$\frac{d[X]}{dt} = -(k_1 + k_4[I])[X][H^+] \qquad (1)$$

$$\frac{d[I]}{dt} = (k_1[X] - k_3[I][F] - k_4[I][X])[H^+] \quad (2)$$

$$\frac{d[F]}{dt} = (k_2[I] - k_3[I][F] - k_5[F]^2)[H^+] \quad (3)$$

$$\frac{d[H]}{dt} = (k_3[F][I] + k_4[X][I] + k_5[F]^2)[H^+] \quad (4)$$

Here [X], [I], [F], and [H] are the concentrations of xylose, intermediate product, furfural, and humins, respectively. Since intermediates involved in the conversion of xylose-to-furfural were not observed, we can invoke the pseudo-steady-state assumption and set d[I]/dt ≈ 0. Values for k_1, k_2, k_3, k_4, and k_5 were determined by least squares minimization of the residuals between the predicted concentrations of X, F, and H obtained by solving eqns. 1 through 4, and the experimental data shown in Figure 3.2. The best-fit values obtained in this manner are $k_1 = 2.9\text{x}10^{-4}$ L/mol-s, $k_2 = 7.5\text{x}10^{-4}$ L/mol-s, $k_3 = 2.1\text{x}10^{-3}$ L^2/mol^2-s, $k_4 = 7.5\text{x}10^{-4}$ L^2/mol^2-s, and $k_5 = 9.7\text{x}10^{-4}$ L^2/mol^2-s. These results demonstrate that the rate coefficient for the consumption of intermediates produced from xylose is nearly twice as large as that for their production, and that humins are formed *via* condensation of furfural and intermediates involved in xylose dehydration at a rate that is more twice as fast as either the rate of resinification or the rate of condensation between xylose and the intermediates involved in xylose dehydration.

3.3.2 Xylose Dehydration in the Presence of Metal Halides

The effects of metal halides on the Brønsted acid-catalyzed dehydration of xylose in an aqueous solution were investigated using the chloride, bromide, and iodide salts of the monovalent metals lithium, sodium, and potassium. Each of these experiments was carried out at 140 ºC in a 5M metal halide solution containing 50 mM HCl. The results of these experiments are presented in Figures 3.4-3.6.

Figures 3.4A-3.6A show that xylose consumption occurs much more rapidly in brine than in water, the rate depending on the nature of both the cation and anion. For a given anion, the rate of xylose consumption increases in the following order: no salt < K^+ < Na^+ < Li^+. The initial rate of furfural formation increases in the same order, as can be seen from the data presented in Figures 3.4B-3.6B. In each case, the yield of furfural reaches a maximum and then declines with further reaction time, the time at which the maximum occurs decreasing as initial rate of furfural formation increases.

Initial rate data for xylose conversion and furfural formation is summarized in Table 3.1 for all metal halide solutions. The initial rates of both xylose consumption and furfural formation increase in the order no salt < Cl^- < Br^- < I^-. However, it is evident from Figures 3.4-3.6 that for longer reaction times the orders of Br^- and I^- are reversed. This change in order is attributable to the slow oxidation of iodide anions to molecular iodine in aqueous systems at elevated temperatures *via* a sequence of reactions that sums to the following stoichiometric reaction [13].

$$4\ I^- + O_2 + 4\ H^+ \rightarrow 2\ I_2 + 2\ H_2O \quad (5)$$

The occurrence of this reaction leads to a loss of both iodide anions and protons from solution and the formation of iodine. Evidence for this process was observed as a darkening of the reaction solution, and a reduction in the rate of xylose dehydration. Further details of this process are discussed in the Supplemental Information (Figure 3.7).

Table 3.1 also lists the selectivity toward furfural for each salt. In general, the furfural selectivity increases in the order $I^- \approx Br^- < Cl^-$, indicating that bromide and iodide anions play greater roles in degradation reactions than do chloride anions.

3.3.3 Effects of Metal Halides on the Activity of Water

The data presented in Figures 3.4-3.6 and Table 3.1 clearly indicate that the presence of metal halides strongly affects rate of xylose dehydration, as well as the formation of furfural and humins. To understand how halide salts affect these processes, we examined the effect of salt composition on the thermodynamic activity of water and the manner in which salt cations and anions interact with dissolved xylose.

The activity of water was determined for 5M metal halide solutions using data taken from the literature [14]. The results, presented in Table 3.2, show that metal halides reduce the activity of water activity in the order no salt > Cl^- > Br^- > I^- for a given cation and no salt > K^+ > Na^+ > Li^+ for a given anion. Comparison of these trends with the observed trend in the rate of xylose consumption reveals that the rate of xylose dehydration increases with decreasing water activity. This correlation can be attributed to the ability of metal halides cations and anions to interact preferentially with water molecules, thereby reducing the interactions of water molecules with themselves of with other solute species. Such an interaction interrupts the hydrogen bond network within water, promoting a more stable restructuring of water around the metal halides [15, 16]. This "kosmotropic" effect increases with ionic radius and/or charge, and can be estimated by the number of water molecules that hydrate each free ion (for example, 5 for Li^+, 4 for K^+ and Na^+, and to a lesser degree 1 for Cl^-/Br^- and 0 for I^- [16]). In the presence of strong kosmotropic species, water molecules are less able to interact with other solutes, and hence the activity coefficient of these solutes (such as xylose) increases, enabling them to interaction more effectively with metal halide ions and protons. The latter effect is thought to enhance the extent of xylose protonation, as discussed in more detail below.

3.3.4 Effects of Metal Halides on the Distribution of Xylose Conformers

Xylose in its crystalline form is present almost exclusively as a-xylopyranose; however upon dissolution in water it isomerizes to an equilibrium distribution of the five conformers shown in Scheme 3.4 [17]. The distribution of xylose confomers was determined by ^{13}C-NMR (see Figure 3.8 for peak assignments). As shown in Table 3.3, in the absence of acid and salt, only four of the five isomers are evident, the principal forms being b-xylopyranose (63.8%) and a-xylopyranose (35.6%). In 5M salt solutions the ratio a-xylopyranose/b-xylopyranose increases slightly in the order no salt < K^+ < Na^+ < Li^+ for a given halide anion and in the order no salt < Cl^- < Br^- < I^- for a given cation. The observed change in the ratio of a-pyranose/ b-pyranose isomers of xylose is smaller than that reported for isomers of ribose and galactose [18, 19]. The larger effect of salts on these latter sugars is attributable to the presence of pyranose conformers containing axial-equatorial-axial (*ax.-eq.-ax.*) orientations of hydroxyl groups, for which the tri-oxygen core strongly attracts cations. By contrast, the hydroxyl groups in β-xylopyranose are in

eq.-eq.-eq. orientation and those in a-xylopyranose are in *ax.-eq.-eq.* orientation, and hence are less able to interact with cations. The distribution of xylose conformers reported in Table 3.3 was determined at room temperature. Previous studies have shown that the ratio of α-xylopyranose/β-xylopyranose in aqueous solutions increase with increasing temperature and, therefore, it is expected that this ratio will be higher at reaction temperature (140 ºC) than at room temperature [17].

3.3.5 Evidence of Metal Halide Cation and Anion Interactions with Xylose

^{13}C- and ^{1}H-NMR were used to observe the interactions of metal cations and halide anions with molecules of xylose dissolved in water. Evidence for these interactions was given by shifts in the positions of the ^{13}C-NMR peaks or shifts in the ^{1}H-NMR peaks for protons bonded directly to carbon atoms (proton chemical shifts for COH groups were not observed due to deuterium exchange with the D_2O solvent used to preserve the chemical nature of solution interactions). The observed changes in chemical shift ($\Delta\delta C_n$ and $\Delta\delta C_nH$) are presented in Tables 3.4 and 3.5. An example of the ^{13}C shifts observed for sodium halides is shown in Figures 3.9A and 3.9B for α- and β-xylopyranose, respectively (see Figures 3.10A/B for lithium halides and Figures 3.11A/B for potassium halides). With a few exceptions $\Delta\delta C_n$ is positive for all carbons of both xylose conformers regardless of the metal halide composition, indicating the occurrence of electron deshielding at the carbon atoms. Each carbon is covalently bound to an oxygen atom that can interact with the metal cations in solution. These interactions withdraw electron density from the oxygen and in turn from the attached carbons, resulting in electron deshielding of the carbon nucleus. The metal cations interacting with the oxygen atoms of C-O-H groups are associated with the negative end of the dipole moment presented by these groups, whereas charge-compensating halide anions can associate with the positive end of the C-O-H dipole. The location of these anions is presumed to be close to the nearest hydroxyl proton given the steric barrier of such a bulky ions nestling between the attached carbon and proton of the hydroxyl group. The cation-oxygen interaction withdraws electron density from carbon atoms of xylose, whereas the anion-proton interaction provides electron density. Given the charge density disparity between the cations and anions, the influence of the cations on shielding of carbon atoms is expected to dominate over the influence of anions, resulting in positive changes in carbon chemical shifts due to electron deshielding. However, as the anion associated with a given cation becomes larger, the anion becomes increasingly less effective in shielding the C-O-H group and the net deshielding effect of the cation-anion interaction with the sugar increases. This is precisely what is generally observed in Table 3.4 — as the charge density of the anion decreases, the magnitude of $\Delta\delta C_n$ increases, such that the change in chemical shift increases with respect to anion in the following manner: $Cl^- < Br^- < I^-$.

The interactions of metal cations with the ring oxygen atom have a qualitatively different effect from that observed for interactions of metal cation with C-O-H groups. While the direct interaction between cation and ring oxygen is observed, as evidenced by positive values of $\Delta\delta C_5$ in all cases, the C5-O5-C1 dipole is aligned such that the positive end extends within the ring itself, prohibiting interaction with large halide anions. Consequently, the anion interacts with the cation on the periphery of the xylose molecule and consequently electron shielding of the C5 carbon atoms does not occur, and only the effects of the cation interaction with the ring oxygen are observed. This explains why the

$\Delta\delta C_n$ is greater at the C5 position than at any other position. Furthermore, $\Delta\delta C_5$ increases with anion polarizability ($Cl^- < Br^- < I^-$) due to the greater charge separation between a given cation and a more polarizable anion that affords a stronger dipole-ion interaction between the cation and ring oxygen. This effect, coupled with resonance effects from the nearby C4 carbon, can explain the trend in increasing values of $\Delta\delta C_5$ with respect to anion size.

It is also notable that for a given metal halide, $\Delta\delta C_n$ is always greater for α-xylopyranose than for β-xylopyranose at the C1 position, whereas the opposite is true at the C2 position. This trend is indicative of a stronger salt-sugar interaction at the C1OH group when xylose is present in the alpha form, while the interaction at the C2OH is strongest when xylose is present in the beta form. These differences have implications for the reaction mechanism, as discussed below.

The trends in $\Delta\delta C_nH$ shown in Table 3.5 follows the patterns observed for $\Delta\delta C_n$. For all protons, $\Delta\delta C_nH$ is positive and increases with respect to anion for a given cation in the following order: $Cl^- < Br^- < I^-$.

The interactions of chloride anions with xylose were probed by acquiring ^{35}Cl-NMR spectra as a function of xylose concentration. Figure 3.12 shows that as the concentration of xylose increases, the width and the height of the chloride ion peak increase. These data can be used to determine the average number of Cl- anions interacting with glucose using the following correlation [20]:

$$\Delta\delta_{obs} = \Delta\delta_{free} + \left(\Delta\delta_{bound} - \Delta\delta_{free}\right) N \frac{[xylose]_{\%}}{[NaCl]_{\%}} \frac{MW_{NaCl}}{MW_{xylose}} \qquad (6)$$

where: $\Delta\delta_{obs}$ = observed peak width of chloride ion
$\Delta\delta_{free}$ = peak width of chloride unbound to xylose
$\Delta\delta_{bound}$ = peak width of chloride bound to xylose
N = ratio of xylose molecules to chloride ions
$[NaCl]_{\%}$ = weight % of NaCl in solution,
$[xylose]_{\%}$ = weight % of xylose in solution
MW_{NaCl} = molecular weight of NaCl, 58.44 g/mol
MW_{xylose} = molecular weight of xylose, 150.13 g/mol

By fitting Equation 6 to a plot of the measured values of the chloride ion peak width versus the weight percent xylose it was possible to determine a value of N. A value of N ≈ 3.8 is determined, suggesting that every molecule of xylose interacts with ~4 chloride anions or that each hydroxyl group interacts with one chloride anion.

Collectively, these and previous observations lead to the xylose-metal halide-water interaction model depicted by Figure 3.13.

3.3.6 ^{18}O Isotopic Labeling Experiments

The NMR results presented in Table 3.2 clearly show that the presence of metal halides causes a small increase in the ratio of α-xylopyranose relative to β-xylopyranose, and as noted earlier this ratio is expected to increase further when the temperature is raised from room temperature to the reaction temperature (140 ºC). However, these changes do not appear to be sufficiently large to account for the significant effects of metal halides on the rates of xylose consumption and furfural formation presented in

Figures 3.4-3.6. Therefore, it is more likely that these effects are attributable to specific interactions of metal cations and halide anions with molecules of xylose. Of particular note in this connection is the observation that cation and anion interactions are stronger with α-xylopyranose than with β-xylopyranose at the C1 position, whereas the opposite is true at the C2 position.

To further probe how metal halides affect the dehydration of α-xylopyranose and β-xylopyranose, experiments were carried out with xylose labeled with ^{18}O-labeled at the ring oxygen position (D-[5-^{18}O]xylose]) both in the presence and absence of NaCl. At the end of reaction, furfural was extracted from the aqueous solution using toluene and then analyzed by GCMS to determine the location of ^{18}O in the furfural. The relative population of peaks at m/z = 69 versus 67 were used to determine whether ^{18}O in the xylose ring remained within the furan ring or transferred to the carbonyl group, respectively. In the absence of metal halides, 69% of the furfural produced contained ^{18}O within the furan ring and the remaining 31% contained ^{18}O in the carbonyl group. When the reaction was carried out in 5M NaCl, 52% of the furfural produced contained ^{18}O in the furan ring and 48% contained ^{18}O in the carbonyl group. The results of these experiments suggest that the interactions of Na^+ and Cl^- with xylose influence the mechanism and kinetics of xylose dehydration. The interpretation of these results is discussed in the next section.

3.3.7 Mechanism of Xylose Dehydration

Aqueous-phase dehydration of xylose to furfural catalyzed by a Brønsted acid can occur in one of two ways, initiated either by ring-opening to form the acyclic isomer of xylose followed by dehydration or by direct dehydration of either α- or β-xylopyranose. Theoretical studies of xylose dehydration suggest that pyranose ring opening followed by dehydration of the resulting aldose is less favorable energetically than direct dehydration of the pyranose ring followed by intramolecular rearrangement [21]. This study also shows that dehydration initiated at the C2OH position of xylopyranose is favored over that at the C1OH position, and that dehydration initiated at either C3OH or C4OH leads to fragmentation products rather than furfural. Hence, under the conditions investigated in this work, Brønsted acid-catalyzed dehydration of xylose in water with or without metal halides is presumed to proceed *via* either C1OH or C2OH dehydration, since fragmentation products were not observed.

When xylose dehydration is carried out in the presence of metal halides, the metal cations can interact with the hydroxyl groups of the ring oxygen of xylose thereby increasing the C-OH and C-O-C bond lengths and lowering the energy necessary to break such C-O bonds. The use of a metal cation with strong kosmotropic character more effectively interrupts the xylose solvation shell, sterically hindering rehydration of the carbocation formed after dehydration. Moreover, halide anions can interact with the electronegative regions of xylose and stabilize any carbocations formed. The proposed influence of halide anions on Brønsted acid dehydration of xylose initiated at the C2OH and C1OH positions is presented in Schemes 3.5 and 3.6, respectively.

Scheme 3.5 shows the dehydration pathway proposed for xylose dehydration initiated by reversible protonation at the C2OH position of either α- or β-xylopyranose. This step is followed by the loss of water and the formation of a carbocation at the C2 position, which has been established in previous studies to be the rate-limiting step [13].

The carbocation is a reactive intermediate that can undergo rearrangement to form 2,5-anhydroxylose, which then further dehydrates to form furfural. The presence of a halide anion near the C2 carbon of the carbocation intermediate can aid in its stabilization and reduce the extent to which rehydration occurs at that position. As the halide nucelophilicity increases, so does ability of the halide to stabilize the carbocations in protic solvents, i.e., $I^- > Br^- > Cl^-$ [13]. This trend parallels that seen for the effect of halide composition on the rate of xylose dehydration (see Figures 3.4-3.6).

Scheme 3.6 illustrates the proposed pathway for the xylose dehydration initiated by reversible protonation of the C1OH position of α-xylopyranose. As mentioned previously, dehydration of the β-xylopyranose conformer at the C2 position is more energetically favorable than at the C1 position, however, the α-xylopyranose conformer presents an anomeric hydroxyl group in the axial position. Hydroxyl groups in such positions are more easily protonated and removed as water than their equatorial counterparts. Therefore, both C1OH and C2OH initiated dehydration pathways are possible for α-xylopyranose. However, after the initial C1OH dehydration and the formation of the oxocarbinium cation, the next step requires the oxygen of the C2OH group to attack the C5 carbon. This step is expected to have a large energetic barrier because the equatorial C2OH must rotate around the plane of the xylose molecule and attack a carbon without formal charge. The addition of metal halides reduces this energetic barrier by not only elongating the C2-OH bond length allowing for increased mobility (*via* the metal cation-OH interaction), but also by increasing the partial positive charge on the carbon due to electron deshielding provided by the metal halide. Therefore, the salt-sugar interaction facilitates the production of furfural *via* the C1OH pathway by not only increasing the starting concentration of α-xylopyranose, but also by decreasing the barrier for ring reformation following the initial dehydration.

The results obtained from ^{18}O labeling experiments are fully consistent with the observed effects of metal halides on the pathways for xylose dehydration. Dehydration *via* protonation of the C1OH group, which results in the ^{18}O-labeled ring oxygen appearing in the furfural carbonyl group, occurs more rapidly than dehydration initiated *via* protonation of the C2OH group, which results in the ^{18}O-labeled ring oxygen remaining in the ring oxygen of furfural, when metal halides are present.

After primary dehydration at either hydroxyl group followed by ring rearrangement to form the 5-membered oxolane ring (2,5-anhydroxylose intermediate), furfural is formed *via* elimination of the hydroxyl groups at the C3 and C4 positions, as shown in Scheme 3.7. The ring structure is maintained throughout these final dehydrations because oxolane is very stable [22] and particularly resistant to attack by hydrolytic agents [23].

The carbocationic intermediates produced during the dehydration of xylose can participate in condensation processes leading to humins. In the presence of metal halides the selectivity to furfural decreased with increasing anion size, indicating that the ratio of the rates of condensation to dehydration increases with respect to anion in the order $Cl^- < Br^- < I^-$. As larger anions stabilize carbocation intermediates, they form longer, lower energy bonds with the carbon atoms that results in a less polar charge distribution between anion and carbocation. This effect lowers the partial positive charge on the carbon making it a weaker Brønsted acid that is less capable of participating in elimination reactions [13]. Together with the fact that larger anions are better leaving

groups improves the probability that substitution occurs at the carbocation. Hence, while large anions promote the rates of xylose consumption and furfural production, such anions also enhance the rate of promote more nucleophilic substitution and, consequently, lower selectivity to furfural.

Condensation reactions leading to humins can occur *via* a number of pathways involving either furfural or xylose and an intermediate involved in the dehydration offxylose. In Section 1 we showed that condensation involving furfural is preferred kinetically. Scheme 3.3 illustrates a possible mechanism for this process. In this example, xylose is substituted at the C2OH position by the nucleophilic carbonyl of furfural, followed by a nucleophilic attack on the carbonyl carbon by the C1OH oxygen, creating a furfural-xylose condensation product with a dioxolane bridge. The condensation of two furfural molecules (Scheme 3.2) can also be aided by the presence of metal halides. Furan resonance structures forming oxocarbenium ions can be stabilized by halide anions, allowing for the nucleophilic attack of a furfural C5 carbon on the carbonyl carbon of another furfural to form a di-furanyl resinification product.

3.3.8 Improving Overall Furfural Yields

To this point, we have only discussed the effects of salt addition on the rate of xylose dehydration in aqueous solution and on the competing formation of humins. However, as noted in the Introduction, the yield of furfural can be enhanced by *in situ* extraction of furfural into a water-immiscible phase. For this reason, we end our discussion of the effects of salt addition by briefly examining the influence of NaCl on the dehydration of xylose carried out in a two-phase water:toluene system. We note that the partition coefficient of furfural between a toluene phase and an aqueous phase (1:1 by volume) increases from 9 to 20 when 5M NaCl is added to the aqueous phase (measured at 50 ºC). Dehydrating xylose in such a biphasic system also improves the selectivity to furfural from 54% to 72% when 5M NaCl (*aq*) was added to the aqueous phase (see Figure 3.14). Thus, the addition of metal halides to a biphasic reaction system has the thermodynamic benefit of improving the efficacy of the extracting solvent relative to water.

It should be noted that adjustments to reaction conditions can result in similar enhancements in selectivity. For example, lowering the metal halide concentration from 5M reduces the difference between rate of xylose conversion and that of furfural production, resulting in increased selectivity (see Figure 3.1). The furfural selectivity can also be increased by increasing the temperature, which decreases the extent of side reactions and thereby increases the furfural selectivity, and at 200 ºC approaches 100% [2].

3.4 Conclusions

This study has shown that the addition of metal halides increases the rate of xylose dehydration in an aqueous phase catalyzed by a Brønsted acid. The enhancement in the dehydration rate is a function of both cation and anion composition and increases in the order no salt < K^+ < Na^+ < Li^+ and no salt < Cl^- < Br^- < I^-. The selectivity to furfural is also affected by salt composition, increasing in the order K^+ < Na^+ < Li^+ and I^- < Br^- < Cl^-. At 140 ºC, the maximum furfural selectivity was 44% when the reaction was

carried out in a 5M LiCl solution. The effects of salt on the rates of xylose dehydration and humin formation are complex and involve interactions of the salt cations and anions with both water and xylose. Metal cations disrupt the solvation of xylose by water and interact with the hydroxyl groups and ring oxygen atoms of xylose, leading to a weakening of C-O bonds. Halide anions interact to a lesser degree with water than do cations, but do interact with the positive end of hydroxyl group on xylose, such that on average 4 Cl^- ions interact with each xylose molecule. These interactions stabilize cationic intermediates formed during the dehydration of the sugar, the degree of stabilization increasing with the nucleophilicity of the anion. Significantly, more nucleophilic anions also enhance reactions involving these intermediates to form humins, and consequently furfural selectivity decreases in the order $Cl^- < Br^- < I^-$. The addition of metal halides was also found to increase the dehydration of xylose initiated by protonation of C1OH versus C2OH groups. These findings demonstrate that alkali metal halides dissolved in water can be used to enhance the rate of xylose dehydration and the selectivity towards furfural versus humin formation. By coupling these effects with the extraction of furfural into an organic phase, high yields of furfural can be achieved.

3.5 Supplemental Information

3.5.1 Effect of Metal Iodide Oxidation to I_2 on Solution pH

Figure 3.7 shows the qualitative results of heating various 5M metal iodide salt solutions (*aq*) to 140 ºC over the course of 120 min in the presence of 50 mM HCl and absence of xylose. The darkening of each solution with time is a qualitative indication of the formation of increasing amounts of I_2 species, which is produced concurrently with metal carbonate species capable of buffering each solution. Salts with iodide anions are known to oxidize to molecular iodine and their metal carbonate analogs (Equation 7) [11], which is evidenced by solutions containing them changing color over time. In the presence of a strong acid, these metal carbonates react to create carbonic acid (Equation 8), which is highly unstable and quickly converts into water and carbon dioxide (Equation 9):

$$4MI + 2\ CO_2 + O_2 \text{ --> } 2M_2CO_3 + 2I_2 \quad (7)$$

$$2M_2CO_3 + 4HCl \text{ --> } 2H_2CO_3 + 4MCl \quad (8)$$

$$2H_2CO_3 \text{ --> } 4H_2O + 2CO_2 \quad (9)$$

The loss of iodide has less of an impact on the chemistry than does the loss of HCl (due to the relative starting concentrations), which could result in a significant drop in reaction rate (which has a first order dependence on $[H^+]$). Reaction (8) is the limiting reaction, due to limited solubility of the gases (approximately 35 mM CO_2 and 130 uM O_2 in pure water at room temperature [16]). As a result of such low gas concentrations, acid neutralization is highly unlikely during the course of reaction; however, pH buffering is a real possibility and likely explanation for the lower rate of xylose dehydration/furfural production in the presence of 5M metal iodides relative to 5M metal bromides in the long time studies. This phenomena is not evident in short time studies, as not enough time is

allowed for appreciable I_2 concentrations to form, allowing initial Brønsted acid catalyst concentration to remain constant. Thus, rate trends observed in initial time studies (as presented in Table 3.1) provide a more representative measure of anion effect.

3.5.2 Effects of Divalent Metal Chlorides on Xylose Dehydration

The effects of divalent metal halides on the Brønsted acid-catalyzed dehydration of xylose in an aqueous solution were investigated using magnesium and calcium chlorides. These experiments were carried out at 140 ºC in 5M metal chloride solutions containing 50 mM HCl. The results are presented in Figure 3.15.

Figure 3.15A shows that xylose consumption occurs much more rapidly in brine than in water, with a dependence on metal cation in the order no salt < Ca^{2+} < Mg^{2+}. The initial rate of furfural formation increases in the same order, as can be seen from the data presented in Figure 3.15B. Comparisons with Figures 3.4A/B reveal that both divalent metal chlorides have greater positive impacts on the rate of xylose consumption and initial rate of furfural formation than do monovalent metal chlorides. Within 2 h of reaction, both magnesium and calcium chlorides promoted the complete conversion of xylose. Maximum furfural yields exceeded 35% for both cations, and were reached after 50 min for magnesium and 75 min for calcium. Selectivites to furfural at these maximums were >40% for both metals. The superior rate performance achieved using divalent versus monovalent cations is attributed to a greater interaction between the higher valency cations and water, with 5M solutions of the divalent species reducing water activities to a greater extent than the monovalent species. Water activities as low as 0.339 and 0.401 have been measured for 5M solutions (*aq*) of magnesium and calcium chlorides, respectively, at 25 ºC [14].

3.5.3 Investigation of Metal Cation Interactions with Water Using Raman Spectroscopy

Figure 3.16 shows the Raman spectra of various 5M metal chloride solutions (*aq*) in the 2800-3700 cm^{-1} region, characteristic of O-H bond stretching. As the metal cation is varied, the O-H stretch band of water broadens and intensifies in the order K^+ < Na^+ < Li^+ < Ca^{2+} < Mg^{2+}, which is indicative of increased hydrogen bonding. Therefore, as the charge density of the metal cation increases, its interaction with water also increases. This corroborates the conclusions drawn in Section 3.3.3.

Scheme 3.1 A representative reaction pathway for xylose dehydration and degradation catalyzed by a Brønsted acid. Major products shown include furfural from the direct dehydration of xylose, condensation products from the reaction between furfural and xylose intermediate(s), condensation products from the reaction between xylose and xylose intermediate(s), and resinification products from furfural.

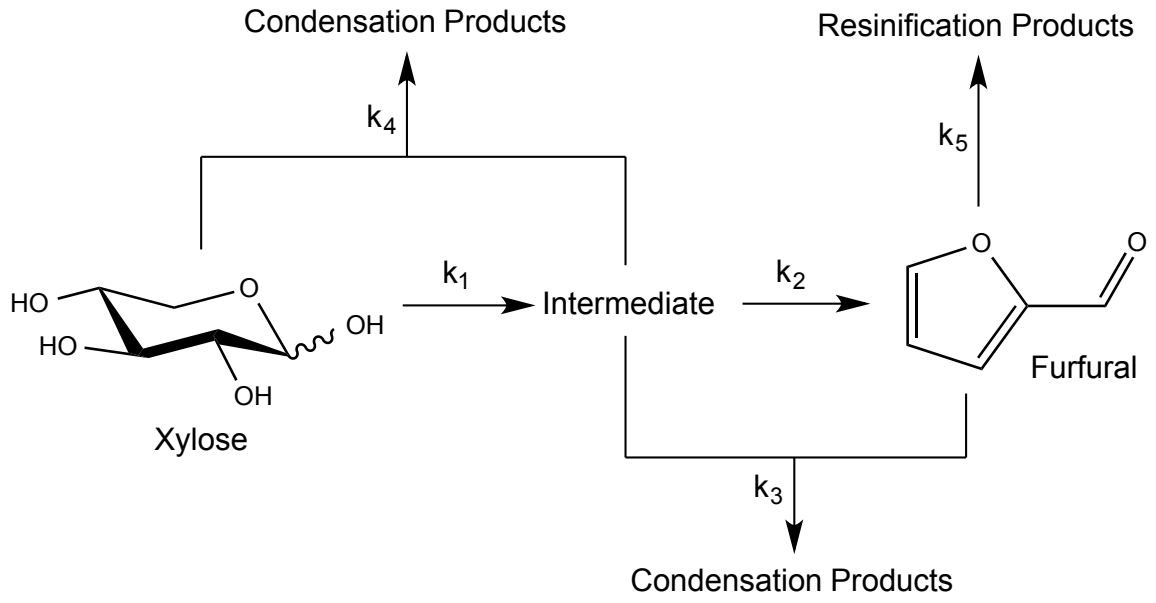

Scheme 3.2 A representative reaction pathway for furfural resinification *via* the self-coupling of two furfural molecules.

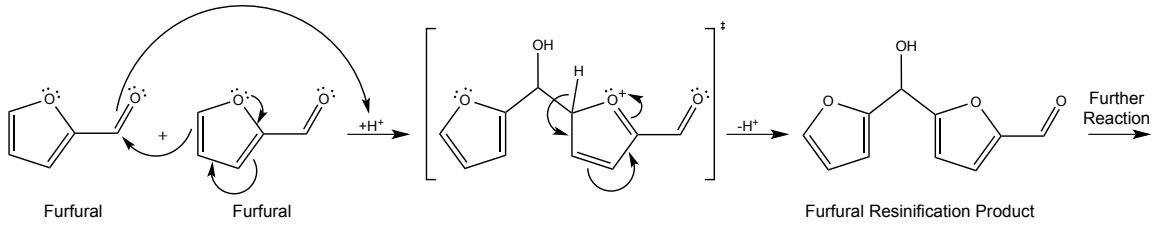

Scheme 3.3 A representative reaction pathway for furfural condensation with a xylose intermediate (mono-dehydrated at the C2 position). Adapted from Ref. [2].

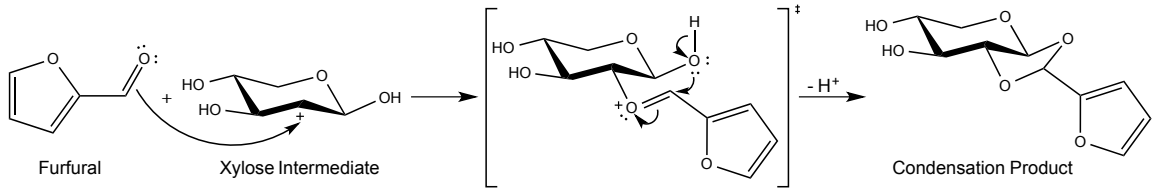

Scheme 3.4 The five isomers of xylose formed after dissolving crystalline xylose in water.

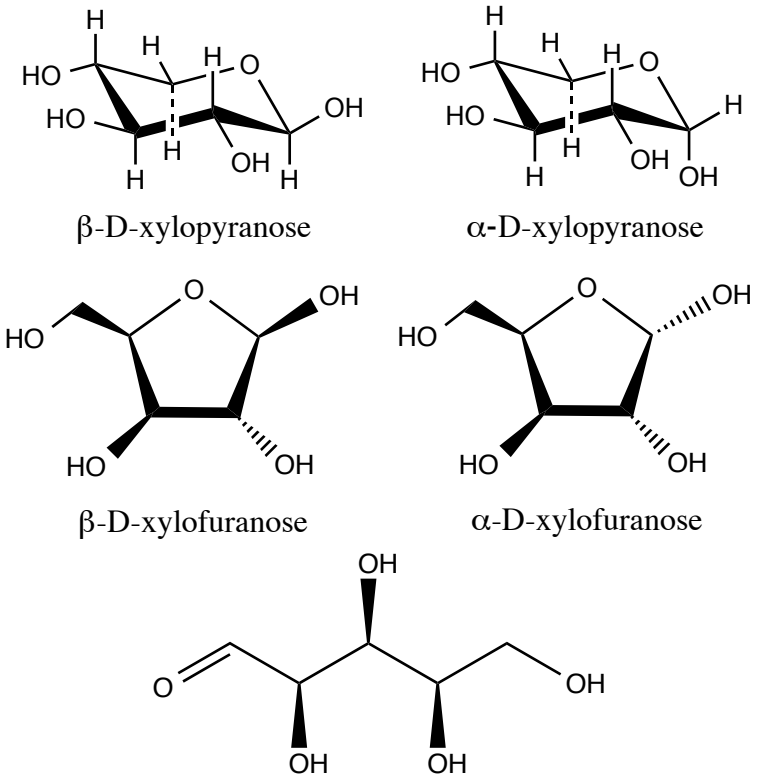

Scheme 3.5 Detailed reaction scheme showing the involvement of halide anions in stabilizing the carbocation formed during the initial dehydration of xylose at the C2 position.

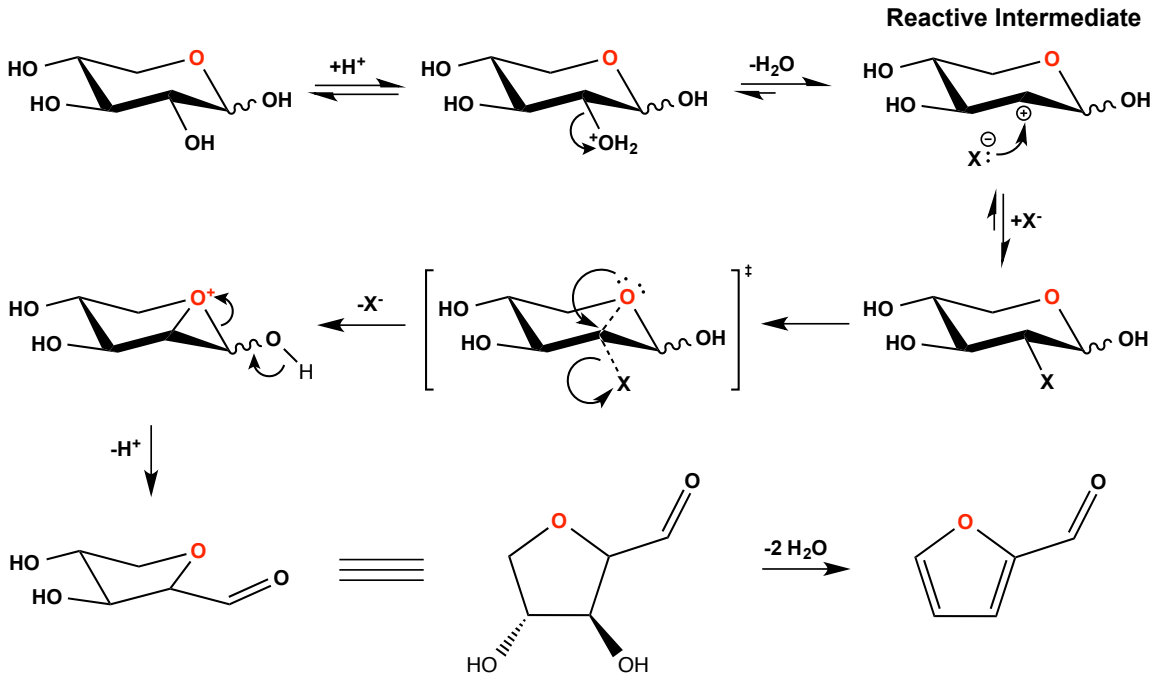

Scheme 3.6 Detailed reaction scheme showing the involvement of halide anions in stabilizing the carbocation formed during the initial dehydration of xylose at the C1 position.

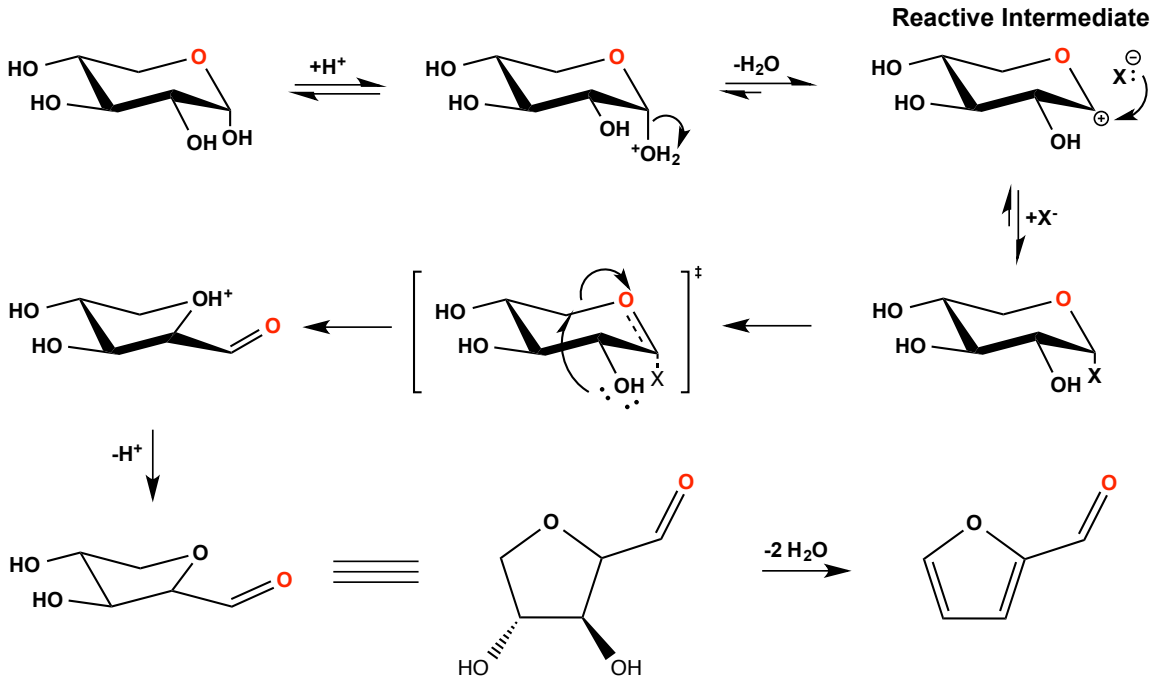

Scheme 3.7 Detailed reaction scheme showing the dehydration of 2,5-anhydroxylose at the C3 position (top) and C4 position (bottom), respectively.

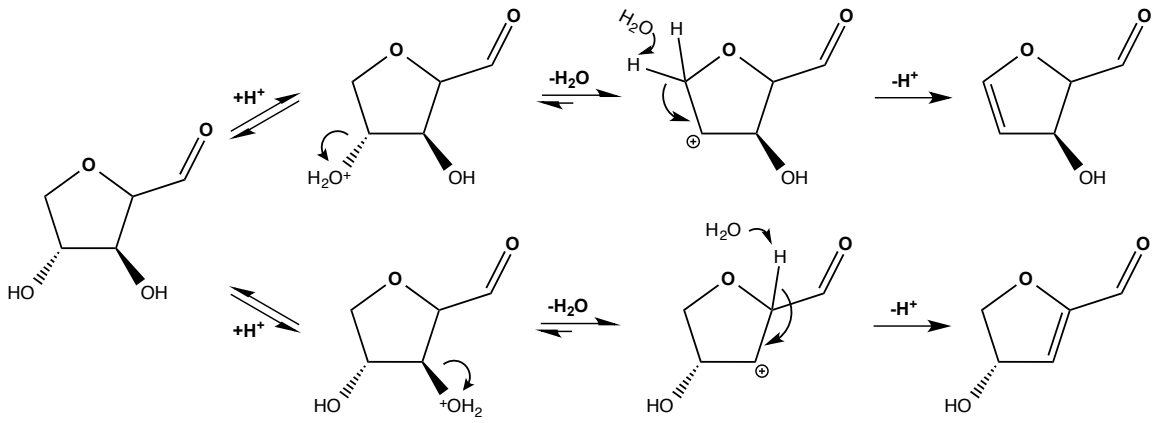

Figure 3.1 Initial rates of xylose (750 mM) dehydration and furfural formation at 140 ºC catalyzed by HCl (50 mM) in various concentrations of NaCl (*aq*) solutions ranging from 0-5M. The natural log of initial rate (r_0) of both xylose conversion and furfural formation are plotted as functions of NaCl concentration to determine the rate order dependence of initial reaction rate on metal halide concentration.

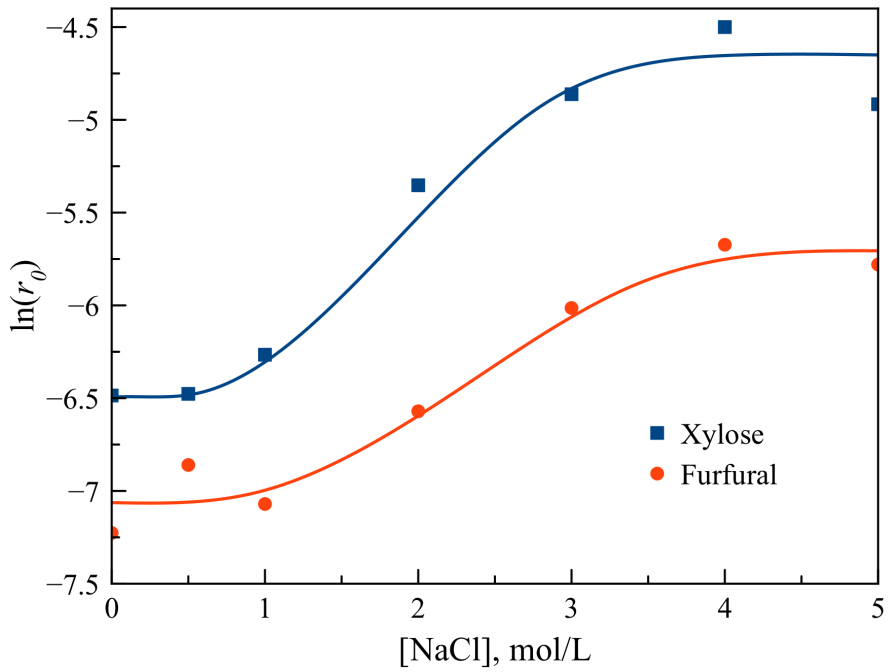

Figure 3.2 Dehydration of xylose (750 mM) at 140 ºC catalyzed by HCl (200 mM) in water. Humins as presented represent the molar sum of soluble and insoluble degradation products.

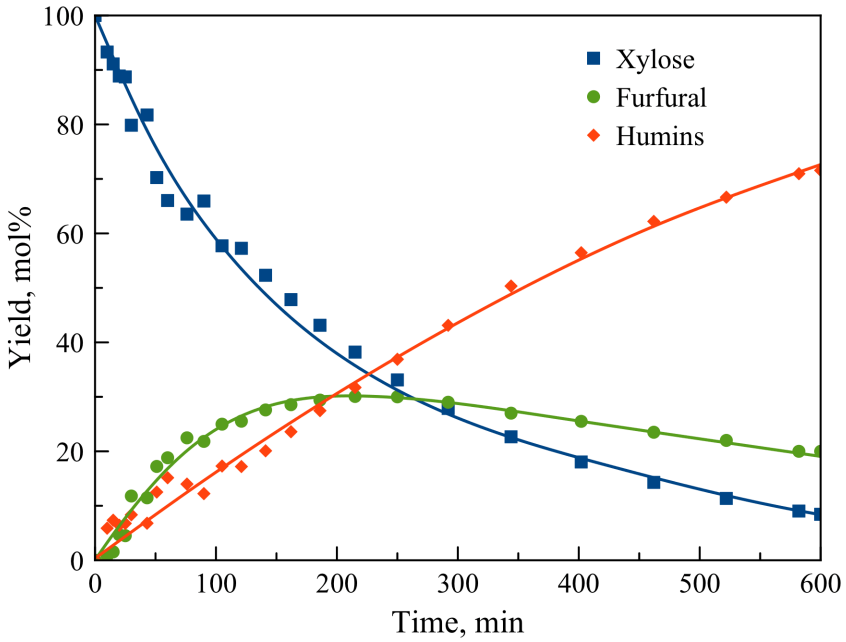

Figure 3.3 Dehydration of xylose (750 mM) at 140 ºC catalyzed by HCl (200 mM) in water with and without an initial concentration of furfural ($[F]_0$ = 400 mM). Furfural yields shown only represent furfural produced directly from xylose, such that in the experiment starting with xylose and furfural, furfural yield = [Total Furfural] - $[F]_0$.

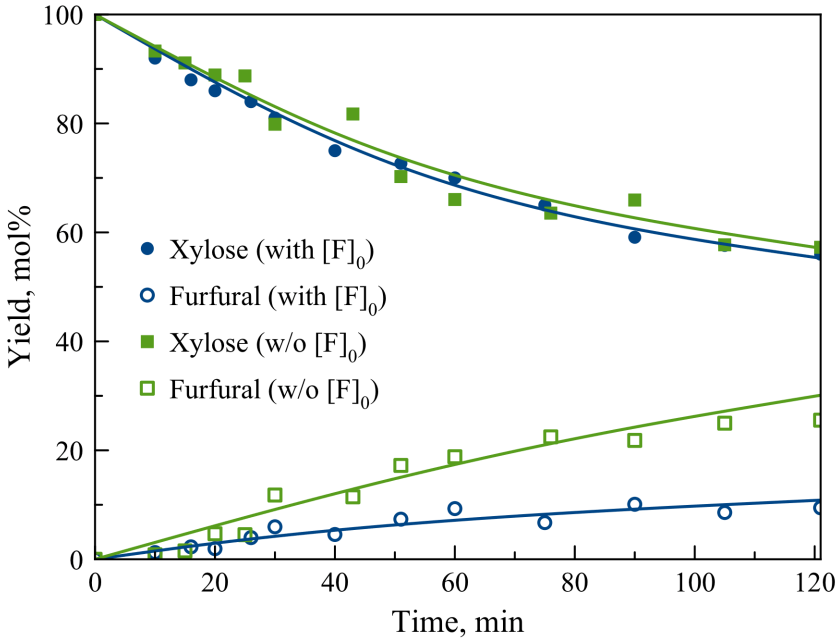

Figure 3.4 A: dehydration of xylose (750 mM) at 140 ºC catalyzed by HCl (50 mM) in various 5M metal chloride (*aq*) solutions. B: resultant furfural formation.

A.

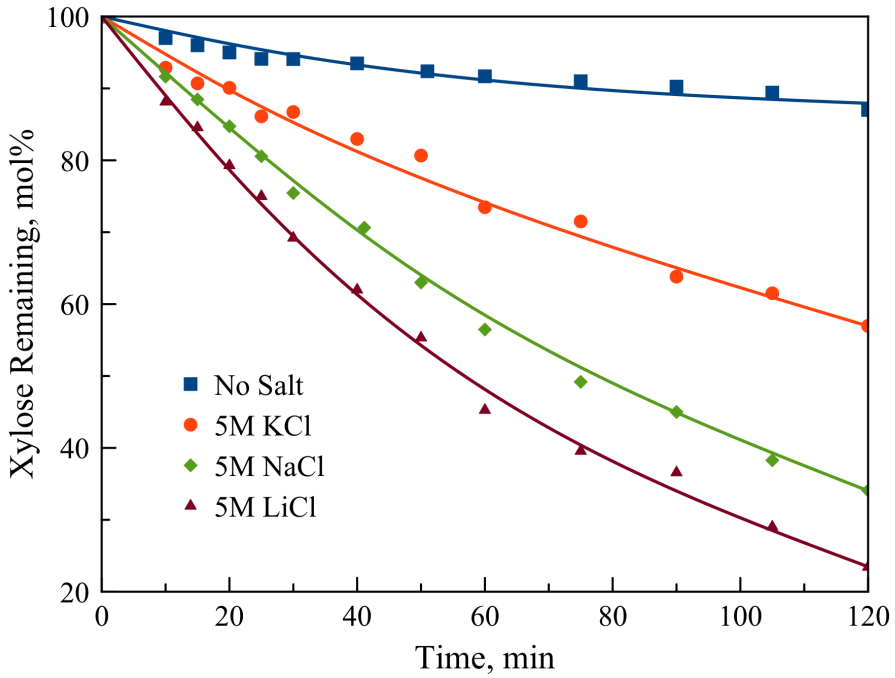

B.

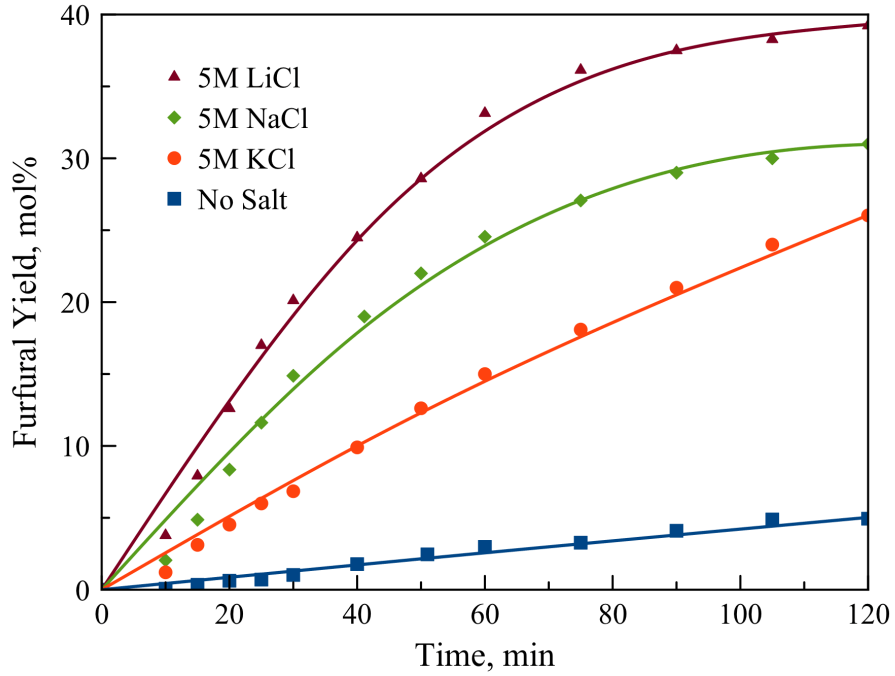

Figure 3.5 A: dehydration of xylose (750 mM) at 140 ºC catalyzed by HCl (50 mM) in various 5M metal bromide (*aq*) solutions. B: resultant furfural formation.

A.

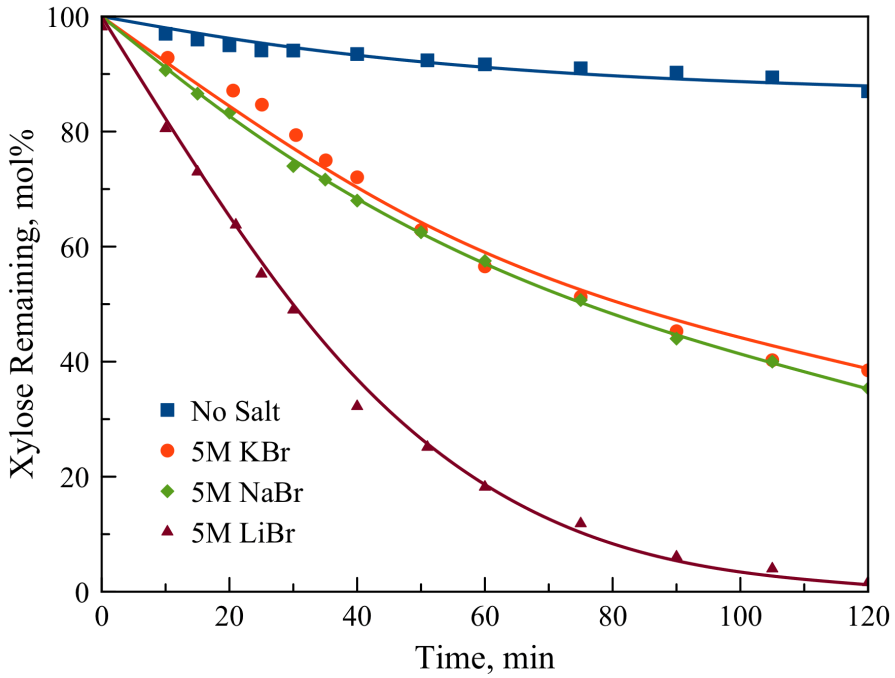

B.

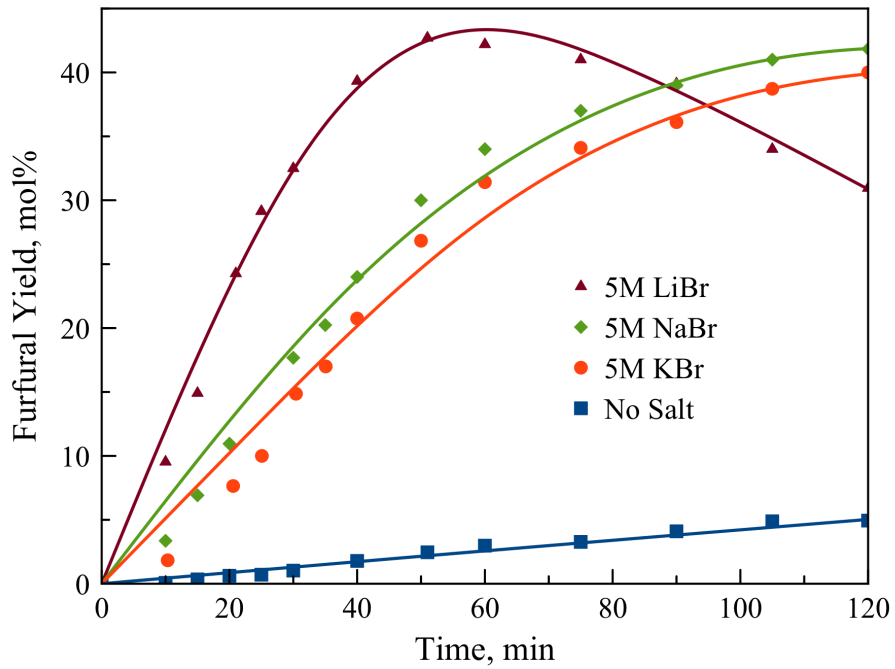

Figure 3.6 A: dehydration of xylose (750 mM) at 140 ºC catalyzed by HCl (50 mM) in various 5M metal iodide (*aq*) solutions. B: resultant furfural formation.

A.

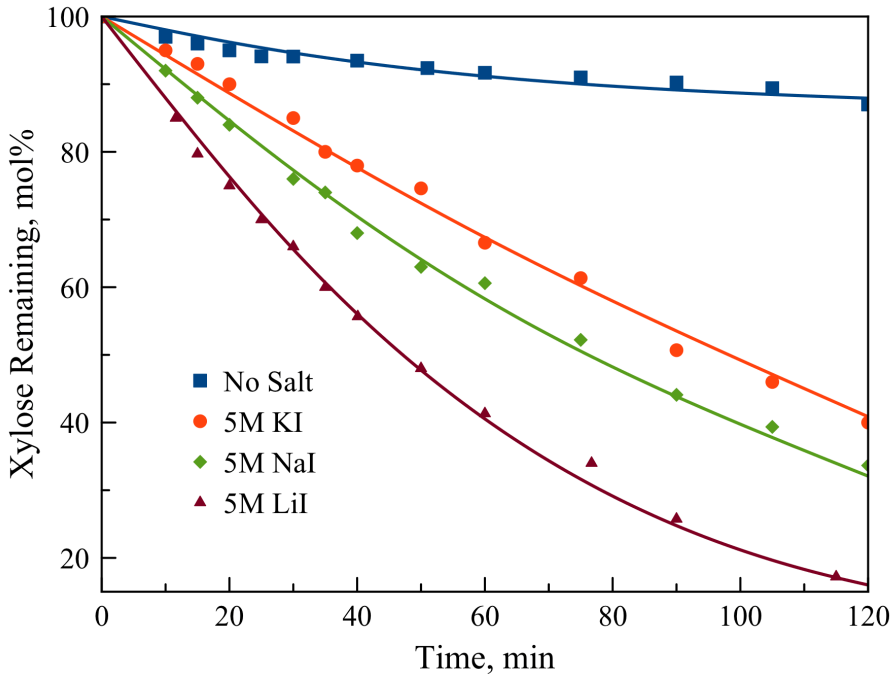

B.

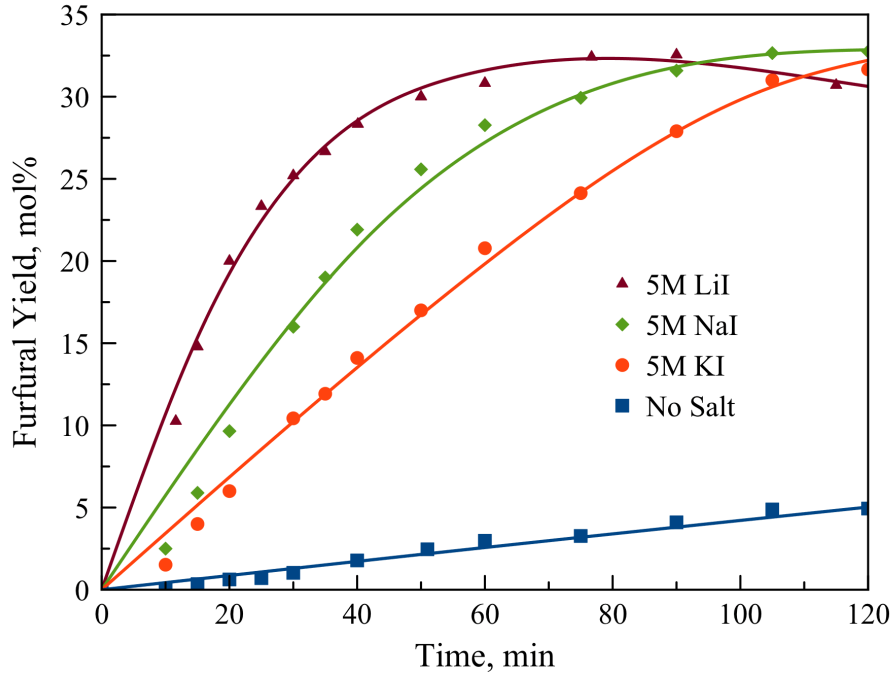

Figure 3.7 Qualitative evidence of the partial oxidation of various 5M metal iodide (*aq*) solutions to I_2 upon heating to 140 ºC over the course of 120 min in the presence of 50 mM HCl and absence of xylose.

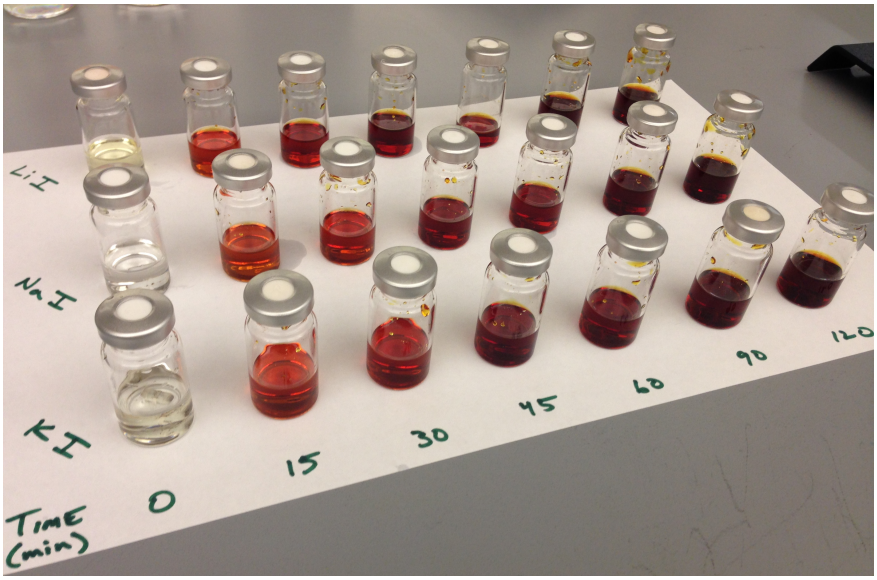

Figure 3.8 ^{13}C-NMR spectrum of 750 mM 1-^{13}C-xylose in D_2O at 298 K, with peak assignments for each carbon of the α- and β-xylopyranose forms.

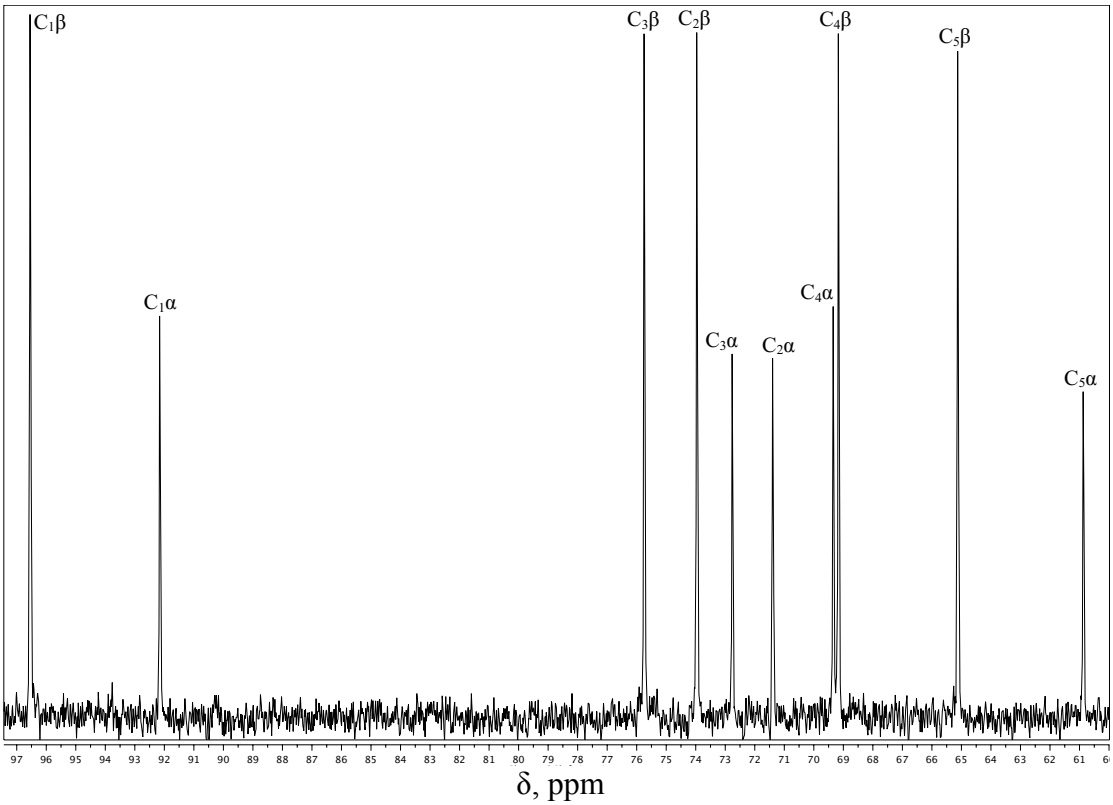

Figure 3.9 Dependence of chemical shift (Δδ) for each carbon of the α-xylopyranose (A) and β-xylopyranose (B) forms on halide anion for the sodium salts as determined by ^{13}C-NMR analysis of 750 mM xylose in D_2O at 298 K in the presence of 5M sodium halides.

A.

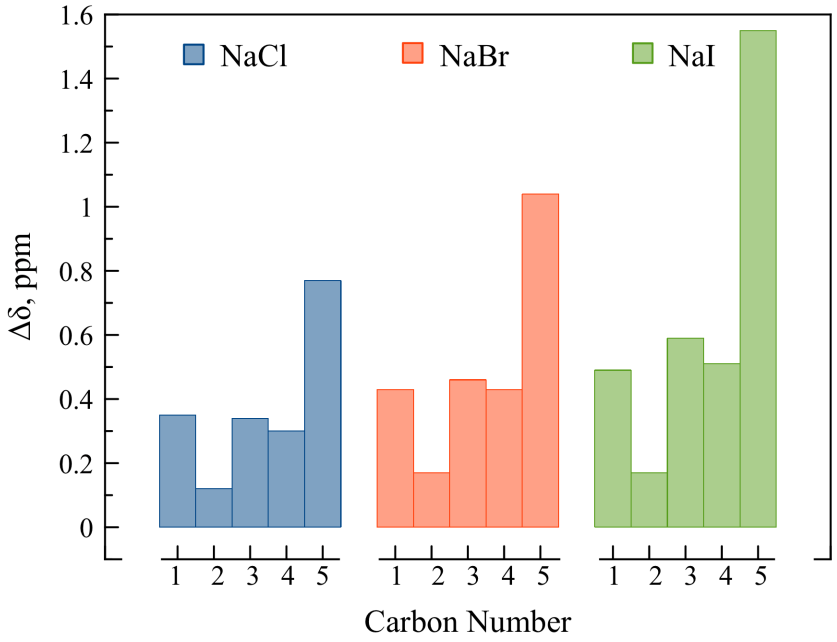

B.

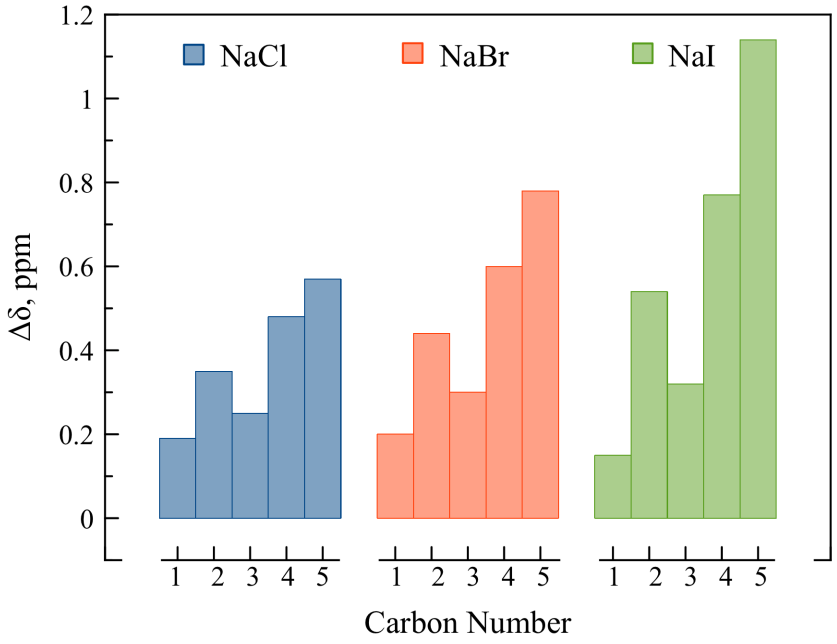

Figure 3.10 Dependence of chemical shift (Δδ) for each carbon of the α-xylopyranose (A) and β-xylopyranose (B) forms on halide anion for the lithium salts as determined by ^{13}C-NMR analysis of 750 mM xylose in D_2O at 298 K in the presence of 5M lithium halides.

A.

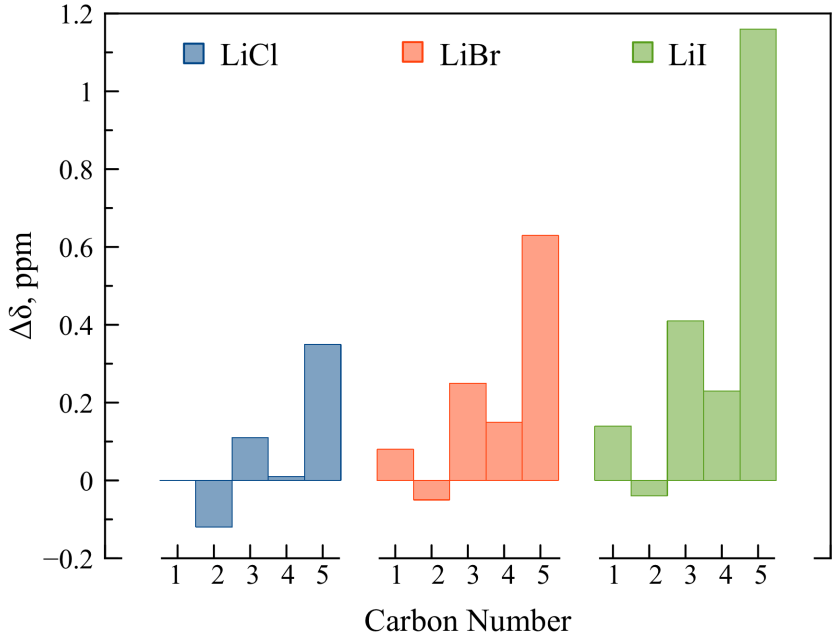

B.

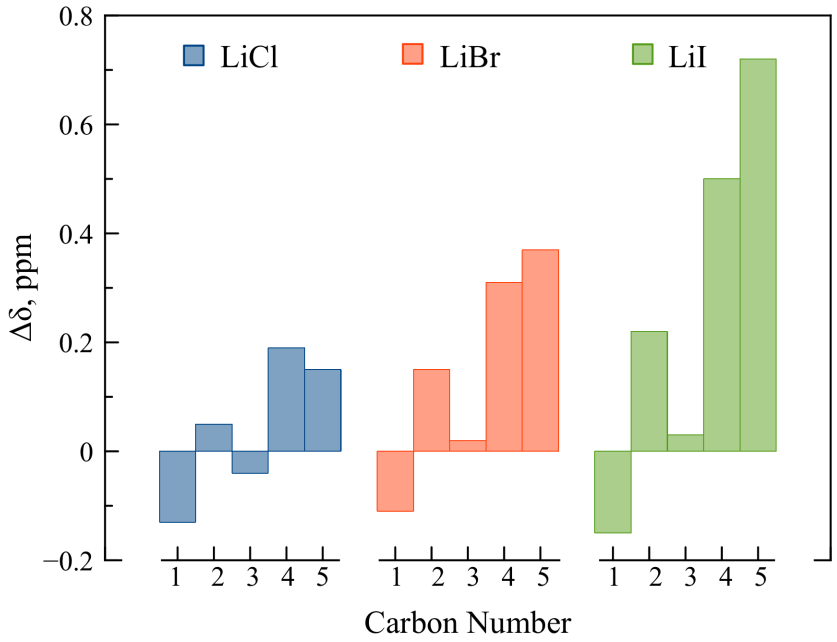

Figure 3.11 Dependence of chemical shift (Δδ) for each carbon of the α-xylopyranose (A) and β-xylopyranose (B) forms on halide anion for the potassium salts as determined by ^{13}C-NMR analysis of 750 mM xylose in D_2O at 298 K in the presence of 5M potassium halides.

A.

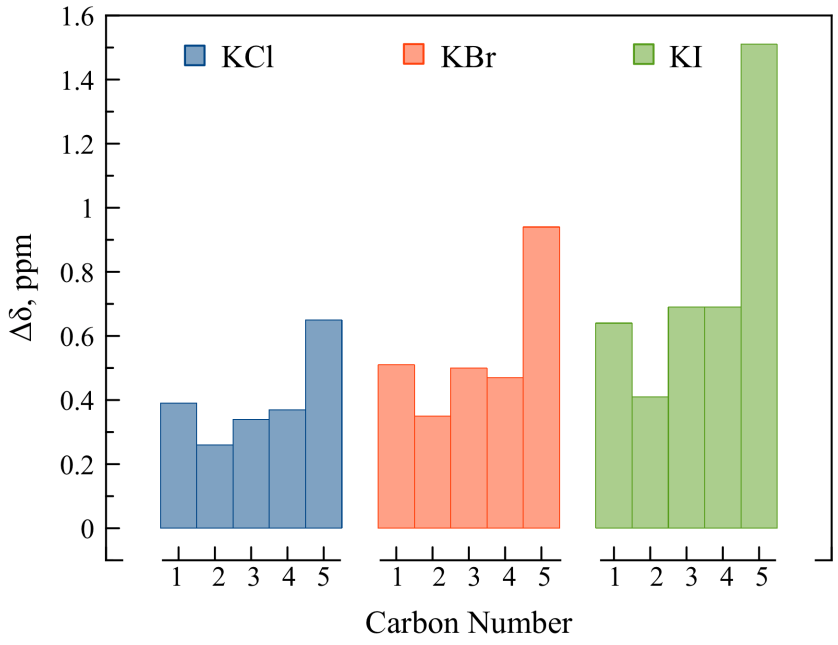

B.

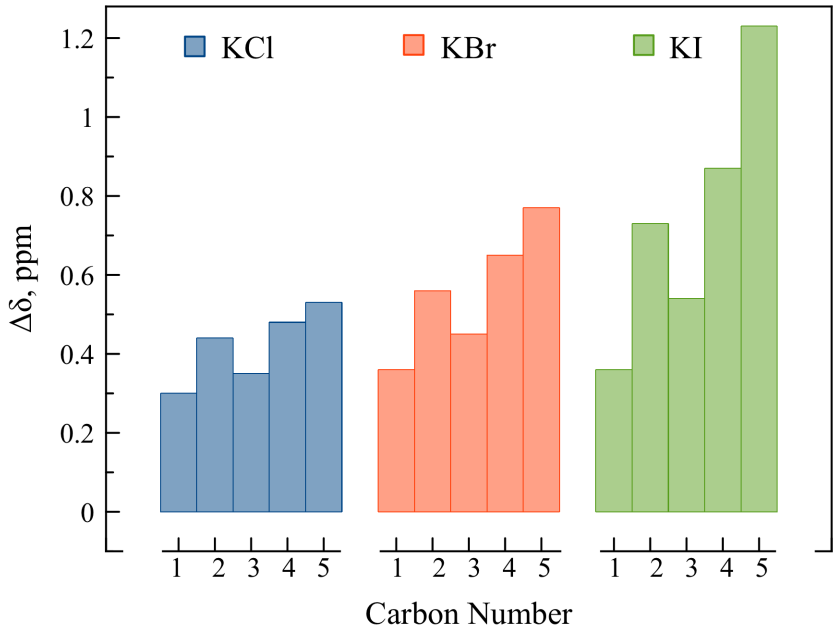

Figure 3.12 1-D ^{35}Cl-NMR of the Cl^- peak of 5M NaCl as a function of varying xylose concentration from 0-10 wt% in D_2O at 298 K.

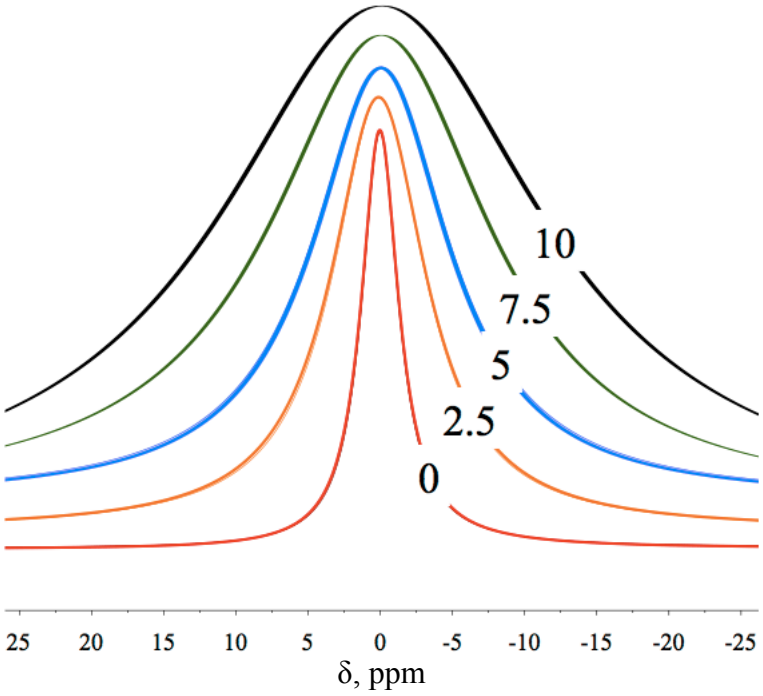

Figure 3.13 A graphical depiction of the relative interactions between xylose, metal cations, halide anions, and water molecules supported by previously discussed observations.

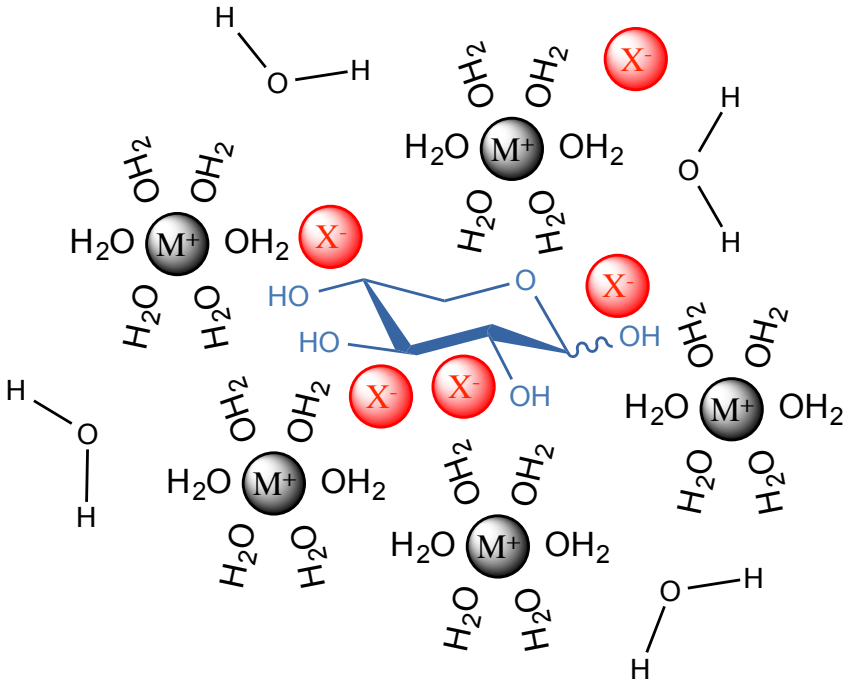

Figure 3.14 Dehydration of xylose (375 mM) at 150 ºC catalyzed by HCl (200 mM) in a 1:4 (by volume) water:toluene biphasic system, with and without 5M sodium chloride.

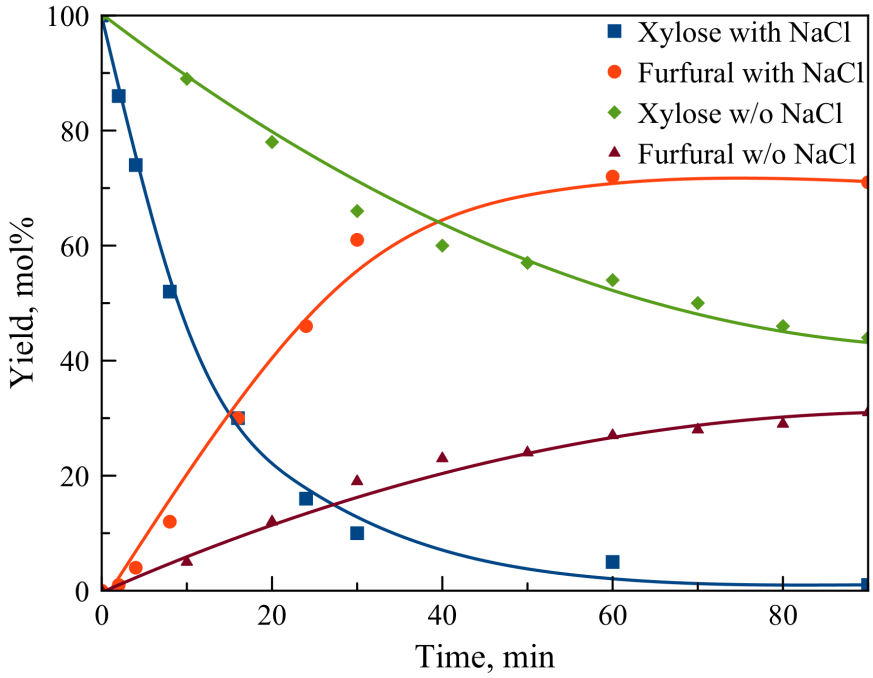

Figure 3.15 A: dehydration of xylose (750 mM) at 140 ºC catalyzed by HCl (50 mM) in 5M (*aq*) solutions of $CaCl_2$ and $MgCl_2$. B: resultant furfural formation.

A.

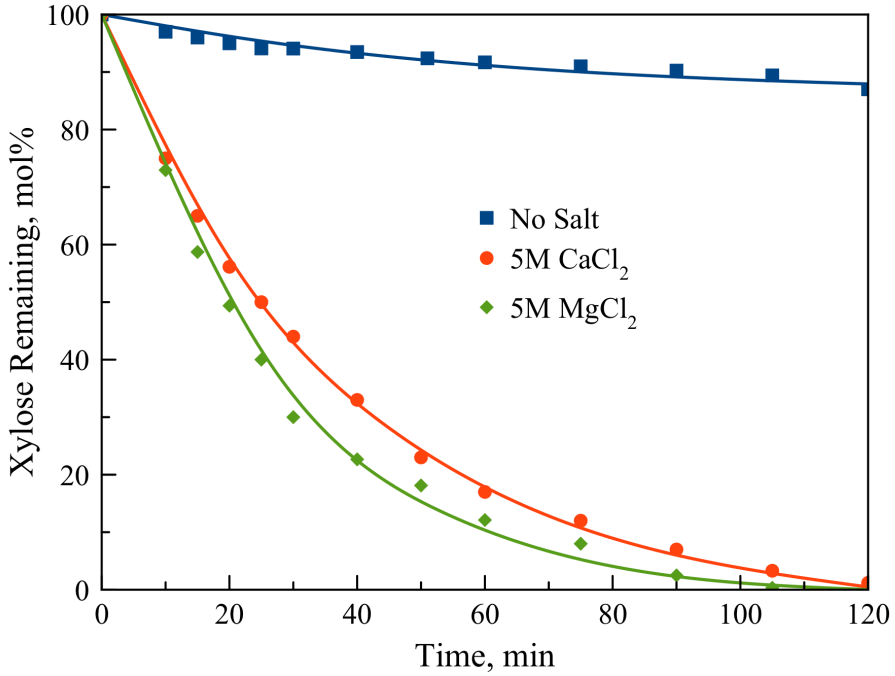

B.

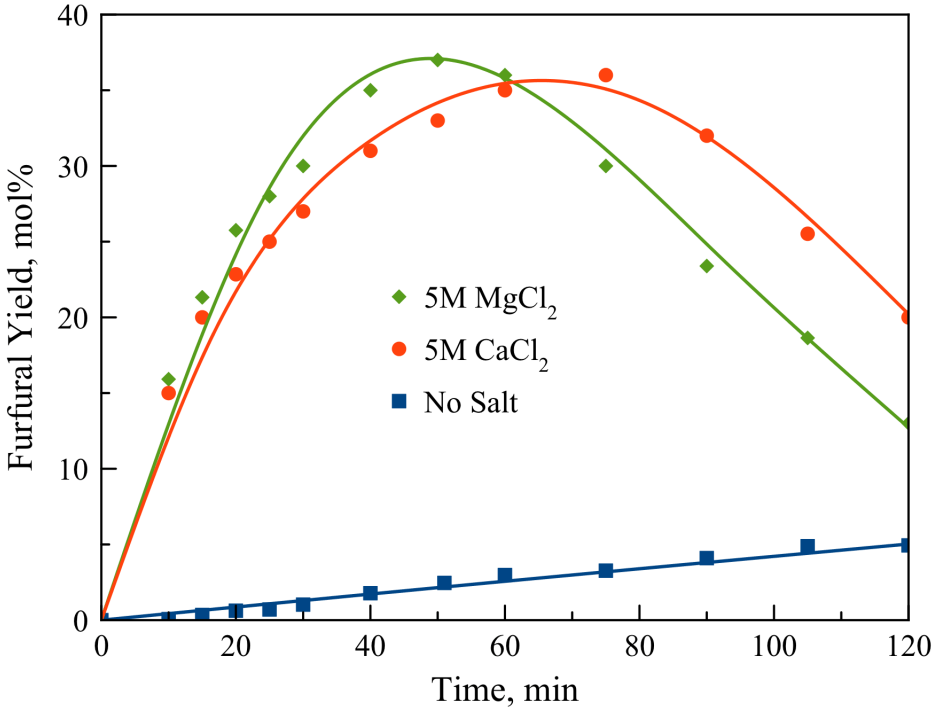

Figure 3.16 Effect of varying cation on the O-H stretching band of water in 5M metal chloride solutions (*aq*), as determined *via* Raman spectroscopy.

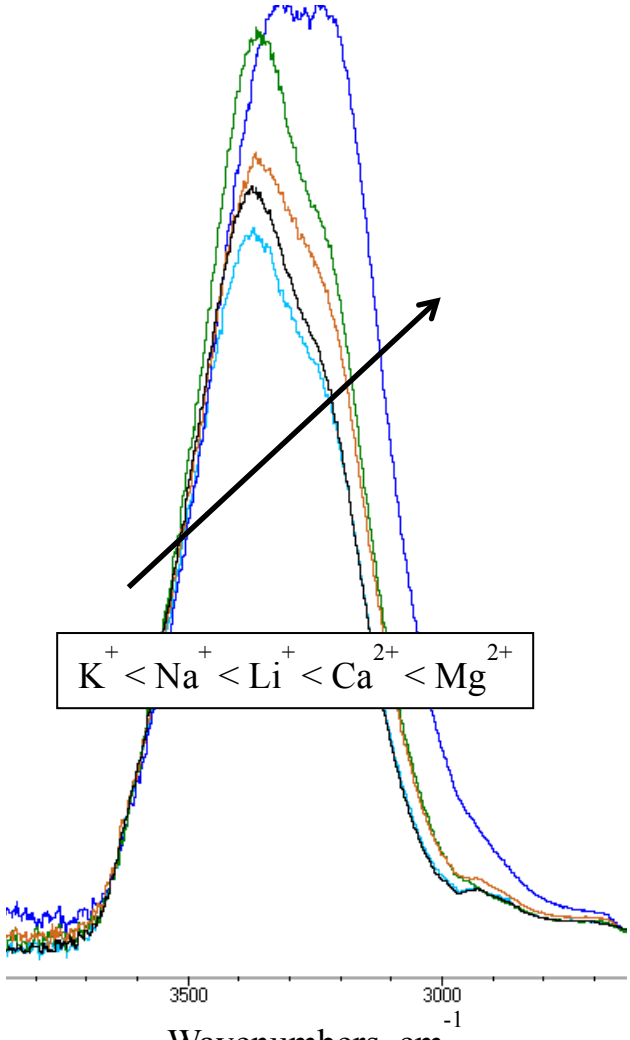

Table 3.1 Initial rates of xylose (750 mM) dehydration and furfural formation at 140 ºC catalyzed by HCl (50 mM) in various 5M metal halide (*aq*) solutions. Includes furfural selectivity data for each salt. Data taken over the course of the first 5 min of each reaction.

Salt	r_0, Xylose, μmol/L-s	r_0, Furfural, μmol/L-s	Furfural Selectivity, mol%
None	19.1	5.8	30.4
LiCl	156.3	69.3	44.3
LiBr	277.7	75.1	27.0
LiI	356.4	86.8	24.4
NaCl	91.3	38.6	42.3
NaBr	118.7	41.1	34.6
NaI	148.7	50.8	34.2
KCl	89.6	35.0	39.1
KBr	107.6	41.2	38.3
KI	126.3	48.8	38.6

Table 3.2 Molalities, salt activity coefficients, osmotic coefficients, and water activities of various 5M metal halide (*aq*) solutions at 298 K. Adapted from Ref. [13].

Salt	Salt Molality, kg/mol	Salt Activity Coefficient	Osmotic Coefficient	Water Activity
None	-	-	1	1
LiCl	5.593	2.404	1.748	0.703
LiBr	6.467	4.785	2.093	0.614
LiI	7.888	7.001	3.132	0.411
NaCl	5.595	0.939	1.238	0.779
NaBr	5.800	1.224	1.368	0.751
NaI	6.198	1.804	1.854	0.661
KCl	5.927	0.781	1.030	0.803
KBr	6.173	0.652	1.048	0.792
KI	6.635	0.734	1.097	0.769

Table 3.3 Xylose isomer distribution (%) of 1-^{13}C-xylose (750 mM) in D_2O (no salt), D_2O with 50 mM HCl (no salt w/50 mM HCl), and various 5M metal halide (*aq* – D_2O) solutions as determined by measuring the ^{13}C-NMR signals for the C1 carbons of individual xylose isomers at 298 K. Dashes in place of numbers indicate that the isomer was not identified in solution. Data was recorded at room temperature after allowing 24 h to achieve an equilibrium distribution.

Salt	Xylopyranose		Xylofuranose		Acyclic Xylose
	β-	α-	β-	α-	
None	63.8	36.2	1.2	0.8	-
None w/50 mM HCl	64.4	35.6	-	-	-
LiCl	63.1	36.9	-	-	-
LiBr	60.3	39.7	-	-	-
LiI	57.2	42.8	-	-	-
NaCl	63.0	37.0	-	-	-
NaBr	62.6	37.4	-	-	-
NaI	62.0	38.0	-	-	-
KCl	67.5	32.5	-	-	-
KBr	66.9	33.1	-	-	-
KI	66.8	33.2	-	-	-

Table 3.4 Chemical shifts, δ (ppm), of ^{13}C-NMR signals for the C1-C5 carbons of the β- and α-xylopyranose forms of xylose (750 mM) in pure D_2O, D_2O with 50 mM HCl, and various 5M metal halide (*aq* – D_2O) solutions at 298 K. Changes in chemical shifts, Δδ (ppm), are shown relative to the chemical shifts associated with the carbon signals of 750 mM xylose in pure D_2O.

Atom	δ, No Salt	Δδ	δ, No Salt w/50 mM HCl	Δδ	δ, LiCl	Δδ	δ, LiBr	Δδ	δ, LiI	Δδ	δ, NaCl	Δδ	δ, NaBr	Δδ	δ, NaI	Δδ	δ, KCl	Δδ	δ, KBr	Δδ	δ, KI	Δδ
C1β	96.58	0.00	96.54	-0.04	96.45	-0.13	96.47	-0.11	96.43	-0.15	96.77	0.19	96.78	0.20	96.73	0.15	96.88	0.30	96.94	0.36	96.94	0.36
C2β	73.99	0.00	73.96	-0.03	74.04	0.05	74.14	0.15	74.21	0.22	74.34	0.35	74.43	0.44	74.53	0.54	74.43	0.44	74.55	0.56	74.72	0.73
C3β	75.78	0.00	75.75	-0.03	75.74	-0.04	75.80	0.02	75.81	0.03	76.03	0.25	76.08	0.30	76.10	0.32	76.13	0.35	76.23	0.45	76.32	0.54
C4β	69.20	0.00	69.16	-0.04	69.39	0.19	69.51	0.31	69.70	0.50	69.68	0.48	69.80	0.60	69.97	0.77	69.68	0.48	69.85	0.65	70.07	0.87
C5β	65.16	0.00	65.12	-0.04	65.31	0.15	65.53	0.37	65.88	0.72	65.73	0.57	65.94	0.78	66.30	1.14	65.69	0.53	65.93	0.77	66.39	1.23
C1α	92.19	0.00	92.15	-0.04	92.19	0.00	92.27	0.08	92.33	0.14	92.54	0.35	92.62	0.43	92.68	0.49	92.58	0.39	92.70	0.51	92.83	0.64
C2α	71.42	0.00	71.39	-0.03	71.30	-0.12	71.37	-0.05	71.38	-0.04	71.54	0.12	71.59	0.17	71.59	0.17	71.68	0.26	71.77	0.35	71.83	0.41
C3α	72.79	0.00	72.76	-0.03	72.90	0.11	73.04	0.25	73.20	0.41	73.13	0.34	73.25	0.46	73.38	0.59	73.13	0.34	73.29	0.50	73.48	0.69
C4α	69.38	0.00	69.34	-0.04	69.39	0.01	69.53	0.15	69.61	0.23	69.68	0.30	69.81	0.43	69.89	0.51	69.75	0.37	69.85	0.47	70.07	0.69
C5α	60.90	0.00	60.87	-0.03	61.25	0.35	61.53	0.63	62.06	1.16	61.67	0.77	61.94	1.04	62.45	1.55	61.55	0.65	61.84	0.94	62.41	1.51

Table 3.5 Chemical shifts, δ (ppm), of ^{1}H-NMR signals for the H1-H5 protons of the β- and α-xylopyranose forms of xylose (750 mM) in pure D_2O, D_2O with 50 mM HCl, and various 5M metal halide (*aq* – D_2O) solutions at 298 K. Changes in chemical shifts, Δδ (ppm), are shown relative to the chemical shifts associated with the carbon signals of 750 mM xylose in pure D_2O. The chemical shifts of the C3H, C4H, and C5H (both equatorial and axial) signals for the α-xylopyranose isomer are presented as a combined peak, as they were indistinguishable. Unidentifiable peaks are marked with a '-'.

Atom	δ, No Salt	Δδ	δ, No Salt w/50mM HCl	Δδ	δ, LiCl	Δδ	δ, LiBr	Δδ	δ, LiI	Δδ	δ, NaCl	Δδ	δ, NaBr	Δδ	δ, NaI	Δδ	δ, KCl	Δδ	δ, KBr	Δδ	δ, KI	Δδ
H_2O	4.76	0.00	4.77	0.01	4.75	-0.01	4.75	-0.01	4.73	-0.03	4.77	0.01	4.75	-0.01	4.74	-0.02	4.76	0.00	4.76	0.00	4.74	-0.02
C1Hβ	4.52	0.00	4.47	-0.05	4.72	0.20	4.92	0.40	5.22	0.70	5.01	0.49	5.20	0.68	5.46	0.94	4.91	0.39	5.12	0.60	5.48	0.96
C2Hβ	3.17	0.00	3.11	-0.06	3.36	0.19	3.51	0.34	3.83	0.66	3.65	0.48	3.83	0.66	4.08	0.91	3.55	0.38	3.76	0.59	4.10	0.93
C3Hβ	3.37	0.00	3.32	-0.05	3.58	0.21	3.77	0.40	4.08	0.71	3.87	0.50	4.06	0.69	4.33	0.96	3.76	0.39	3.97	0.60	4.34	0.97
C4Hβ	3.57	0.00	3.52	-0.05	-	-	-	-	-	-	-	-	-	-	-	-	3.94	0.37	4.13	0.56	4.46	0.89
C5Hβ Equitorial	3.87	0.00	3.82	-0.05	4.03	0.17	4.18	0.32	4.41	0.55	4.33	0.46	4.48	0.61	4.66	0.80	4.24	0.38	4.42	0.55	4.70	0.83
Axial	3.26	0.00	3.21	-0.05	3.44	0.18	3.64	0.38	3.87	0.61	3.73	0.47	3.90	0.64	4.12	0.86	3.63	0.37	3.82	0.56	4.13	0.87
C1Hα	5.14	0.00	5.09	-0.05	5.31	0.18	5.48	0.34	5.73	0.59	5.61	0.47	5.77	0.63	5.97	0.83	5.52	0.38	5.70	0.57	6.01	0.87
C2Hα	3.46	0.00	3.41	-0.05	3.68	0.22	3.85	0.39	-	-	3.97	0.51	4.14	0.68	-	-	3.87	0.41	4.06	0.60	4.39	0.93
C3Hα C4Hα C5Hα	3.62	0.00	3.57	-0.05	-	-	-	-	-	-	-	-	-	-	-	-	3.97	0.35	4.15	0.53	4.49	0.87

References

[1] T. Werpy, G. Petersen, Report No. NREL/TP-510– 35523, *Top Value Added Chemicals from Biomass: Vol. 1—Results of Screening for Potential Candidates from Sugars and Synthesis Gas*, National Renewable Energy Laboratory, Golden, CO, **2004**.
[2] K. J. Zeitsch, *Sugar Ser*. **2000**, *13*, 1-353.
[3] S. Bayan, E. Beati, *Chim. Ind. (Milan, Italy)* **1941**, *23*, 432.
[4] a) J. N. Chheda, G. W. Huber, J. A. Dumesic, *Angew. Chem. Int. Ed.* **2007**, *46*(38), 7164; b) G. A. Tompsett, N. Li, G. W. Huber, *Thermochemical Processing of Biomass: Conversion into Fuels, Chemicals and Power* (Ed.: Robert C. Brown), John Wiley & Sons, Chichester, **2011**, pp. 223-279.
[5] B. Madhesan, E. R. Sacia, A. T. Bell, *ChemSusChem* **2014**, *7*, 1078.
[6] a) G. W. Huber, J. N. Chheda, C. J. Barrett, J. A. Dumesic, *Science* **2005**, *300*, 2075; b) G. W. Huber, J. A. Dumesic, *Catal. Today* **2006**, *111*, 119.
[7] C. Moreau, R. Durand, D. Peyron, J. Duhamet, P. Rivalier, *Ind. Crops Prod.* **1998**, *7*(2-3), 95.
[8] a) G. W. Huber, S. Iborra, A. Corma, *Chem. Rev.* **2006**, *106*, 4044; b) C. E. Wyman, S. R. Decker, M. E. Himmel, J. W. Brady, C. E. Skopec, L. Viikari, *Polysaccharides: Structural Diversity and Functional Versatility, Vol. 2* (Ed.: S. Dumitriu), Marcel Dekker, New York, **2005**, pp. 995-1033.
[9] R. Weingarten, J. Cho, W. C. Conner, G. W. Huber, *Green Chem.* **2010**, *12*(8), 1423.
[10] J. N. Chheda, Y. Roman-Leshkov, J. A. Dumesic, *Green Chem.* **2007**, *9*(4), 342.
[11] a) E. O. Eisen, J. Joffe, *J. Chem. Eng. Data* **1966**, *11*, 480; b) E. I. Gürbüz, S. G. Wettstein, J. A. Dumesic, *ChemSusChem* **2012**, *5*(2), 383; c) B. Saha, N. S. Mosier, M. M. Abu-Omar, *Advances in Plant Biology: Plants and BioEnergy, Vol. 4* (Eds.: M. McCann, M. S. Buckeridge, and N. C. Carpita), Springer, New York, **2013**, pp. 267-276; d) Y. Roman-Leshkov, J. A. Dumesic, *Top. Catal.* **2009**, *52*, 297.
[12] a) G. Marcotullio, W. D. Jong, *Green Chem*. **2010**, *12*, 1739; b) G. Marcotullio, W. D. Jong, *Carbohydr. Res.* **2011**, *346*, 1291.
[13] T. W. G. Solomons, C. B. Fryhle, *Organic Chemistry 8th ed.*, John Wiley & Sons, Hoboken, NJ, **2004**.
[14] a) W. J. Hamer, Y. C. Wu, *J. Phys. Chem. Ref. Data* **1972**, *1*, 1047;b) R. N. Goldberg, R. L. Nuttall, *J. Phys. Chem. Ref. Data* **1978**, *7*(1), 263.
[15] a) C. D. Cappa, J. D. Smith, K. R. Wilson, B. M. Messer, M. K. Gilles, R. C. Cohen, R. J. Saykally, *J. Phys. Chem. B* **2005**, *109*(15), 7046; b) J. D. Smith, R. J. Saykally, P. L. Geissler, P. L. *J. Am. Chem. Soc*. **2007**, *129*(45), 13847.
[16] J. Israelachvili, *Intermolecular and Surface Forces 2nd ed.*, Academic Press, London, UK, **1991**.
[17] J. P. Mikkola, R. Sjoholm, T. Salmi, P. Maki-Arvela, *Catal. Today* **1999**, *48*(1-4), 73.
[18] S. J. Angyal, *Adv. Carbohydr. Chem. Biochem*. **1989**, *47*, 1.
[19] P. Ortiz, J. Fernandez-Bertran, E. Reguera, *Spectrochim. Acta. Part A* **2005**, *61*(8), 1977.
[20] a) R. C. Remsing, R. P. Swatloski, R. D. Rogers, G. Moyna, *Chem. Comm.* **2006**, *12*, 1271; b) J. J. Falke, R. J. Pace, S. I. Chan, *J. Biol. Chem*. **1984**, *259*, 6472; c) J. J. Falke, K. J. Kanes, S. I. Chan, *J. Biol. Chem.* **2005**, *260*, 9545.

[21] M. R. Nimlos, X. Qian, M. Davis, M. E. Himmel, D. K. Johnson, *J. Phys. Chem. A* **2006**, *110*(42), 11824.
[22] X. H. Qian, M. R. Nimlos, D. K. Johnson, M. E. Himmel, *Appl. Biochem. Biotechnol*. **2005**, *121*, 989.
[23] M. J. Antal, T. Leesomboon, W. S. Mok, G. N. Richards, *Carbohydr. Res*. **1991**, *217*, 71.

Chapter 4

Lewis Acid-Catalyzed Conversion of Xylose and Glucose to Furanics in Water

Abstract

A number of Lewis acid catalysts were screened for their effectiveness in converting both xylose and glucose in aqueous media to furfural and 5-HMF, respectively. While other catalysts were found to be more active, $SnCl_4$ was identified as the most selective Lewis acid. Hydrolysis of $SnCl_4$ was observed at various concentrations and temperatures resulting in the production of Brønsted acidic protons in a 3.5:1 ratio to Sn^{4+} at all $SnCl_4$ concentrations above 60 ºC. As a consequence, there was no need to add a Brønsted acid in order to promote the dehydration of either xylose or glucose. $SnCl_4$-promoted isomerization/dehydration of xylose and glucose at 140 ºC in water resulted in conversions of 55% and 33%, respectively, after 2 h of reaction, and furfural and 5-HMF selectivities of up to 58% and 27%, respectively. Significant conversion of sugars to humins was observed in both cases, and in the case of glucose, degradation of 5-HMF to levulinic and formic acids was also noted. The effects of secondary reactions could be greatly suppressed by extraction of the furanic product as it was produced. Using *n*-butanol as the extracting agent, xylose and glucose conversions of 90% and 75%, respectively, were observed after 5 h of reaction, and the selectivities to furfural and 5-HMF increased to 85% and 69%, respectively. Small additional increases in the furfural and 5-HMF selectivities were obtained by adding LiCl to the aqueous phase without much effect on the conversion of either sugar. In this case, the selectivities to furfural and 5-HMF were 88% and 72%, respectively, after 5 h of reaction at 140 ºC.

4.1 Introduction

Furfural and 5-hydroxymethyl furfural (5-HMF) are of great interest as platform molecules for the production of specialty chemicals and fuels [1]. Both products can be obtained from the carbohydrate portion of lignocellulosic biomass. Furfural is produced by dehydration of xylose, obtained by hydrolysis of hemicellulose, and 5-HMF is produced by dehydration of glucose, obtained by hydrolysis of cellulose. The primary reactions occurring during both dehydration processes are shown in Schemes 4.1 and 4.2 (adapted from [2, 3]), with the pathways shown in black catalyzed by Brønsted acids and those shown in blue catalyzed by Lewis acids. The dehydration of xylose can occur directly to furfural catalyzed by a Brønsted acid. However, intermediates involved in this process can react with either xylose or furfural to condense and form humins, undesired soluble and insoluble degradation products. In the presence of a Lewis acid, xylose can epimerize to lyxose, and either carbohydrate can isomerize to xylulose. This aldose to ketose isomerization (shown in Scheme 4.3) is thought to occur *via* enolization [4]. Xylulose can then dehydrate with the aid of a Brønsted acid to form furfural. Scheme 4.2 shows an analogous set of reaction pathways for the conversion of glucose to 5-HMF in the presence of Brønsted and Lewis acids. It should be noted that furfural and 5-HMF can both undergo Brønsted acid-catalyzed secondary reactions. In the case of furfural, self-

condensation or resinification leads to humins, and in the case of 5-HMF, hydrolysis of the primary product leads to levulinic and formic acids.

While high yields of furfural and 5-HMF have been reported in organic solvents [5-7], similar yields have not been achieved for dehydration occurring in water at moderate reaction temperatures. Higher conversions and yield of furanics can be achieved using a mixture of Brønsted and Lewis acids than is possible using only a Brønsted acid catalyst [2, 3, 7]. The higher conversion of xylose and glucose is a consequence of the lower apparent activation energy barrier for Brønsted acid-catalyzed dehydration of xylulose and fructose, and the higher selectivity to furanics is a consequence of the lower susceptibility of the furanose isomers to participate in degradation reactions compared to the corresponding pyranose isomers [7]. Additional improvements in the yields of furanics can be attained by *in situ* extraction of the product from the aqueous phase into an immiscible organic phase [1, 7-9].

In this work we investigate a number of Lewis acid catalysts and evaluate their ability to selectively dehydrate both xylose and glucose to their corresponding furanics, furfural and 5-HMF, in water at moderate temperatures. Screening studies revealed that the highest yields of furfural and 5-HMF could be achieved using $SnCl_4$ and hence all further work was carried out with this catalyst. Minimization of the effects of secondary reactions by means of *in situ* solvent extraction of the furanic products was also investigated.

4.2 Methods

4.2.1 Materials

D-xylose (99%, Sigma-Aldrich), D-glucose (≥99.5%, Sigma), D-xylulose (≥98%, Santa Cruz Biotechnology), D-fructose (≥99% Sigma), 2-furaldehyde (furfural, 99%, Sigma-Aldrich), 5-hydroxymethylfurfural (5-HMF, 98%, Acros Organics), levulinic acid (≥97%, Aldrich), formic acid (≥99.5%, Fisher Chemical), and α-angelica lactone (98%, Sigma-Aldrich) were used as reagents and standards (for quantification).

Aluminum chloride hexahydrate ($AlCl_3$ x $6H_2O$, 99.0%, crystalline), cerium(III) chloride heptahydrate ($CeCl_3$ x $7H_2O$, 99.999%, trace metals basis), chromium(II) chloride ($CrCl_2$, 95%, water soluble), chromium(III) chloride hexahydrate ($CrCl_3$ x $6H_2O$, 98%), iron(II) chloride tetrahydrate ($FeCl_2$ x $4H_2O$, 99.0%), iron(III) chloride hexahydrate ($FeCl_3$ x $6H_2O$, ACS reagent, 98.0-102%, crystalline), indium(III) trifluoromethanesulfonate ($In(OTf)_3$, 99%), lithium chloride (LiCl, BioXtra, ≥99.0% (titration)), scandium(III) triflate ($Sc(OTf)_3$, 99%), tin(II) chloride dihydrate ($SnCl_2$ x $2H_2O$, 99.995%, trace metals basis), tin(IV) chloride pentahydrate ($SnCl_4$ x $5H_2O$, 98%), tin(II) trifluoromethanesulfonate ($Sn(OTf)_2$, 98%), and ytterbium(III) trifluoromethanesulfonate ($Yb(OTf)_3$, 99.99%) were purchased from Sigma-Aldrich. Hydrochloric acid (HCl, 37% v/v, Fisher Scientific) was used as the Brønsted acid catalyst. *n*-Butanol (ACS Reagent, ≥99%, Fluka) was used as the organic extracting agent in biphasic experiments. All materials were used as purchased, without further purification or modification.

4.2.2 Experimental Approach

All experiments were performed in 10 ml glass vials (from Sigma-Aldrich *via*

supplier Supelco) sealed with 20 mm aluminum-crimped PTFE septa and heated using a silicon oil bath to maintain constant reaction temperature and stirring rate. In a representative glucose dehydration experiment, glucose was dissolved in nanopure water, to which $SnCl_4$ and HCl were added to create a solution (750 mM glucose, 25 mM $SnCl_4$, 50 mM H^+). A 4 ml aliquot of this solution was sealed into a 10 ml glass vial. The vial was then placed in a silicone oil bath heated to 140 ºC and stirred at 600 rpm. Upon completion of the reaction, the sample was removed and quenched in an ice bath. An internal standard (1 ml of 75 mg/ml 1,6-hexanediol in water) was added and the sample centrifuged to remove all water insoluble particulates. A portion of the reaction mixture (500 µl) was diluted in a 1:1 ratio with nanopure water and taken for HPLC analysis. For reactions involving an additional organic phase, the aqueous phase volume was reduced to 1 ml and *n*-butanol (4 ml) was added prior to sealing the reaction vial. At reaction end, the organic phase was separated *via* centrifuging. The aqueous phase was treated as above and analyzed *via* HPLC while a different internal standard (1 ml of 5 mg/ml guaiacol in toluene) was added to the organic phase prior to GC/MS analysis.

4.2.3 Product Analysis

A Shimadzu HPLC equipped with a Phenomenex Rezex RFQ-Fast Acid H+ column (100 x 7.8 mm; 0.01 N H_2SO_4; 1.0 ml/min; 55 ºC) and a refractive index detector (RID) was used to analyze all aqueous samples. Product quantities were determined by converting integrated HPLC peak areas into concentrations using a 7-point calibration curve generated from purchased standards.

A Varian CP-3800 Gas Chromatograph equipped with a FactorFour Capillary Column (UF-5ms 30 m, 0.25 mm, 0.25 µm, P/N CP8944) connected to a Varian quadrupole-mass spectrometer (MS) and flame ionization detector (FID) was used to analyze all organic phase samples. After product identification by mass spectrometer, product concentrations were determined from integrated FID peak areas using a 6-point calibration curve generated from purchased standards.

Reagent and product yields are reported as molar percentages relative to initial molar concentrations of carbohydrate (i.e. furfural yields = moles furfural/initial moles xylose). All reported yields were typically reproducible to within a +/- 5% relative error (based upon the calculation of one standard deviation).

4.3 Results and Discussion

4.3.1 Xylose and Glucose Isomerization/Dehydration in Water

Various metal chlorides and triflates were screened in order to establish their effectiveness as Lewis acid catalysts in converting xylose and glucose to furfural and 5-HMF, respectively. The results are summarized in Tables 4.1 and 4.2. Glucose product selectivity is tabulated to reflect 5-HMF and levulinic/formic acid production, as 5-HMF was found to hydrolyze to the acid products in all cases. For both sugars, all Lewis acids increased the rate of sugar conversion and the total product yield when compared to the results observed for Brønsted acid-catalyzed reactions. Of the metal triflates, $In(OTf)_3$ converted both sugars at the highest rate (in excess of 93% after 2 h), however, $Sn(OTf)_2$ was the most selective to dehydration products (41% for xylose and 70% for glucose). Chromium(II) and (III) chloride exhibited the highest activities for sugar conversion of

all metal chlorides (in excess of 90% after 2 h); however, $SnCl_4$ was the most selective to dehydration products (58% for xylose and 70% for glucose). For this reason, $SnCl_4$ was used exclusively for the remainder of this study.

The temporal evolution of products for $SnCl_4$-catalyzed dehydration of xylose and glucose is shown in Figures 4.1 and 4.2, respectively. For both sugars, the isomeric products lyxose, xylulose, mannose, and fructose were either not observed or were present in negligible quantities. Figure 4.1 shows xylose conversion reaching 55% over 2 h, with furfural production increasing toward 32% over the same period. Any unaccounted mass is attributed to the formation of soluble degradation products and humins. Figure 4.2 shows that glucose is converted to 67% of its initial concentration in 2 h, while 5-HMF is produced in small quantities and goes through a maximum of 6% after 1 h of reaction. The low concentration of 5-HMF is due to its hydrolysis to levulinic and formic acids, shown to reach yields of 12% and 19%, respectively, after 2 h of reaction. Produced in a 1:1 molar ratio from 5-HMF, the two acid yields are not found in the expected stoichiometric ratio because levulinic acid undergoes cyclization to form α-angelica lactone (found to be present in <5%) [9]. A proposed pathway for this side reaction is given in Scheme 4.4, wherein the cyclization is shown to be initiated *via* either carbonyl or hydroxyl group attack of the ketone carbon, followed by dehydration.

4.3.2 Lewis Acid Hydrolysis in Water

The production of any dehydration product from xylose and glucose is an indication of the presence of a Brønsted acid, as protons in solution are necessary for hydroxyl group removal during all dehydration steps leading to furfural and 5-HMF [9]. Furthermore, levulinic and formic acid formation from 5-HMF and α-angelica lactone formation from levulinic acid can also only occur in the presence of a Brønsted acid [9]. Therefore it is important to evaluate the extent to which $SnCl_4$ generates Brønsted acidity in water.

When $SnCl_4$ is added to water, it dissociates into Sn^{4+} and Cl^-, followed immediately by the complexation of Sn^{4+} ions with 6 water molecules to form the octahedrally-coordinated aquachlorotin(IV), $[SnCl_x(H_2O)_{6-x}]^{(4-x)+}$, and hexaaquatin(IV), $[Sn(OH)_y(H_2O)_{6-y}]^{(4-y)+}$, complexes [10-12]. However, at $SnCl_4$ concentrations of 100 mM and lower, only a single peak is observed when such solutions are analyzed *via* ^{119}Sn-NMR. This peak has been exclusively attributed to hexaaquatin(IV) ions, indicating that any chloride-containing complexes are completely dissociated at low $SnCl_4$ concentrations [10]. The $[Sn(OH)_y(H_2O)_{6-y}]^{(4-y)+}$ complex ions can undergo hydrolysis, releasing a proton for each stage of hydrolysis, for example:

$$[Sn(H_2O)_6]^{4+} + H_2O \leftrightarrows [Sn(OH)(H_2O)_5]^{3+} + H_3O^+ \qquad (1)$$

It has also been reported that $SnCl_4$ can hydrolyze to form water-insoluble SnO_2, releasing 4 protons per oxide formed [11, 13]. Small quantities of white precipitate were observed after allowing aqueous $SnCl_4$ solutions of concentrations 10, 20, 40, and 60 mM to sit at room temperature over 24 h, which is likely an indication that the metal oxide forms under the conditions used in the present study.

The exact distribution of hexaaquatin(IV) complexes and SnO_2 existing in sub-100 mM $SnCl_4$ solutions is undefined and consequently an assessment of aggregate

Lewis acidity cannot be made. However, the distinction does not appear to be important. A recent study has found that chitosan could be converted to 27.4% levulinic acid *via* 5-HMF when either $SnCl_4$ or the equivalent of SnO_2 and HCl were used, indicating either complete oxidation of tin in the first case or a relatively similar Lewis acidity exists for hexaaquatin(IV) cationic complexes and SnO_2 species [14]. In either case, we investigated the overall extent of hydrolysis by measuring solution pH as a function of $SnCl_4$ concentration in water. Figure 4.3 shows that proton concentration increases with both $SnCl_4$ concentration and temperature over the range of 20-80 ºC. For a given $SnCl_4$ concentration, the proton concentration increase appears to decrease with increasing temperature such that beyond at high temperatures, the proton concentration is no longer a function of temperature. This conclusion is reinforced by the observation that at 140 ºC, a 25 mM $SnCl_4$ solution has a pH of 1.1 ($[H^+]$ = 80 mM). Figure 4.3 also shows that for all conditions tested, the H^+:Sn ratio is always less than 4, an indication that $SnCl_4$ does not hydrolyze completely to SnO_2 nor do $[Sn(OH)_y(H_2O)_{6-y}]^{(4-y)+}$ complexes hydrolyze to form neutral or negative charged Sn species.

We note that regardless of the exact distribution of Sn(IV) complexes in solution, $SnCl_4$ provides both Lewis- and Brønsted-acid centers for aqueous phase reactions. Previous work has shown that even with 200 mM of HCl, xylose conversion only reached 45% after 2 h using purely Brønsted-acid centers at 140 ºC [15]. When the isomerization/dehydration of xylose is carried out with 25 mM $SnCl_4$ in the absence of added Brønsted acid, 55% of the xylose was converted over 2 h even though tin hydrolysis results in less Brønsted acidity by comparison. Therefore, SnO_2 and $[Sn(OH)_y(H_2O)_{6-y}]^{(4-y)+}$ complexes evolved from $SnCl_4$ hydrolysis are active as Lewis acids and providers of Brønsted acidity.

Lastly, the fact that little to no xylulose and fructose were observed can be explained by the hydrolysis of the tin increasing the Brønsted acidity of our aqueous solutions such that the rate of ketose carbohydrate dehydration became competitive with the isomerization of xylose and glucose under these conditions.

4.3.3 Effect of Lewis Acid Concentration and Reaction Temperature on Selectivity

The initial rates of xylose/glucose conversion and furfural/5-HMF production were evaluated as a function of $SnCl_4$ initial concentration and temperature. The results are presented in Table 4.3. As the $SnCl_4$ concentration increases from 25 to 75 mM at either 140 ºC or 160 ºC, the rates of both xylose and glucose conversion increase, as do those of furfural and 5-HMF production. The selectivity toward furfural does not change with Lewis acid concentration, however, 5-HMF selectivity increases with $SnCl_4$ concentration. As previously noted, Sn^{4+} hydrolysis increases linearly with $SnCl_4$ concentration at temperatures above 40-60 ºC, such that proton concentration increases proportionally with the amount of metal cations dissolved (about 3.5 protons per Sn^{4+} cation). Since xylose selectivity to furfural is unaffected by $SnCl_4$ concentration, Brønsted acid- and Lewis acid-catalyzed reaction pathways shown in Scheme 4.1 must have the same rate-order dependencies on proton and Sn^{4+} concentrations, respectively. With glucose selectivity toward 5-HMF increasing with $SnCl_4$ concentrations, however, Lewis acid-catalyzed reaction pathways shown in Scheme 4.2 must have higher rate-order dependencies on Sn^{4+} concentration than the Brønsted acid-catalyzed reaction pathways have on proton concentration.

Comparing the results from 140 ºC and 160 ºC for a given catalyst concentration, the rates of carbohydrate conversion and furanic production increase with temperature, however, selectivities toward furanics decrease for both furfural and 5-HMF. This is due to differences in the activation energies for the direct sugar dehydration pathways versus the sugar isomerization-initiated pathways (see Schemes 4.1 and 4.2). For xylose, the activation energies for direct dehydration to furfural, isomerization to xylulose, and dehydration of xylulose to furfural are reported to be 32, 15.5, and 23.1 kcal/mol, respectively (where $CrCl_3$ was used for isomerization) [2]. Similarly, the activation energies for direct dehydration of glucose to 5-HMF, isomerization to fructose, dehydration of fructose to 5-HMF, and hydrolysis of 5-HMF to levulinic and formic acids have been found to be 36.4, 20, 29.4, 23.1 kcal/mol, respectively [7]. Reactions with higher activation energy barriers are more sensitive to increases in temperature. For example, by taking the ratio of Arrhenius rate constants at two temperatures, one finds that the rate of the direct dehydration of xylose increases by 6.2-fold whereas the rate of xylose isomerization only increases by 2.4-fold when the temperature is adjusted from 140 ºC to 160 ºC (similarly, 7.8-fold compared to 3-fold for glucose). Therefore, the direct dehydration pathway for both sugars becomes increasingly competitive with the isomerization/dehydration pathway as the temperature increases. The overall selectivity to furanics decreases as a result of the increased production of highly reactive intermediates involved in the direct dehydration process, which are proposed to be the primary participants in degradation pathways leading to humins [15]. Maintaining lower reaction temperatures, therefore, results in a shift in the ratio of direct dehydration to isomerization pathways in favor of isomerization and higher furanic selectivity.

4.3.4 Combination of $SnCl_4$ and a Brønsted Acid

The use of $SnCl_4$ produces very little quantifiable xylulose or fructose since the hydrolysis of the Lewis acid catalyst provides ample Brønsted acidity to catalyze the dehydration of the ketose carbohydrates at a rate equal to or superior than the isomerization of the aldose carbohydrates. Thus, the further addition of a Brønsted acid would only accelerate the competing direct carbohydrate dehydration and furanic degradation reactions. However, a comparison of the $SnCl_4$-catalyzed isomerization/dehydration of either xylose or glucose with and without the addition of a small amount of HCl (50 mM) shows that Brønsted acid addition has little impact on the chemistry (an example for xylose is shown in Figure 4.4). This is so because when low concentrations are added to solutions of $SnCl_4$ under 100 mM, hydrolytic exchange occurs between the positive H_3O^+ and the anionic Sn-OH species, evidenced by a broadening of the ^{119}Sn-NMR peak attributed to $[Sn(OH)_y(H_2O)_{6-y}]^{(4-y)+}$ [10]. This exchange shifts the equilibrium from hydrolyzed variants of Sn^{4+} toward $[Sn(H_2O)_6]^{4+}$ while the solution pH remains approximately the same. As a consequence, the extent to which this hydrolysis occurs is governed by the solution pH, such that for pH values <2, solvated Sn^{4+} exists primarily as cationic hexaaquatin(IV) species [12].

4.3.5 Xylose and Glucose Isomerization/Dehydration in a Biphasic System

The dehydration of xylose and glucose in the presence of Brønsted acidity, whether added extrinsically or derived *via* Lewis acid cation hydrolysis, is necessary for furanic production but also detrimental because it promotes furanic-consuming side

reactions that lead to the formation of humins. Furanic consumption can be avoided by removing furfural and 5-HMF immediately as they are produced. One way to accomplish this is through the employment of a biphasic system that utilizes an appropriate solvent capable of extracting furfural and 5-HMF from the reactive aqueous phase *in situ*. Such systems have been observed to be successful in curtailing degradation and improving overall furanics yields [8]. However, identifying a solvent that is serviceable for the removal of both furfural and 5-HMF is complicated due to the structural differences in the two molecules affecting solvation. Instead of performing an exhaustive screening of organic solvent candidates by physically performing biphasic extraction experiments, we used the UNIFAC (**UNI**versal quasichemical **F**unctional-group **A**ctivity **C**oefficients) method to rapidly determine activity coefficients for both furfural and 5-HMF in water and various organic solvents [16, 17]. This method has been found to accurately predict activity coefficients for small molecule solvents and solutes at temperatures below 200 ºC [17]. After acquiring these activity coefficients, we calculated the partition coefficient for each solute between water and a given organic solvent as:

$$\log(K) = -\log\left(\frac{\gamma_{organic}^{solute}}{\gamma_{water}^{solute}}\right) \quad (2)$$

where K is the partition coefficient and γ is the activity coefficient of the solute in either the water or organic phase. Partition coefficient values >1 calculated in such a fashion indicated a preference for the organic phase. After qualitative comparison of solvent K values, *n*-butanol was found to strike the best balance of partition coefficients for both furanics of interest. The UNIFAC results for both furfural and 5-HMF in some optimal biphasic systems at 140 ºC are shown in Figure 4.5. For the low mole fractions of furanics expected under the typical reaction conditions (<0.02), the partition coefficients for furfural and 5-HMF between *n*-butanol and water were found to be ≥11.3 and ≥3.8, respectively.

Using *n*-butanol as an extracting agent, we performed the $SnCl_4$-catalyzed isomerization/dehydration of xylose and glucose, separately, in a biphasic system consisting of a 1:2 ratio of water:butanol (by volume). The results for this experiment are shown in Figures 4.6A and 4.6B for xylose and glucose, respectively. Xylose conversion proceeds at a rate similar to that observed for its reaction in water alone, reaching a conversion of 90% after 5 h. The furfural selectivity for the biphasic system was nearly constant at 85% throughout the reaction, resulting in a yield of 77% after 5 h of reaction. The initial conversion of glucose in the biphasic system was lower than in the single-phase system, but reached a conversion of 75% after 5 h. The selectivity of 5-HMF tracked the conversion of its glucose and remained nearly constant at 69%, resulting in a 5-HMF yield of 52% after 5 h. Furthermore, formic acid (10%) and levulinic acid (5%) production was reduced in the biphasic system after 5 h, indicating less 5-HMF degradation to these products as compared to the reaction in water alone (19% and 12%, respectively, after only 2 h). Including formic acid yields with those of 5-HMF, selectivity to desirable products from glucose increases to 83% in a biphasic system. Levulinic acid degradation was also lower in the two-phase system, with only 5% degradation products (mainly angelica lactone) produced when *n*-butanol was used compared to 7% after 2 h with water alone.

Despite the employment of a biphasic system, selectivities to furfural and 5-HMF never reach 100%. A review of Schemes 4.1 and 4.2 reveals that reaction pathways to degradation products not involving furanics exist, which can consume carbohydrates in the aqueous phase regardless of the extraction of furfural/5-HMF and result in the reduction of apparent product selectivity. These reactions can be mitigated by controlling the Brønsted acidity of the aqueous phase, though, this can be difficult to accomplish when using hydrolyzable Lewis acid catalysts as in this study. Also, while *n*-butanol is a good extracting agent, the partitioning of either furanic compound does not reach 100%, resulting in an observable amount of furanics remaining within the aqueous phase capable of participating in Brønsted acid-catalyzed side reactions. The latter issue can be moderated through the use of aqueous phase modifiers, which is addressed in the next section.

4.3.6 Effect of LiCl on Xylose and Glucose Isomerization/Dehydration in a Biphasic System

The addition of metal halides to aqueous solutions has been observed to improve the thermodynamics of solute extraction from aqueous phases into organic phases, with higher metal halide concentrations found to be more effective [18, 19]. However, previous work has also shown that, while the addition of metal halides to the Brønsted acid-catalyzed dehydration of xylose increases the rate of xylose consumption and furfural production, product selectivity decreases with increasing salt concentrations because the metal halide can also promote the undesired formation of humins [15]. Therefore, it is important to select an appropriate metal halide concentration such that additives can improve the partitioning efficacy of a biphasic system by reducing water activity and increasing the activity coefficients of furanics in water without interfering in the dehydration chemistry. The concentration at which the metal halide activity coefficient in water is also the point it is at its lowest chemical potential and least likely to interact with other solutes, namely carbohydrates. LiCl was selected based on earlier work showing this salt to be an optimal additive for the dehydration of xylose in a biphasic system [19]. The activity coefficient minimum in water was found to be 0.734 with a water activity of 0.983 [20] for a concentration of 500 mM LiCl.

The biphasic experiment described previously was repeated with the addition of 500 mM LiCl to the aqueous phase. These results are presented in Table 4.4. Xylose and glucose conversion rates increased slightly, such that 95% of the xylose and 81% of the glucose was consumed after 5 h. Similarly, the furfural yield reached 84% and the 5-HMF yield reached 58%, raising the furanic selectivities to 88% for furfural and to 72% for 5-HMF. The slight increase in carbohydrate conversion is likely due to dissolved LiCl assisting in the dehydrations of xylulose and fructose, while selectivity increases toward furanics can be attributed to a minor enhancement in partitioning from the reactive aqueous phase to the *n*-butanol phase.

The present observations of glucose dehydration in a biphasic system catalyzed by $SnCl_4$ in the aqueous phase are similar to those found for glucose dehydration in a water/THF biphasic system catalyzed by Sn-BEA zeolite and HCl [6]. However, the biphasic Lewis acid-catalyzed xylose conversion results exceed those typically reported in aqueous media (for example, selectivities of ~80% were found when $CrCl_3$ was used as catalyst [2]).

4.4 Conclusions

$SnCl_4$ was investigated as a selective Lewis acid catalyst for the production of furfural and 5-HMF from xylose and glucose, respectively, in aqueous media. At moderate concentrations and reaction temperature, $SnCl_4$ to provides the Lewis acidity necessary for isomerization of xylose to xylulose and glucose to fructose, as well as the Brønsted acidity necessary to dehydrate xylulose to furfural and fructose to 5-HMF. The significant Brønsted acidity resulting from hydrolysis of $SnCl_4$ also catalyzes secondary reactions that consume furfural and 5-HMF to produce humins and hydrolyze 5-HMF to produce levulinic and formic acid, both processes limiting the selectivities to the desired furanic product. *n*-Butanol was found to be an appropriate solvent for removing both furanics from water. Working in a 1:1 water:butanol biphasic system with $SnCl_4$ in the aqueous phase, conversions of both carbohydrates in excess of 75% with selectivities of 85% toward furfural and 69% toward 5-HMF could be achieved at 140 ºC in 5 h. The addition of LiCl to the aqueous phase increased the conversion of xylose to 95% and that of glucose to 81%, and increased the selectivity to furfural to 88% and that to 5-HMF to 72%.

4.5 Supplemental Information

4.5.1 Effect of Temperature on the Partition Coefficients of Furanics in Water:Butanol Determined Using UNIFAC

The partition coefficients of varying concentrations of furfural and 5-HMF within a water:butanol biphasic system were determined over the temperature range 20-160 ºC using UNIFAC. These results are shown in Figure 4.7. For both furanics, partition coefficients decrease with temperature and solute concentration; however, furfural partition coefficients more strongly depend on temperature than 5-HMF. Overall, reducing reaction temperature results in a higher partition coefficient for both furanic compounds, and thus to improve product partitioning, lower reaction temperatures are more useful.

Scheme 4.1 Reaction network for xylose dehydration catalyzed by a Brønsted acid (shown in **black**) and a Lewis acid (shown in **blue**).

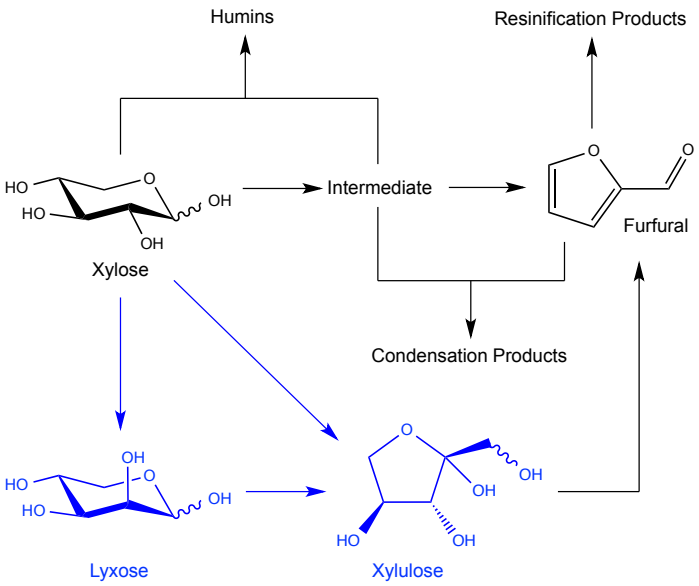

Scheme 4.2 Reaction network for glucose catalyzed by a Brønsted acid (shown in **black**) and a Lewis acid (shown in **blue**).

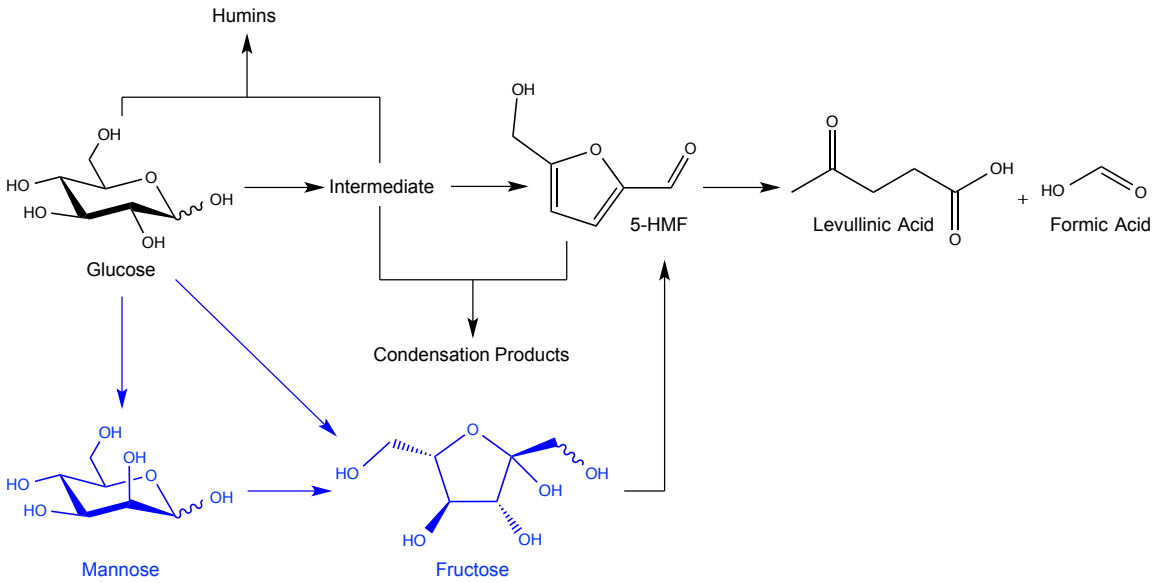

Scheme 4.3 Lewis acid-catalyzed aldose to ketose isomerization reaction pathway for xylose and glucose to xylulose and fructose, respectively.

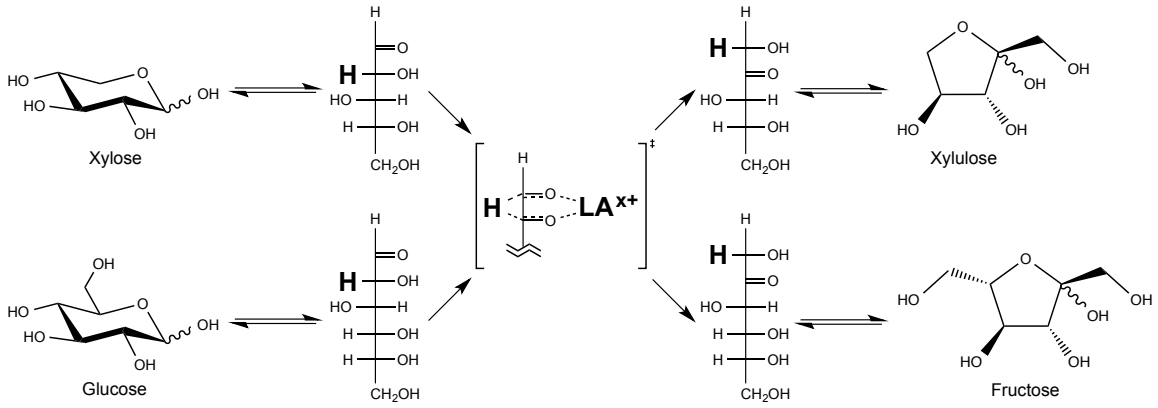

Scheme 4.4 Proposed reaction scheme for the Brønsted acid-catalyzed cyclization of levulinic acid to an equilibrium mixture of α- and β-angelica lactone.

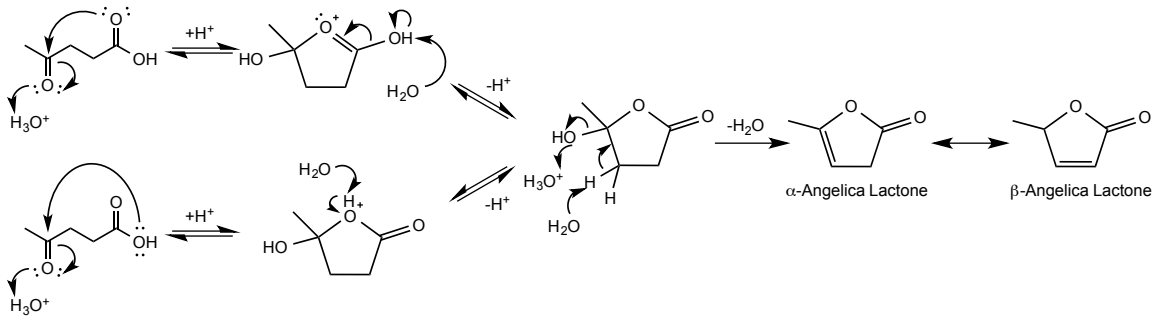

Figure 4.1 The conversion of xylose (750 mM) and the yield of furfural at 140 ºC catalyzed by 25 mM $SnCl_4$ in a single aqueous phase.

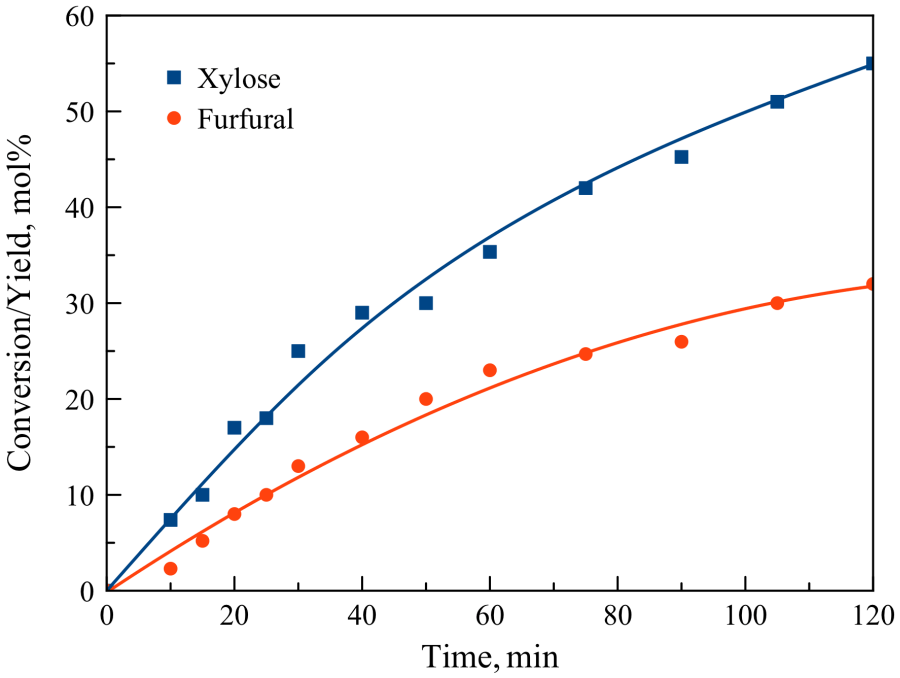

Figure 4.2 The conversion of glucose (750 mM) and the yields of 5-HMF, levulinic acid, and formic acid at 140 ºC catalyzed by 25 mM $SnCl_4$ in a single aqueous phase.

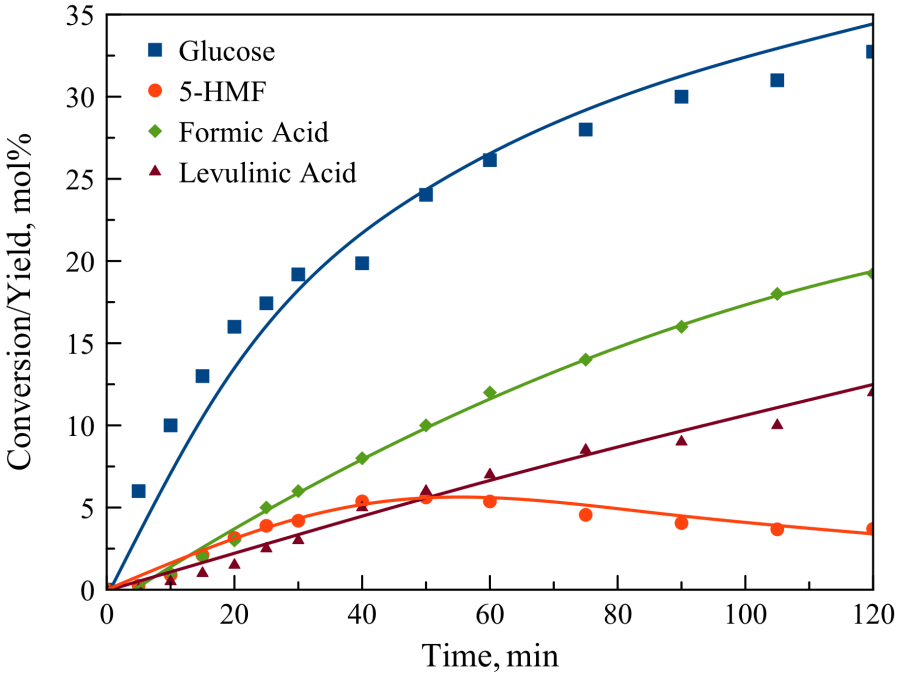

Figure 4.3 Effect of $SnCl_4$ concentration on H^+ concentration observed for temperatures between 20 ºC and 80 ºC. Measurements were taken after solutions were allowed to equilibrate for 12 h.

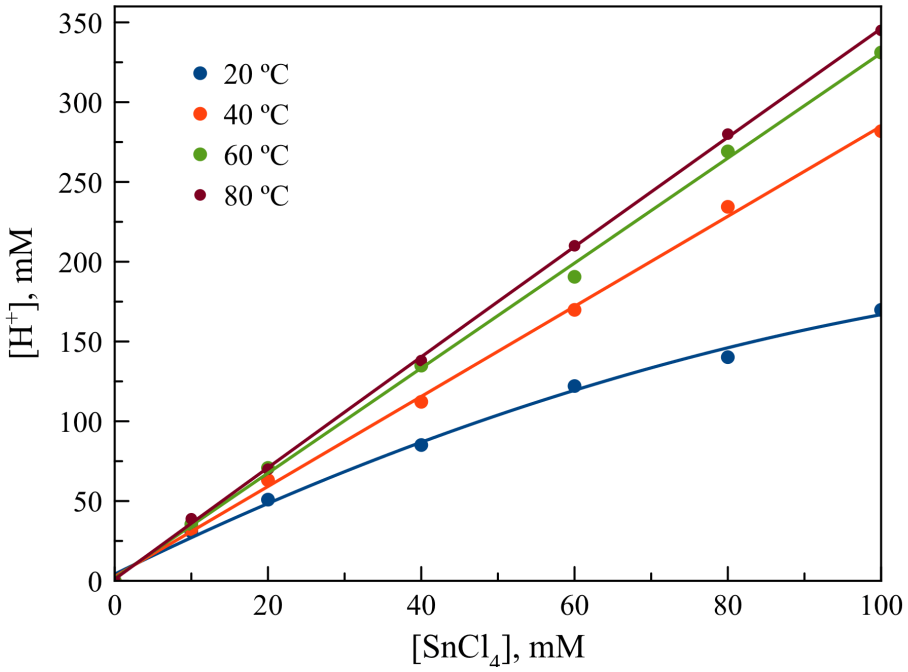

Figure 4.4 The conversion of xylose (750 mM) and the yield of furfural at 140 ºC catalyzed by 25 mM $SnCl_4$ in a single aqueous phase with and without 50 mM HCl.

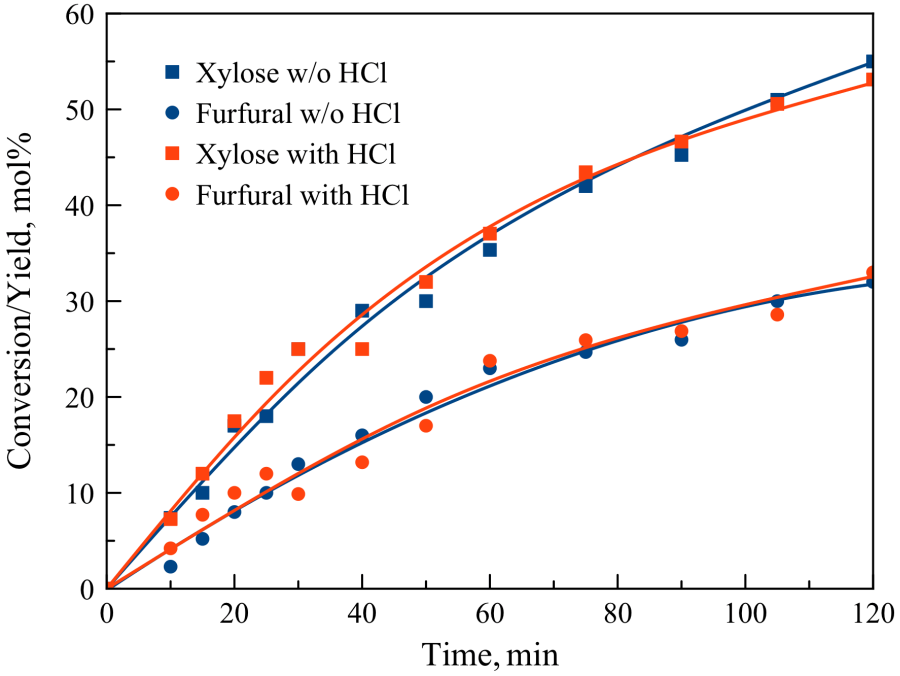

Figure 4.5 The partition coefficients for furfural (A) and 5-HMF (B) between water and the organic solvents benzene, toluene, *n*-butanol, and MIBK at 140 ºC determined using UNIFAC.

A.

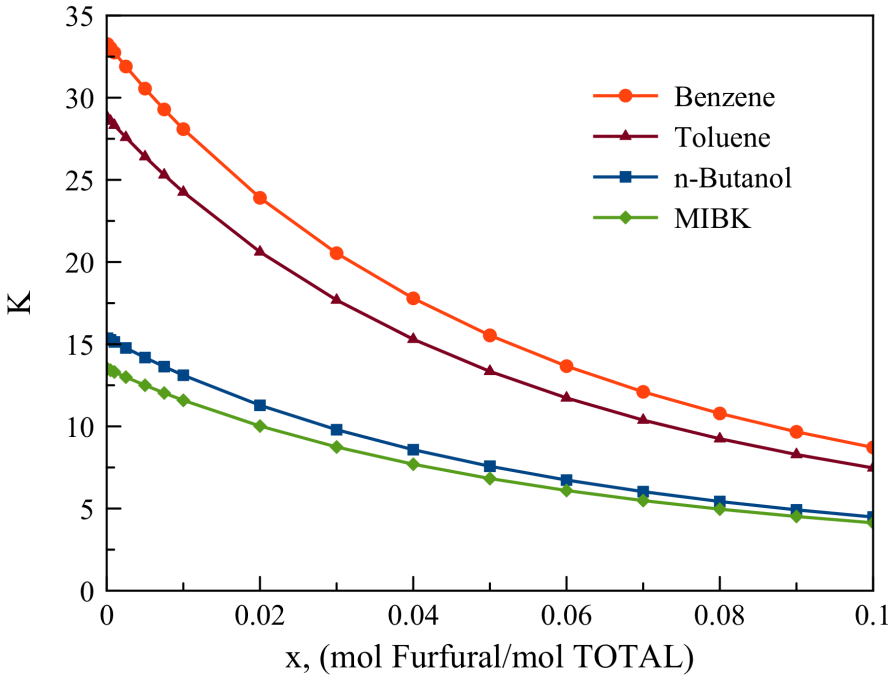

B.

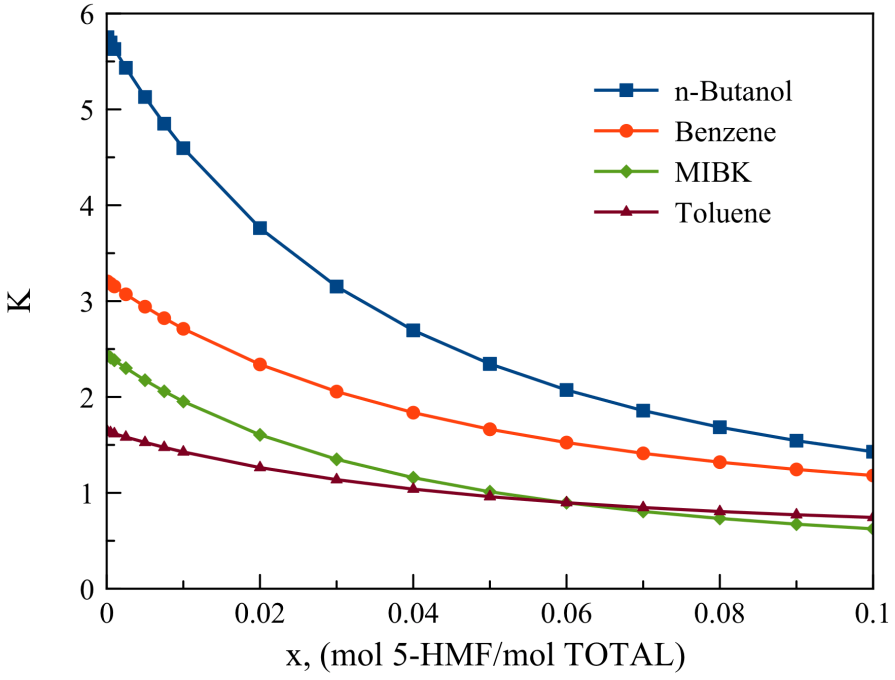

Figure 4.6 The $SnCl_4$-catalyzed conversion of xylose (A) and glucose (B) in a 1:2 water:butanol (v/v) biphasic system. Conditions: 750 mM initial sugar concentration, 25 mM $SnCl_4$, 140 ºC. All concentrations based upon the aqueous phase.

A.

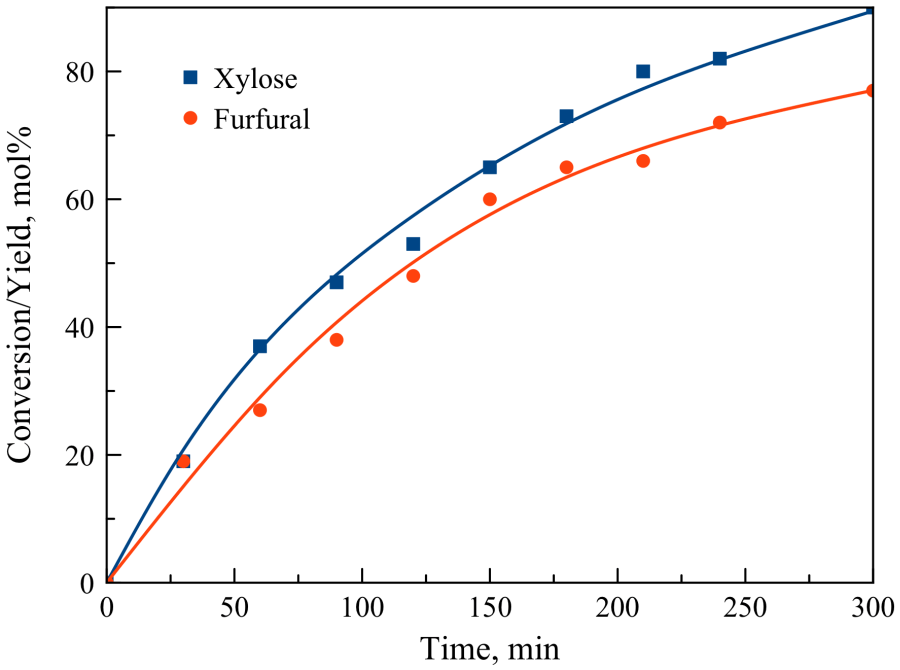

B.

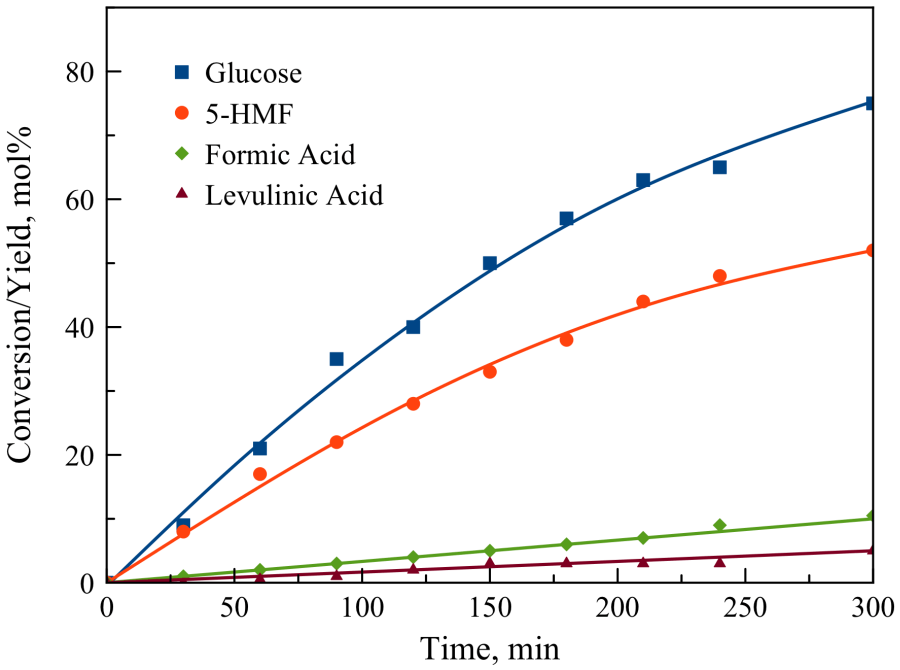

Figure 4.7 The partition coefficients for furfural (A) and 5-HMF (B) between water and *n*-butanol over the temperature range 20-160 ºC determined using UNIFAC.

A.

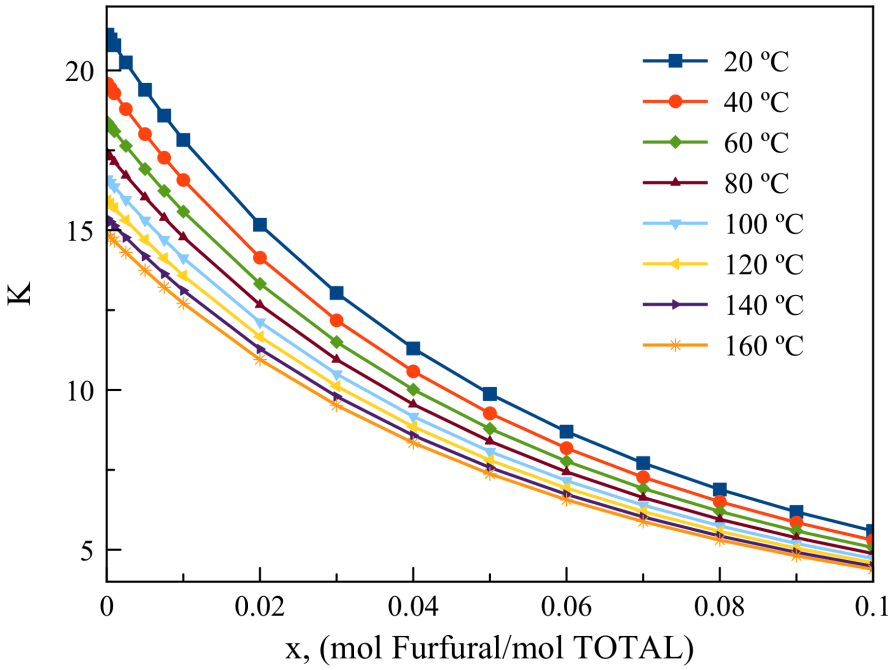

B.

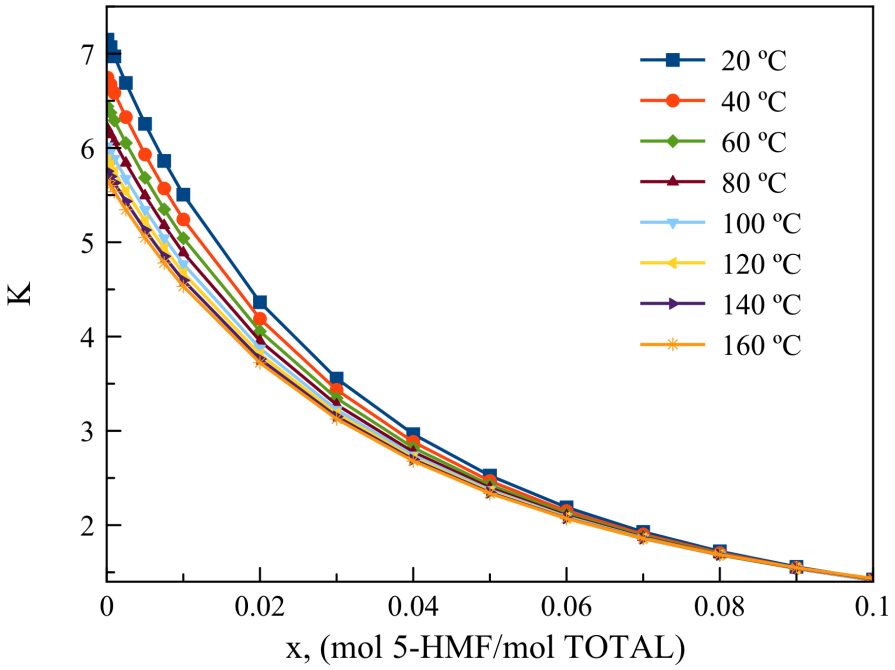

Table 4.1 The conversion of xylose (750 mM) and the yield of furfural at 140 ºC catalyzed by various Lewis acidic metal chlorides and triflates (25 mM) in a single aqueous phase measured after 1 and 2 h of reaction. Data for the HCl-catalyzed (25 mM) dehydration under the same conditions is shown for comparison.

Catalyst	Time, h	Xylose Conversion, mol%	Furfural Yield, mol%	Selectivity, mol%
HCl	1	4	1.3	32
	2	8	2.4	30
$AlCl_3$ x $6H_2O$	1	75	31	41
	2	91	29	32
$CeCl_3$ x $7H_2O$	1	28	4	14
	2	35	7	20
$CrCl_2$	1	75	25	33
	2	92	28	30
$CrCl_3$ x $6H_2O$	1	70	32	46
	2	92	36	39
$FeCl_2$ x $4H_2O$	1	18	5	27
	2	30	8	25
$FeCl_3$ x $6H_2O$	1	24	7	30
	2	40	12	31
$SnCl_2$ x $2H_2O$	1	29	14	48
	2	42	20	48
$SnCl_4$ x $5H_2O$	**1**	**35**	**23**	**65**
	2	**55**	**32**	**58**
$In(OTf)_3$	1	89	22	25
	2	96	24	25
$Sc(OTf)_3$	1	48	14	29
	2	64	16	25
$Sn(OTf)_2$	1	32	11	35
	2	39	16	41
$Yb(OTf)_3$	1	32	9	30
	2	45	14	31

Table 4.2 The conversion of glucose (750 mM) and the yields of 5-HMF, levulinic acid (LA), and formic acid (FA) at 140 ºC catalyzed by various Lewis acidic metal chlorides and triflates (25 mM) in a single aqueous phase measured after 1 and 2 h of reaction. Data for HCl-catalyzed (25 mM) dehydration of glucose under the same conditions are shown for comparison. Product selectivity is the sum of glucose selectivity toward 5-HMF and formic acid.

Catalyst	Time, h	Glucose Conversion, mol%	5-HMF Yield, mol%	LA/FA Yield, mol%	Product Selectivity, mol%
HCl	1	2	-	-	-
	2	3	0.6	-	20
$AlCl_3$ x $6H_2O$	1	68	10	4	21
	2	80	18	10	35
$CeCl_3$ x $7H_2O$	1	21	3	2	24
	2	25	4	2	24
$CrCl_2$	1	70	9	7	23
	2	89	10	10	22
$CrCl_3$ x $6H_2O$	1	68	11	5	24
	2	90	13	10	26
$FeCl_2$ x $4H_2O$	1	9	2	0	22
	2	15	3	1	27
$FeCl_3$ x $6H_2O$	1	11	4	0	36
	2	18	6	1	39
$SnCl_2$ x $2H_2O$	1	22	4	9	60
	2	26	5	11	63
$SnCl_4$ x $5H_2O$	**1**	**26**	**5**	**13**	**69**
	2	**33**	**4**	**19**	**70**
$In(OTf)_3$	1	87	11	39	57
	2	93	9	46	59
$Sc(OTf)_3$	1	59	5	22	46
	2	66	5	25	45
$Sn(OTf)_2$	1	49	12	20	65
	2	58	17	24	70
$Yb(OTf)_3$	1	21	4	9	61
	2	31	7	12	61

Table 4.3 The initial rates of reaction of xylose (A, 750 mM) and glucose (B, 750 mM) and the initial rates of formation of furfural and 5-HMF for different $SnCl_4$ concentrations (25-75 mM) at 140 and 160 ºC. Selectivities toward furanic products are also included. Measurements were taken within the first 10 min of reaction.

A.

Temperature, °C	[$SnCl_4$], mM	Xylose Initial Rate of Reaction, μmol-L^{-1}-s^{-1}	Furfural Initial Rate of Formation, μmol-L^{-1}-s^{-1}	Furfural Selectivity, mol%
140	25	94	56	60
	50	182	108	59
	75	279	170	61
160	25	197	83	42
	50	385	159	41
	75	585	257	44

B.

Temperature, °C	[$SnCl_4$], mM	Glucose Initial Rate of Reaction, μmol-L^{-1}-s^{-1}	5-HMF Initial Rate of Formation, μmol-L^{-1}-s^{-1}	5-HMF Selectivity, mol%
140	25	87	18	20
	50	95	28	30
	75	103	32	31
160	25	199	38	19
	50	215	55	26
	75	230	61	27

Table 4.4 The effects of 500 mM LiCl added to the aqueous phase on the $SnCl_4$-catalyzed conversion of xylose and glucose in a 1:2 water:butanol (v/v) biphasic system. Conditions: 750 mM initial sugar concentration, 25 mM $SnCl_4$, 140 ºC.

Carbohydrate	Time, h	Carbohydrate Conversion, mol%	Furanics Formation, mol%	Furanics Selectivity, mol%
Xylose	1	41	32	78
	2	61	53	87
	3	77	66	86
	4	88	76	87
	5	95	84	88
Glucose	1	26	16	62
	2	45	31	69
	3	60	42	70
	4	71	51	72
	5	81	58	72

References:

[1] a) M. J. Climent, A. Corma, S. Iborra, *Green Chem.* **2011**, *13*, 520; b) G. A. Tompsett, N. Li, G. W. Huber, *Thermochemical Processing of Biomass: Conversion into Fuels, Chemicals and Power* (Ed.: Robert C. Brown), John Wiley & Sons, Chichester, **2011**, pp. 223-279; c) J. N. Chheda, G. W. Huber, J. A. Dumesic, *Angew. Chem. Int. Ed.* **2007**, *46*(38), 7164; d) T. Werpy, G. Petersen, A. Aden, J. Bozell, J. Holladay, J. White, A. Manheim, Report No. NREL/TP-510– 35523, *Top Value Added Chemicals from Biomass: Vol. 1—Results of Screening for Potential Candidates from Sugars and Synthesis Gas*, National Renewable Energy Laboratory, Golden, CO, **2004**; e) K. J. Zeitsch, *Sugar Ser*. **2000**, *13*, 1-353.
[2] a) V. Choudhary, S. Sandler, D. Vlachos, *ACS Catal*. **2012**, *2*(9), 2022; b) V. Choudhary, S. Caratzoulas, D. Vlachos, *Carbohydr. Res.* **2013**, *368*, 89.
[3] V. Choudhary, S. H. Mushrif, C. Ho, A. Anderko, V. Nikolakis, N. S. Marinkovic, A. I. Frenkel, S. I. Sandler, D. G. Vlachos, *J. Am. Chem. Soc.* **2013**, *135*, 3997.
[4] J. B. Binder, J. J. Blank, A. V. Cefali, R. T. Raines, *ChemSusChem* **2010**, *3*(11), 1268.
[5] a) R. Weingarten, A. Rodriguez-Beuerman, F. Cao, J. S. Luterbacher, D. M. Alonso, J. A. Dumesic, G. W. Huber, *ChemCatChem* **2014**, *6*(8), 2229; b) E. I. Gürbüz, J. M. R. Gallo, D. M. Alonso, S. G. Wettstein, W. Y. Lim, J. A. Dumesic, *Angew. Chem. Int. Ed.* **2012**, *52*(4), 1270.
[6] E. Nikolla, Y. Roman-Leshkov, M. Moliner, M. E. Davis, *ACS Catal.* **2011**, *1*(4), 408.
[7] a) R. van Putten, J. C. van der Waal, E. de Jong, C. B. Rasrendra, H. J. Heeres, J. G. de Vries, *Chem. Rev.* **2013**, *113*, 1499; b) P. Gallezot, *Chem. Soc. Rev.* **2012**, *41*, 1538.
[8] Y. Roman-Leshkov, J. A. Dumesic, *Top. Catal*. **2009**, *52*, 297.
[9] G. W. Huber, S. Iborra, A. Corma, *Chem. Rev.* **2006**, *106*(9), 4044.
[10] M. J. Taylor, J. M. Coddington, *Polyhedron* **1992**, *11*(12), 1531.
[11] K. M. O. Jensen, M. Christensen, P. Juhas, C. Tyrsted, E. D. Bojesen, N. Lock, S. J. L. Billinge, B. B. Iversen, *J. Am. Chem. Soc.* **2012**, *134*, 6785.
[12] F. Fringuelli, F. Pizzo, L. Vaccaro, *J. Org. Chem.* **2001**, *66*, 4719.
[13] a) N. Wiberg, A. F. Holleman, *Inorganic Chemistry 34th ed.*, Academic Press, San Diego, CA, **2001**; b) Z. M. Jarzevski, J. P. Marton, *J. Electrochem. Soc.* **1976**, *123*(7), 199; c) M. Nagasawa, S. Shionoya, S. Makishima, *Jpn. J. Appl. Phys.* **1965**, *4*(3), 195.
[14] K. W. Omari, J. E. Besaw, F. M. Kerton, *Green Chem.* **2012**, *14*, 1490.
[15] K. R. Enslow, A. T. Bell, *ChemCatChem* **2014**, *In Review*.
[16] a) A. Fredenslund, R. L. Jones, J. M. Prausnitz, *AIChE J*. **1975**, *21*, 1086; b) T. Magnussen, T. Rasmussen, A. Fredenslund, *Ind. Eng. Chem. Process Des. Dev*. **1980**, *20*, 1269.
[17] R. Wittig, J. Lohmann, J. Gmehling, *Ind. Eng. Chem. Res*. **2003**, *42*, 183.
[18] a) K. Pitzer, J. Kim, *J. Am. Chem. Soc.* **1974**, *96*(18), 5701; b) F. A. Long, W. F. McDevit, *Chem. Rev.* **1952**, *51*(1), 119; c) R. G. Curtis, H. H. Hatt, *Aust. J. Chem.* **1948**, *1*(2), 213; d) F. Hofmeister, *Arch. Exp. Pathol, Pharmacol.* **1888**, *24*, 247.
[19] E. O. Eisen, J. Joffe, *J. Chem. Eng. Data.* **1966**, *11*(4), 480.
[20] W. J. Hamer, Y. C. Wu, *J. Phys. Chem. Ref. Data* **1972**, *1*, 1047.

Chapter 5

Brønsted Acid-Catalyzed Deconstruction of Lignin and Lignin Model Compounds Dissolved in Ionic Liquids and other Solvents

Abstract

Conversion of plant biomass provides a sustainable pathway toward renewable fuels. Lignin, the third most abundant biomass component after cellulose and hemicellulose, can be catalytically converted to provide a range of fuel molecules, including alkanes and aromatics. Using the ionic liquid [Emim][Cl] as solvent and a Brønsted acid as catalyst, we investigated deconstruction reactions involving both lignin and lignin model compounds. We were unable to successfully produce either oligomeric or monomeric cleavage products. Such an incompatibility between lignin and the ionic liquid solvent was determined to be due to unfavorable solvent-solute interactions. The lack of reactivity of lignin and lignin model compounds in [Emim][Cl] makes this ionic liquid a suitable solvent for the hydrolysis of cellulosic biomass in the presence of and without interference from lignin. Despite being unreactive in ionic liquid, lignin model compounds containing glycerol β-O-4 ether linkages could be hydrolyzed successfully in a variety of organic solvents, most notably a combination of 1,4-dioxane and water. The linkage of the guaiacylglycerol β-guaiacyl ether ([G,G]) model compound was found to be cleaved *via* a two-step dehydration/hydrolysis leading to guaiacol and Hibbert ketones. The Brønsted acid-catalyzed reactions of an array of lignin model compounds containing glycerol β-O-4 ether linkages revealed that the nature of phenyl group substitution does not influence the rate of ether cleavage.

5.1 Introduction

The deconstruction of lignocellulosic biomass offers the unique opportunity to access high value fuel molecules in a renewable and carbon-neutral manner. These chemicals represent a wide range of fuel molecules including aromatics, furanics, sugar alcohols, and alkanes that can be blended with gasoline, diesel, and jet fuel or combined to create stand-alone fuels capable of supplanting traditional fuels [1-3].

Biomass consists of three main components: cellulose (25-50%), hemicellulose (20-40%), and lignin (10-30%) [1]. While much attention has been paid to the hydrolysis of cellulose and hemicellulose to their constituent sugars [1, 4] and the dehydration of those sugars to furfural and 5-hydroxymethyl furfural [5], less attention has been given to the deconstruction of lignin [1]. The bulk of lignin research involves the production of bio-oil, a complex slurry of combustible chemicals, and syn-gas, [1] however, the production of these fuels requires extreme conditions and lack the selectivity of their cellulosically-derived counterparts. As the only renewable source of aromatics, developing a way to selectively deconstruct lignin to its oligomeric and monomeric components while maintaining their aromaticity would be invaluable to the chemicals industry, which currently relies heavily on synthetic routes to satisfy demand (for example, 61.9 billion pounds of aromatic chemicals were consumed in the United States

in 2007) [3]. Financial forecasts estimate lignin conversion to aromatic chemicals to be the most profitable use of the material, capable of generating $25 billion versus $11.2 billion from simply burning lignin for power or $23.3 billion from converting lignin to syn-gas (based upon 450 billion pounds of lignin produced) [3].

Figure 5.1 shows a representative fragment of lignin (adapted from reference [6]). Although lignin lacks a defined primary structure, it is largely composed of guaiacyl, syringyl, and p-hydroxyphenol phenylpropanoids. These aromatic compounds are linked together in a variety of ways, most notably *via* arylglycerol-β-aryl ether, biphenyl, diarylpropane, phenylcoumaran, resinol, and diphenyl ether linkages [7]. On average, ether linkages, highlighted in the figure, are the most prominent, constituting over half of the linkages and making them suitable targets for lignin deconstruction. Studies have investigated the use of ether-linked lignin model compounds as a means to understand the fundamental cleavage of these ether linkages [6,8], however, little of the chemistry is known and selectivity toward phenolic monomer compounds have been poor.

Our research has focused on developing an understanding of lignin deconstruction, with the ultimate goal of producing various oligomeric/monomeric aromatic molecules that can be hydrogenated and used as gasoline oxygenates. Ionic liquids have shown promise in dissolving cellulose, hemicellulose, and lignin [9], and have been found to be useful solvents in the hydrolysis of cellulose and hemicellulose [10], therefore we have targeted them as potential solvents for lignin deconstruction in this study. We first explore the solvation characteristics and Brønsted acid-catalyzed deconstruction of higher molecular weight lignin in ionic liquids. We then transition to the use of representative lignin model compounds in an effort to understand the fundamental chemistry involved in selectively cleaving the most common linkage present in lignin, the arylglycerol-β-aryl ether (approximately 45% of all linkages) [7].

5.2 Methods

5.2.1 Materials

Lignin, alkali (Kraft, MW ~28,000 g/mol), lignin, low sulfonate (MW ~60,000 g/mol), phenol (Bio-Xtra, ≥99.5%), 2-methoxyphenol (guaiacol, ≥98%), and 2,6-dimethoxyphenol (syringol, 99%) were all purchased from Sigma-Aldrich and were used as reagents and standards (for quantification). All lignin model compound reagents were synthesized with the exception of guaiacylglycerol β-guaiacyl ether ([G,G], 99%), which was purchased from Tokyo Chemical Industry (TCI, Japan). A sample procedure of this synthesis is described below.

1-Butyl-3-methylimidazolium chloride ([Bmim][Cl], EMD), 1-butyl-3-methylimidazolium acetate ([Bmim][OAc], Fluka), 1-ethyl-3-methylimidazolium chloride ([Emim][Cl], 99%, Sigma-Aldrich), 1-ethyl-3-methylimidazolium acetate ([Emim][OAc], Fluka), 1-ethyl-3-methylimidazolium methyl sulfate ([Emim][MeS], Fluka), acetonitrile (Sigma-Aldrich), dimethylsulfoxide (DMSO, Sigma), dimethylformamide (DMF, Acros), 1,4-dioxane (Sigma-Aldrich), ethanol (Sigma-Aldrich), ethyl acetate (Sigma-Aldrich), and tetrahydrofuran (THF, Fisher Scientific) were used as solvents. Sulfuric acid (H_2SO_4, 96.5-98%, Sigma-Aldrich) and hydrochloric acid (HCl, 37%, Fisher Scientific) were used as acid catalysts.

All reactants, solvents, and acid catalysts were used as purchased, without further

purification or modification, with ionic liquids being the lone exception. All ionic liquids were vacuum dried at 100 ºC for 24 h prior to use to ensure minimal water content (measured *via* Karl-Fischer titration to be approximately 2 wt%).

5.2.2 Synthesis of Lignin Model Compounds

Lignin model compounds were synthesized by modifying methods taken from the literature [11] and purified using flash chromatography (FC). For example, phenylglycerol β-phenyl ether ([P,P]) was synthesized as follows: a 250 mL round-bottomed flask was charged with benzoylethylacetate (5.00 g, 26.0 mmol) in dichloromethane (CH_2Cl_2, 75 mL, 0.33 M). The solution was cooled to 10 ºC (using cold tap water) and stirred rapidly while a solution of bromine (1.2 mL, 23.4 mmol) in CH_2Cl_2 (10 mL) was added dropwise. The solution was warmed to room temperature and left to stir for 1 h. Thin layer chromatography (TLC) indicated consumption of the starting ester (R_f = 0.28 in 10% ethyl acetate/hexanes) to a new product, bromobenzoylethyl acetate (R_f = 0.23 in 10% ethyl acetate/hexanes). The reaction was quenched by adding water (100 mL). The water was extracted with CH_2Cl_2 (3 x 50 mL), and the combined organic layer was dried over magnesium sulfate ($MgSO_4$). Filtration and concentration yielded a clear oil (6.99 g). The oil was taken up in acetone (30 mL). Potassium carbonate (5.4 g, 40.0 mmol) and phenol (3.60 mL, 32.5 mmol) were added, and the reaction was left to stir for 12 h. TLC indicated consumption of bromobenzoylethyl acetate to form two new products (R_f = 0.30-0.40 and R_f = 0.20). This solution was filtered through Celite and then diluted with water (40 mL). The mixture was transferred to a separatory funnel and the aqueous layer was extracted with ether (3x75 mL). The combined ethereal layers were washed with aqueous NaCl (1x75 mL), dried over $MgSO_4$, filtered, and concentrated to yield a pale yellow semi-solid (6.64 g) The recovered material was dissolved in boiling ethanol (30 mL), allowed to cool to room temperature, and then placed in the refrigerator (-20 ºC) for 15 h. The recrystallized material was filtered and washed with cold ethanol to yield a white, amorphous solid (1.43 g, 6.19 mmol). This solid was diluted in THF:H_2O/4:1 (30 mL) to yield a pale yellow solution. $NaBH_4$ (500 mg, 14.37 mmol) in THF:H_2O/4:1 (10 mL) was added drop-wise and the reaction was left to stir for 1.5 h. TLC indicated that the starting material (R_f =0.43 in 10% hexanes/ethyl acetate) had fully converted to product (R_f = 0.05 in the same solvent). The reaction was quenched by slowly adding saturated NH_4Cl (*aq*, 40 mL). The quenched solution was transferred to a separatory funnel, diluted with water (100 mL), and extracted with ether (3x100 mL). The combined ethereal extracts were washed with saturated NaCl (*aq*, 1x150 mL), dried over $MgSO_4$, filtered, and concentrated to yield a pale, yellow oil. The oil was loaded onto a Biotage 25-M FC column and eluted with a hexanes:ethyl acetate gradient (2-60%). Two large peaks were observed with absorbances in the range of 254 and 220 nm. Ten fractions were collected for the peak with a retention volume of 6 column volumes (CV) and concentrated to yield a clear oil (Product A, 624 mg). Eleven fractions were collected for the peak at 10 CV and concentrated to yield a clear oil (Product B, 562 mg). ^{1}H NMR indicated that Product A was a combination of diastereomers of partially reduced material, while Product B was the target product, [P,P], in a 2:3 diastereomer ratio.

5.2.3 Experimental Approach

All experiments were performed within 5 ml glass vials with threaded caps using a Symx core module deck to maintain constant reaction temperature and stirring rate. In a representative lignin hydrolysis experiment, either high molecular weight lignin or a lignin model compound (50 mg) was allowed to dissolve in 1 ml of [Emim][Cl] for three h at 100 ºC at 200 rpm of stirring. Ten molar equivalents of 96.5-98% H_2SO_4 and water per mole of ether linkage was then added. Upon completion of the reaction, samples were removed and quenched in an ice bath. An internal standard (1 ml of 10 mg/ml anthracene in acetonitrile) was added and the samples were centrifuged to remove all insoluble particulates. The sample was then extracted three times with THF, and the organic layer was analyzed using GC/MS. In experiments involving high molecular weight lignin, excess water was used to precipitate lignin from the [Emim][Cl] at reaction end, with the precipitate being characterized using MALDI to observe whether any molecular weight changes occurred over the course of the reaction (an indication of lignin deconstruction).

5.2.4 Product Analysis

A Brookfield viscometer was used to measure ionic liquid solution viscosities. A Thermo Scientific Nicolet 6700/Smart iTR FTIR-ATR was used to analyze the infrared spectra of solid samples of lignin. A Shimadzu AXIMA-CFR^{TM} MALDI-TOF mass spectrometer was used to monitor changes in the molecular weight of polymeric lignin after subjection to various reaction conditions. A Bruker AVQ-400 console with a Bruker 9.39 T magnet was used to perform ^{1}H nuclear magnetic resonance (NMR) experiments to identify products from lignin model compound syntheses. A Varian CP-3800 Gas Chromatograph (GC) equipped with a FactorFour Capillary Column (UF-5ms 30 m, 0.25 mm, 0.25 μm, P/N CP8944) connected to a Varian quadrupole-mass spectrometer (MS) and flame ionization detector (FID) was used to analyze all catalytic samples. After product identification by mass spectrometery, product concentrations were determined from integrated FID peak areas using a 6-point calibration curve generated from purchased standards.

Reagent and product yields are reported as molar percentages relative to initial molar concentrations of lignin ether linkages (i.e. guaiacol yields = moles guaiacol/initial moles β-O-4 ether linkages). All reported yields were typically reproducible to within a +/- 5% relative error (based upon the calculation of one standard deviation).

5.3 Results and Discussion

5.3.1 Dissolution of Lignin in Ionic Liquids

A number of di-alkylimidazolium ionic liquids were screened for lignin solubility and the results are summarized in Table 5.1. It was determined that anion selection had the greatest impact on the solubility of high molecular weight lignin in the order methyl sulfate > acetate > chloride. While ionic liquids with chloride anions showed the lowest solubilities, it has been reported and observed that in the presence of strong acids (such as the H_2SO_4 and HCl acid catalysts used in this study), acetate and methyl sulfate anions tend to abstract catalytic protons from solution, effectively forming weaker acids that decrease and, in the case of acetate anions, eliminate reactivity [12]. Furthermore, interchanging the cation between 1-ethyl-3-methylimidazolium ([Emim]) and 1-butyl-3-

methylimidazolium ([Bmim]) had little effect on solubility. Ultimately, [Emim][Cl] was chosen as the ionic liquid used for the remainder of this study, with solubilized lignin maintained below the 11 wt% threshold.

At low pH (<2) and at temperatures exceeding 150 ºC, we found that [Emim][Cl] undergoes degradation *via* loss of the proton at position 2 of the 1,3-alkylsubstituted imidazolium moiety as well as through various ring opening reactions. This thermal instability has also been reported in the literature *via* thermogravimetric analysis of [Emim][Cl] over the range of 150-200 ºC [13]. With a melting point of about 77 ºC (depending upon moisture content), low temperatures are also of concern for solutions of lignin in [Emim][Cl], where viscosities can be as high as 110 cP near the melting point of the ionic liquid. Such high viscosities can critically affect mass transfer rates to the extent that reaction rates are reduced in imidazolium-based ionic liquids [14]. Raising the temperature can considerably reduce solution viscosity, as is shown in Figure 5.2. In order to ensure the stability of the ionic liquid while mitigating high solution viscosities and any associated mass transfer limitations, subsequent reaction temperatures were maintained between 100-120 ºC.

The chemical stability of lignin within [Emim][Cl] was also investigated to ensure that the ionic liquid does not chemically alter lignin or catalyze the deconstruction of the material as has been observed with [Hmim][Cl] [15]. Figure 5.3 shows the spectra for dry lignin as well as lignin that has been dissolved in [Emim][Cl] at 100 ºC for 3 h and then precipitated out of solution. In the wavenumber region of 1500 ± 100 cm^{-1}, the characteristic region for aromatic absorbance, there is no difference in the spectrum for either case indicating that lignin is unaltered by the ionic liquid. Furthermore, analysis of both materials using MALDI-TOF spectrometry showed no difference in molecular weight between the untreated and treated lignin samples.

5.3.2 Deconstructing Lignin in [Emim][Cl]

The Brønsted acid-catalyzed deconstruction of lignin dissolved in [Emim][Cl] was investigated over the temperature range 100-120 ºC. In all cases investigated, we found high molecular variants of lignin to be recalcitrant to acid-catalyzed deconstruction in [Emim][Cl], with no changes in lignin molecular weight observed *via* MALDI-TOF. These results are similar to those found in the literature [15, 16], which has exhaustively screened other sources of lignin (i.e. organosolv), acid catalysts (i.e. solid acid catalysts), and ionic liquids (imidazolium and pyridinium based cations paired with varying anions) to the same end.

Commercially available lignin, such as that used in this study, is obtained through methods that can leave the lignin highly substituted with unnatural elements and functional groups (such as alkali metals and sulfur compounds) [7] that could contribute adversely to depolymerization chemistries. Furthermore, the complex combination of varied linkages within lignin makes it difficult to pinpoint the actions necessary to successfully deconstruct lignin. To better understand the fundamental chemistry of lignin depolymerization in the absence of a natural, unaltered source of lignin, we have developed a subset of representative dimer molecules that could be used to study the cleavage of the most common bond within the lignin motif, the glycerol β-O-4 linkage.

5.3.3 Cleaving Lignin Model Compounds in [Emim][Cl]

Figure 5.4 shows the nine possible glycerol β-O-4 lignin model compounds, differing only in their phenyl group substitutions. These model compounds are commonly designated with a two letter code describing the substitution of each phenyl group (for example, **P**henylglycerol β-**G**uaiacyl with a phenyl group at the α-Ph and guaiacyl group at the β-Ph would be designated [**P**,**G**]). The [P,P], [P,G], [P,S], [G,G], and [S,G] lignin model compounds within boxes in the figure were those that were synthesized for this study. In the presence of a Brønsted acid, the β-O-4 linkage can by cleaved in a variety of ways. By first protonating the ether oxygen as shown in Scheme 5.1, a given model compound ether can be cleaved to produce a substituted phenol and either a substituted phenyl glycerol molecule *via* hydrolysis at the β position or a phenyl prop-1-ene-1,3-diol *via* double bond formation between the α and β carbons. Alternatively, as shown in Scheme 5.2, dehydration first at the α position followed by hydrolysis of the β-O-4 ether produces a substituted phenol and either a Hibbert ketone or a derivative isomer. While the production of the substituted phenol (phenol, guaiacol, and syringol for lignin model compounds [*i*,P], [*i*,G], and [*i,*S], respectively) is indicative of β-O-4 ether cleavage, the nature of the secondary product(s) reveals which of the proposed pathways is correct.

Beginning with guaiacylglycerol β-guaiacyl ether ([G,G]), we investigated the Brønsted acid-catalyzed hydrolysis of this dimer dissolved in [Emim][Cl]. At 100 ºC, the [G,G] lignin model compound yielded less than 1% guaiacol after 2 h of reaction time. Similar results were found for the lignin model compounds [P,P], [P,G], [P,S], and [S,G] for the same reaction conditions. Using [G,G], the above reaction was repeated with the addition of increasing amounts of acetonitrile. Guaiacol production was followed as a function of increasing acetonitrile:[Emim][Cl] solvent ratio (by mass), as shown in Figure 5.5. As the proportion of acetonitrile increases to 60%, guaiacol yields remain low, reaching only about 2% after 2 h. Further increases in the percentage of acetonitrile, however, result in increasing amounts of guaiacol up to 26% in the case of pure acetonitrile (also after 2 h). Guaiacol production was accompanied by the appearance of Hibbert ketones and associated isomers (as evidenced *via* GC/MS), indicating that the reaction pathway presented in Scheme 5.2 occurs while that in Scheme 5.1 does not.

The question now arises as to why [Emim][Cl] is an ineffectual solvent for the cleavage of lignin model compound ether linkages under conditions suitable for extensive hydrolysis of both cellulose and hemicellulose [10]. To investigate this issue, we performed the Brønsted acid-catalyzed cleavage of [G,G] in acetonitrile with varying amounts of either 1-butylimidazole or NaCl to determine whether any ionic liquid imidazole or chloride anion interference occurs. The results of this experiment are shown in Table 5.2. The addition of NaCl to the reaction had no effect on guaiacol yields. However, when 1-butylimidazole was added in increasing amounts, guaiacol yields dropped continuously, reaching only 3.3% when 500 mg was added. It is clear from this experiment that imidazole compounds are responsible for reducing the rate of [G,G] ether cleavage to guaiacol. 1-Butyl imidazole and 1-ethyl-3-methyl imidazolium are not basic, and therefore not likely to interact more favorably with catalytic protons than the α hydroxyl group or ether oxygen of [G,G]. However, their aromaticity lends itself to potentially engage in π-π or cation-π stacking interactions with the phenyl rings that could: (1) sterically hinder access of protons to dehydration and hydrolysis sites; (2) chemically "restrain" phenyl rings to the extent that upon protonation at the β-O-4 ether

linkage the phenyl glycerol and phenyl components are incapable of separating to a degree sufficient to effectuate cleavage; or (3) withdraw electron density from the ether phenyl ring and reduce the nucleophilicity of the ether oxygen such that protonation energies are prohibitively heightened. In any case, the imidazole-phenyl ring interaction results in a higher apparent hydrolysis activation energy that reduces the rate of ether cleavage relative to cases where solvents (and/or solutes, as in the case of cellulose and hemicellulose) lacking conjugation are utilized. Higher temperatures than investigated are likely necessary to promote ether linkage catalysis in [Emim][Cl], although, further investigation would be necessary to confirm such a hypothesis.

5.3.4 Effect of Lignin Model Compound Phenyl Substitution on the Extent of Cleavage

With a suitable reaction medium identified, pure acetonitrile was used as the reaction solvent to determine whether varying phenyl group substitution of the lignin model compounds has any effect on the extent of ether cleavage. These results are presented in Table 5.3. While there exists a slight increase in substituted phenol yield when the glycerol phenyl group is held constant and the ether phenyl is substituted increasingly (i.e. in going from phenyl to guaiacyl to syringyl), there appears to be no pattern in varying glycerol phenyl group substitution for a given ether phenyl group. Simulations using DFT methods discussed in the Supplemental Information show that the Gibb's free energy of reaction for the ether cleavage of all lignin model compounds follows the trends observed experimentally, with the [G,G] lignin model compound having the lowest Gibb's free energy of reaction. Overall, each lignin model compound yielded between 20-26% of their respective phenolic monomers, with [G,G] being cleaved to the greatest extent of the five lignin model compounds investigated. As a result, [G,G] was used as the representative lignin model compound for the remainder of this study.

5.3.5 [G,G] Hydrolysis in Various Organic Solvents

With [Emim][Cl] ineffective as a solvent for the hydrolysis of [G,G] when compared to acetonitrile at 100 ºC, we turned to investigating the impact of using various organic solvents on the extent of ether hydrolysis. Table 5.4 summarizes our findings. All solvents screened were found to be effective in assisting the Brønsted acid-catalyzed ether cleavage of [G,G] to guaiacol in the order acetonitrile < dioxane < DMSO < ethanol < ethyl acetate < dioxane:water (1:1 v/v). The case of a 50/50 by volume mixture of dioxane and water was capable of producing 40% guaiacol from [G,G] over the course of 2 h. The effect of temperature and acid loading on [G,G] cleavage was examined for this solvent system, the results of which are shown in Figure 5.6. As expected, higher temperatures resulted in greater yields of guaiacol. While the same trend was observed for increasing acid loading, increases in guaiacol production rates decay with the acid:[G,G] ratio resulting in minimized enhancements in guaiacol production at high acid loadings.

5.4 Conclusions

Although an effective solvent for the hydrolysis of cellulose and hemicellulose, [Emim][Cl] was found to inhibit the hydrolytic cleavage of high molecular weight lignin

and β-O-4 lignin model compounds. This inhibition of β-O-4 ether cleavage in [Emim][Cl] is likely due to adverse electrostatic interactions between imidazolium cations and lignin phenyl groups. Cellulose and hemicellulose are comprised of saturated ring structures, a feature which prohibits a similar interaction with imidazolium and can explain why these two biopolymers are capable of being hydrolyzed in [Emim][Cl] under conditions where lignin and lignin model compounds are not. This finding suggests that [Emim][Cl] may be capable of hosting the Brønsted acid-catalyzed transformation of biomass with selectivity toward cellulose and hemicellulose conversion, and without interference from lignin. Upon reaction termination, lignin could then be easily separated from the cellulosic sugars in [Emim][Cl] through the addition of sufficient amounts of water to precipitate out the unaltered lignin. In this fashion, the three biopolymers would not need to be separated from lignin before performing the hydrolysis of either cellulose or hemicellulose as is currently done [1, 16].

Using lignin model compounds we determined that phenyl ring substitution has little impact on the extent of ether cleavage, and that cleavage occurs *via* the dehydration/hydrolysis scheme described in Scheme 5.2. Such compounds could be easily hydrolyzed in a variety of organic solvents, with a 1:1 by volume ratio of dioxane and water permitting yields of 40% guaiacol from the [G,G] lignin model compound at 100 ºC after only 2 h. Experiments with this reaction medium have shown that [G,G] hydrolysis would benefit more greatly from higher reaction temperatures than from increased acid concentrations.

Despite success in cleaving lignin model compounds, the challenges of deconstructing lignin are clear, with ionic liquids appearing to be unsuitable for the role. Systematic studies investigating the reactivities of lignin model compounds bound in other fashions are necessary to develop a complete understanding of the complex cocktail of chemistries necessary to deconstruct lignin selectively.

5.5 Supplemental Information

5.5.1 DFT-Calculated Lowest Energy Conformation of [G,G]

Figure 5.7 shows the lowest energy 3-dimensional conformation of the [G,G] model compound as determined by DFT calculations performed using the software Gaussian 09.

5.5.2 DFT-Calculated Free Energies of Hydrolysis of the Lignin Model Compounds

The lowest energy conformations of the remaining 8 β-O-4 lignin model compounds were optimized and frequency calculations were performed to determine various thermodynamic values for all compounds at 298K (# freq opt b3lyp/6-31+g(df,pd) geom=connectivity). These values were used to calculate the enthalpy, entropy, and Gibb's free energy for the ether hydrolysis of each compound at 298K. Table 5.5 summarizes these thermodynamic reaction parameters. When increasing the degree of substitution of the α-Ph (while maintaining a constant β-Ph substitution scheme), there is a decrease in $\Delta_r G^o$ (298 K). However, this is not the case when varying the degree of β-Ph substitution. In this case, the syringyl-substituted β-Ph is more stable than the phenol-substituted β-Ph, which is more stable than the guaiacyl-substituted β-Ph.

Overall, the [G,G] model compound was found to have the lowest Gibb's free energy of reaction for the cleavage of the β-O-4 ether linkage.

Scheme 5.1 A potential reaction pathway for the Brønsted acid-catalyzed cleavage of lignin model compounds, with the highlighted phenolic compound (**blue**) serving as an identifier for successful β-O-4 ether cleavage and either phenyl prop-1-ene-1,3-diols or substituted phenyl glycerol serving as secondary products.

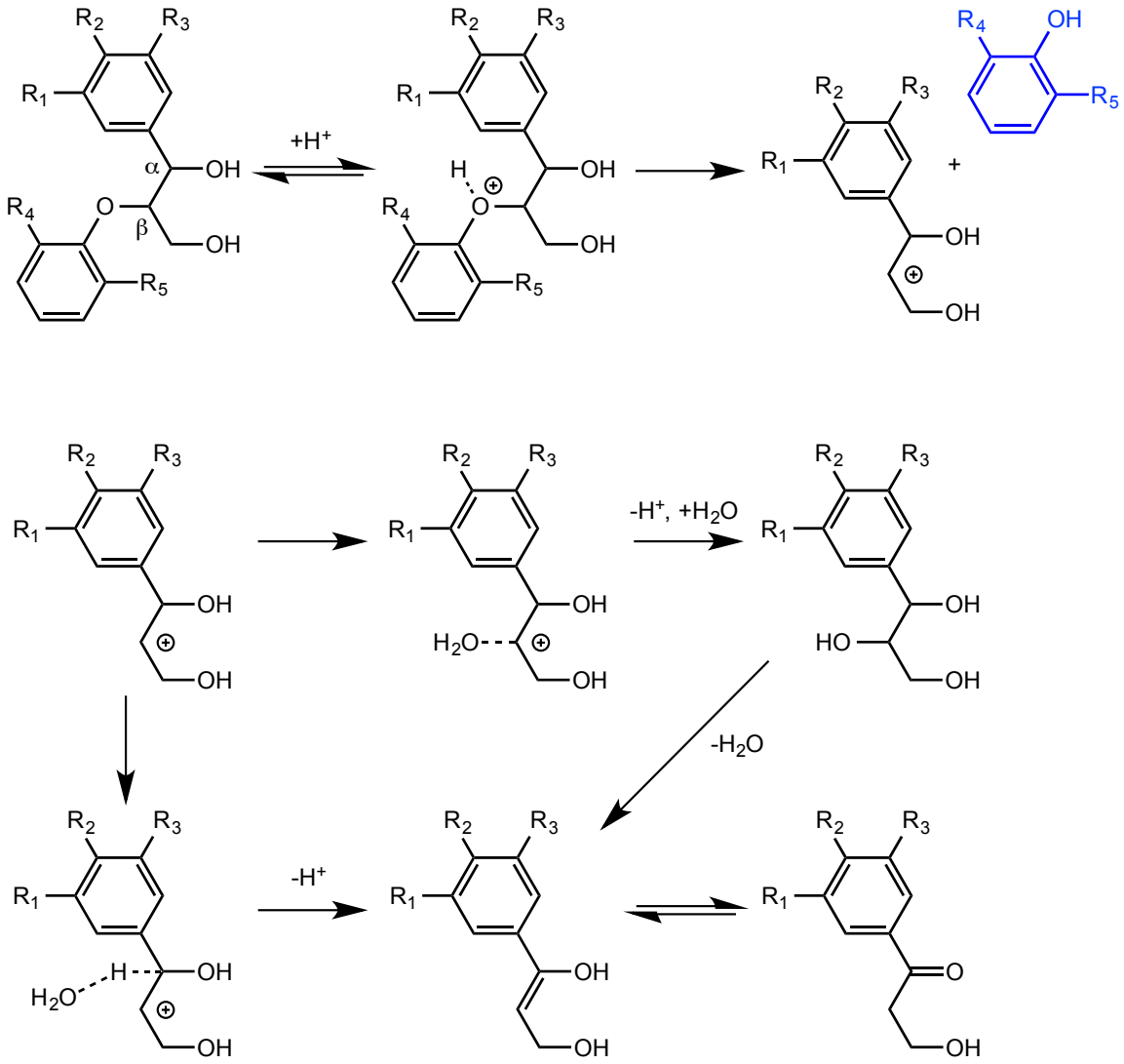

Scheme 5.2 A potential reaction pathway for the Brønsted acid-catalyzed cleavage of lignin model compounds, with the highlighted phenolic compound (**blue**) serving as an identifier for successful β-O-4 ether cleavage and Hibbert ketones or derivative isomers serving as secondary products.

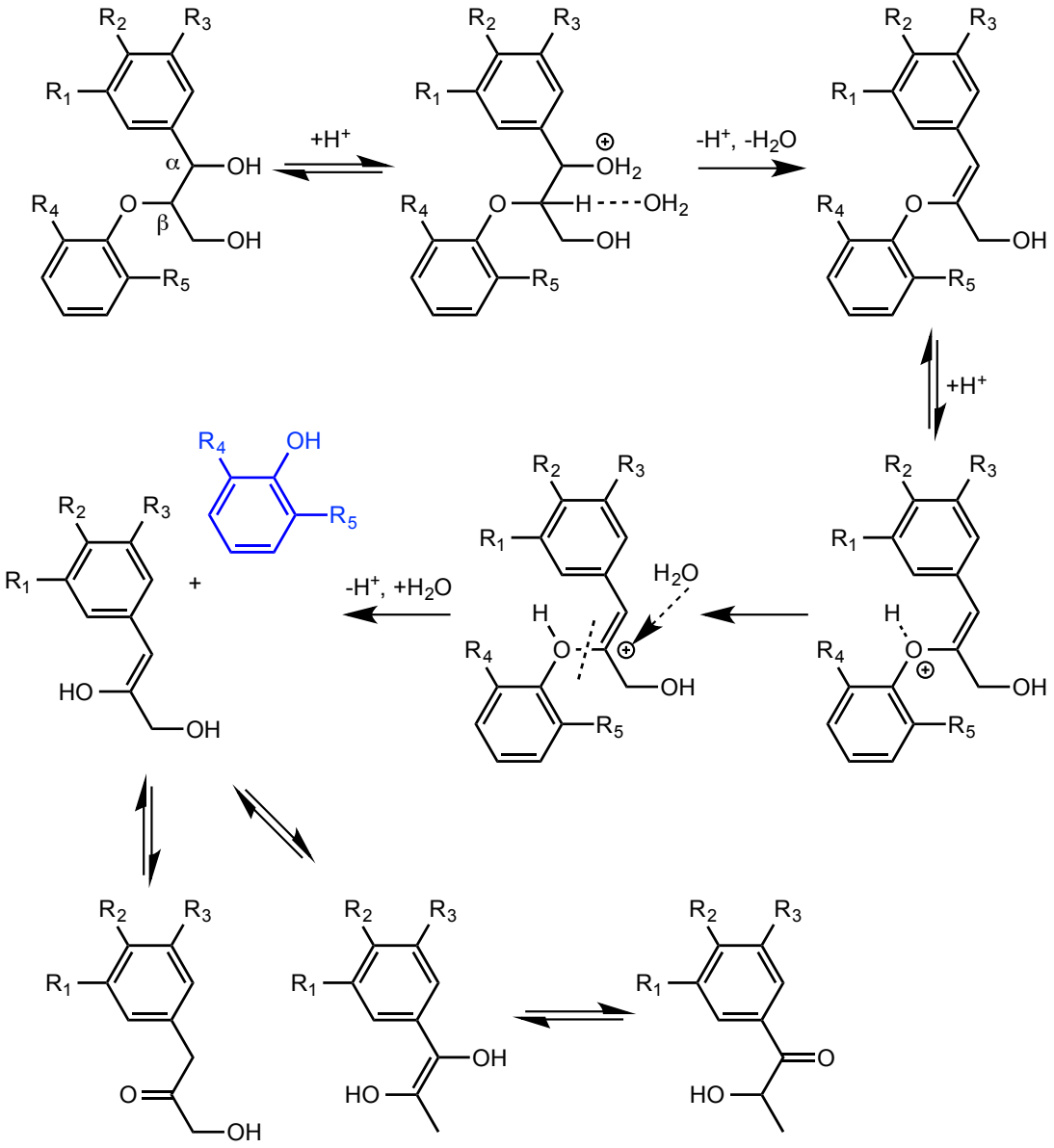

Figure 5.1 Representative structure of a possible lignin fragment. Bonds in **bold** highlight targeted ether bonds, such as arylglycerol-β-aryl ether (**blue**) and diphenyl ether (**red**). Adapted from Ref. [6].

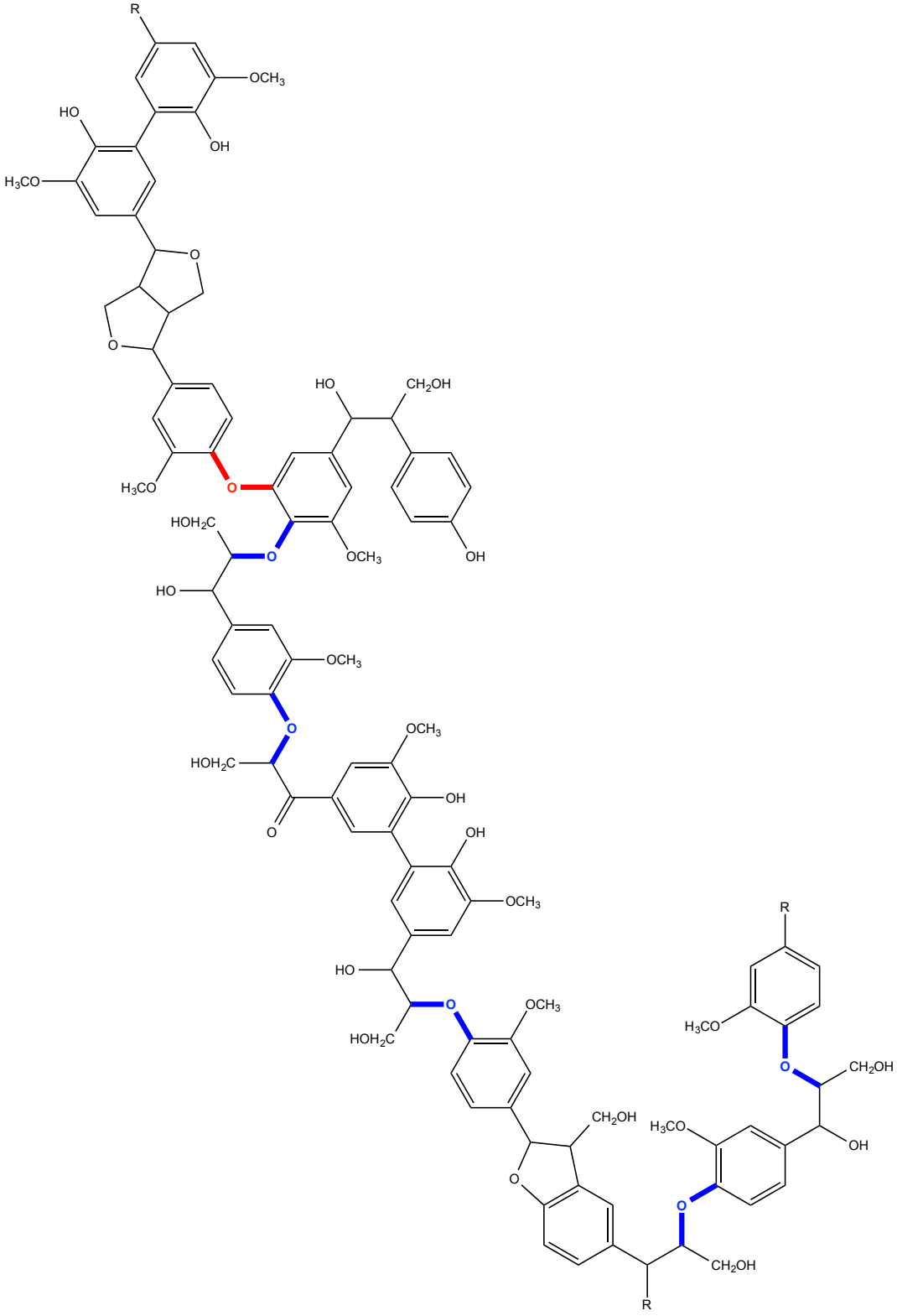

Figure 5.2 The viscosity of 10 wt% solutions of high molecular weight lignin in [Emim][Cl] as a function of temperature.

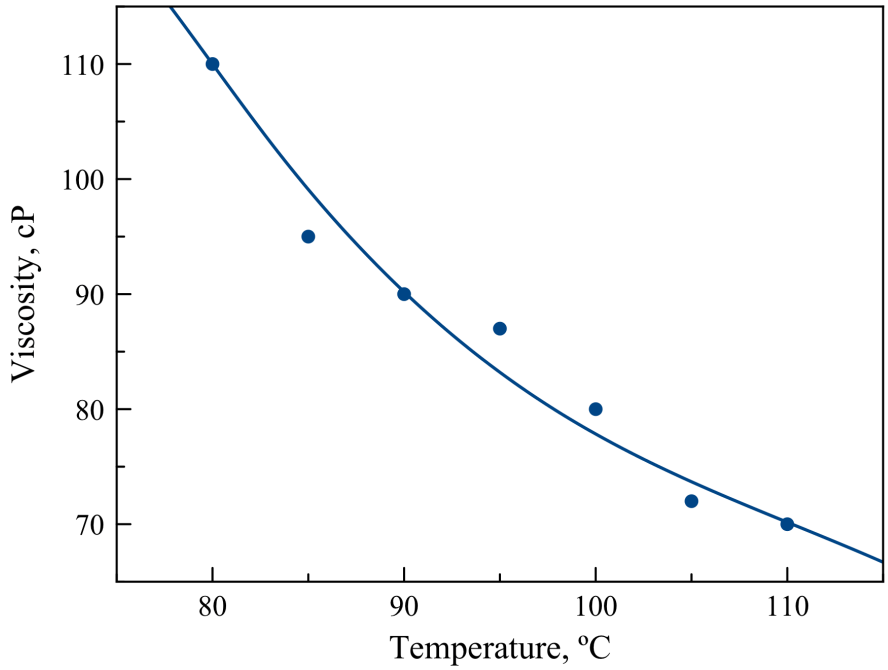

Figure 5.3 FTIR-ATR analysis of high molecular weight lignin before (**green**) and after (**red**) dissolution/precipitation from [Emim][Cl] at 100 ºC (10 wt% lignin).

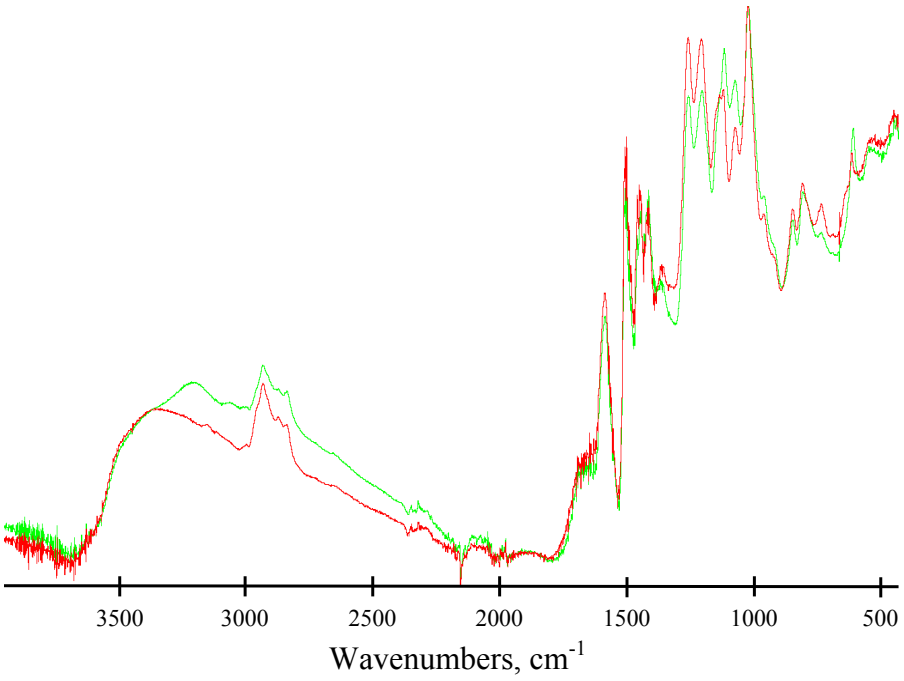

Figure 5.4 The complete array of variously substituted [*i*,*i*] glycerol β-O-4 lignin model compounds. Those compounds in boxes were synthesized for use in this study.

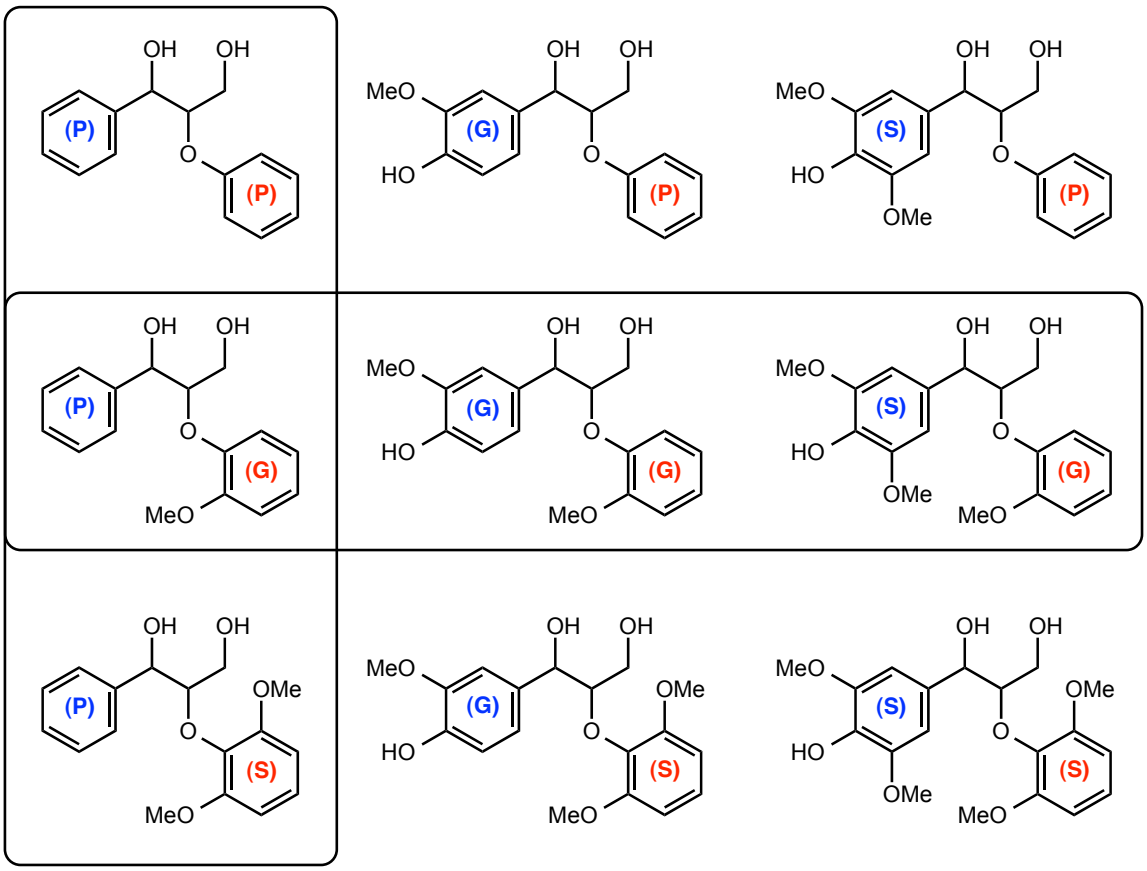

Figure 5.5 Effect of acetonitrile:[Emim][Cl] solvent ratio on the Brønsted acid-catalyzed ether cleavage of the [G,G] lignin model compound to guaiacol at 100 ºC after 2 h. Reaction conditions: 50 mg (156 µmol) [G,G] in 1 ml varying acetonitrile/[Emim][Cl] mixtures with 85 µL (1.56 mmol) H_2SO_4 and 28 µL (1.56 mmol) water.

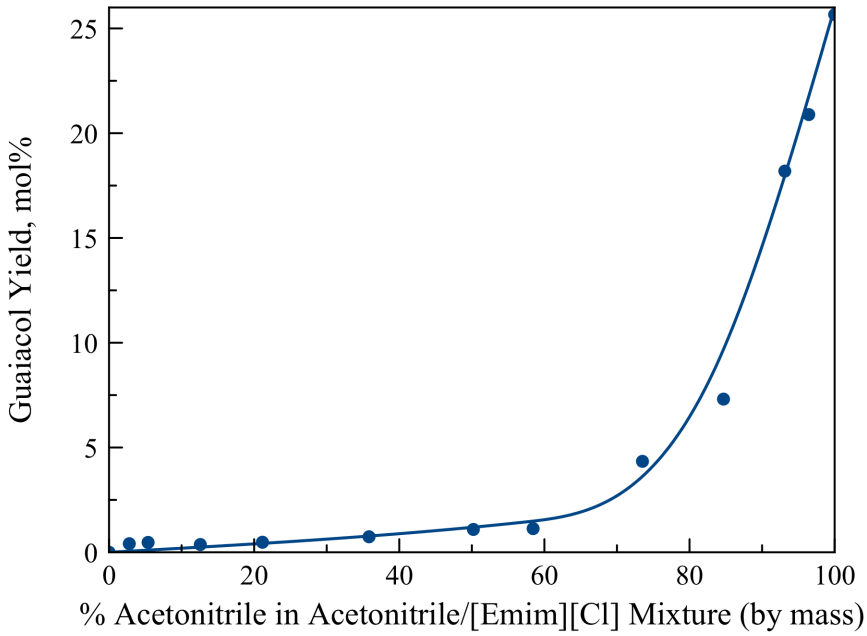

Figure 5.6 Effect of acid loading and temperature on the Brønsted acid-catalyzed ether cleavage of the [G,G] lignin model compound to guaiacol after 2 h. Reaction conditions: 50 mg (156 µmol) [G,G] in 1 ml dioxane:water mixtures with varying concentrations of H_2SO_4.

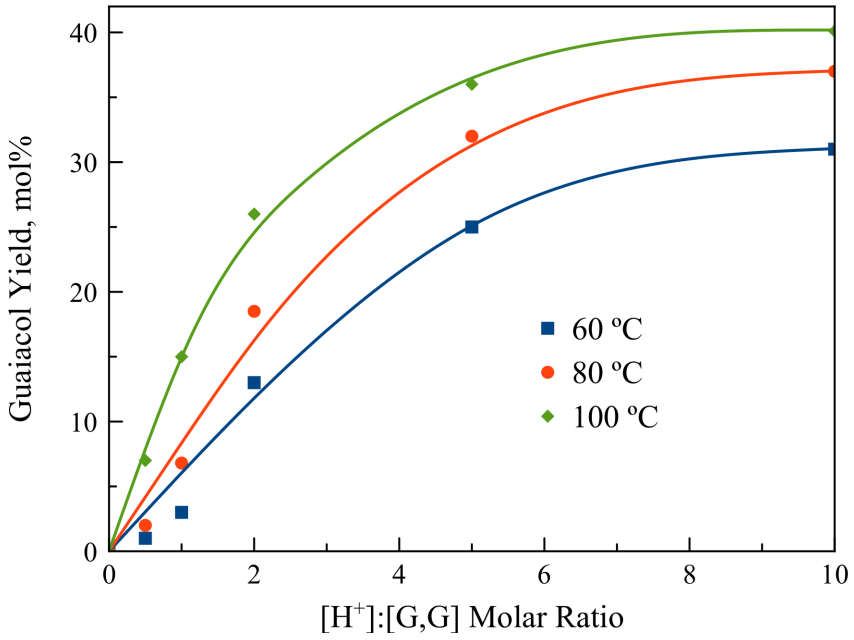

Figure 5.7 Lowest energy conformation of the [G,G] lignin model compound at 298 K as determined from DFT calculations performed using the software Gaussian 09.

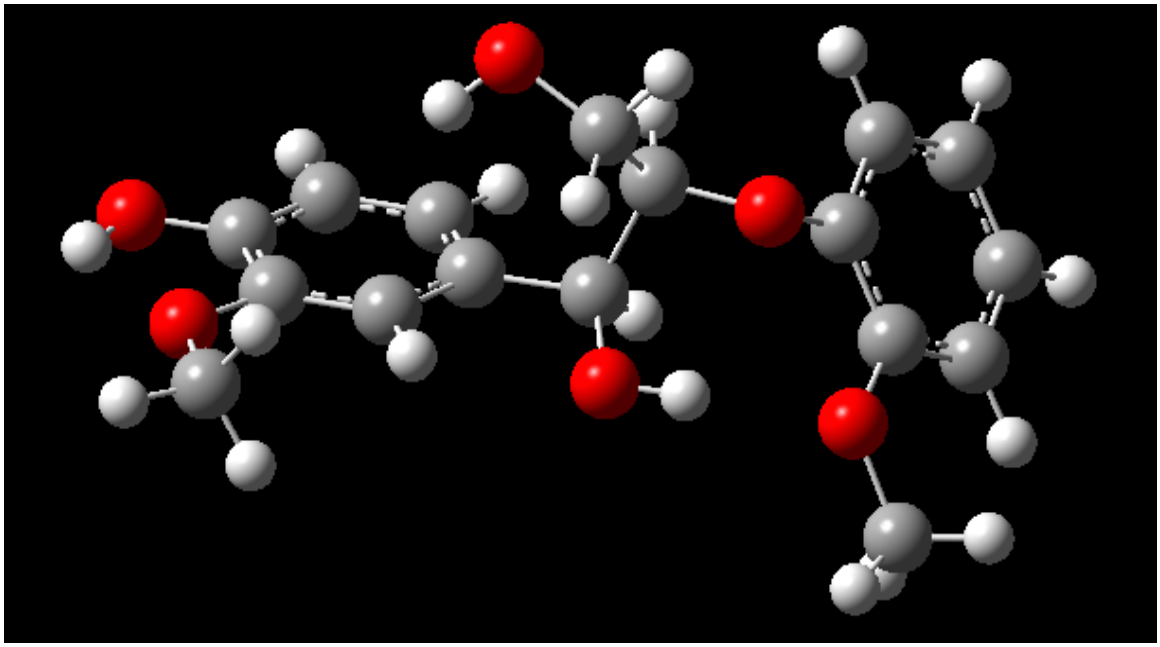

Table 5.1 The maximum determined solubilities of high molecular weight lignin (alkali) in various di-alkylimidazolium ionic liquids at 75 ºC after 3 h and 200 rpm of stirring.

Ionic Liquid	Weight % Lignin Dissolved
[Emim][Cl]	11.1
[Emim][OAc]	24.3
[Emim][MeS]	45.2
[Bmim][Cl]	10.2
[Bmim][OAc]	23.3

Table 5.2 Effect of NaCl and 1-butylimidazole concentrations on the Brønsted acid-catalyzed ether cleavage of the [G,G] lignin model compound to guaiacol in acetonitrile at 100 ºC after 2 h and 200 rpm of stirring. Reaction conditions: 50 mg (156 μmol) [G,G] in 1 ml acetonitrile with 85 μL (1.56 mmol) H_2SO_4 and 28 μL (1.56 mmol) water.

Additive	Amount, mg	Guaiacol Yield, mol%
None	-	26.0
	-	27.9
1-butylimidazole	10	24.8
	50	16.4
	100	9.7
	500	3.3
NaCl	10	25.3
	50	26.8
	100	25.8
	500	25.7

Table 5.3 Yields of substituted phenol monomers derived from the Brønsted acid-catalyzed cleavage of various lignin model compounds in acetonitrile at 100 ºC after 2 h and 200 rpm of stirring. Reaction conditions: 150 μmol [*i*,*i*] in 1 ml acetonitrile with 82 μL (1.5 mmol) H_2SO_4 and 27 μL (1.5 mmol) water.

Lignin Model Compound	Substituted Phenol Yield, mol%
[P,P]	20.6
[P,G]	22.0
[P,S]	23.4
[G,G]	25.5
[S,G]	20.5

Table 5.4 Effect of organic solvent choice on the Brønsted acid-catalyzed ether cleavage of the [G,G] lignin model compound at 100 ºC after 2 h and 200 rpm of stirring. Reaction conditions: 50 mg (156 μmol) [G,G] in 1 ml solvent with 85 μL (1.56 mmol) H_2SO_4 and 28 μL (1.56 mmol) water (except in the dioxane:water case).

Organic Solvent	Guaiacol Yield, mol%
Acetonitrile	25.7
Ethyl Acetate	37.4
Ethanol	33.7
Dioxane	27.3
Dioxane:Water (1:1 v/v)	40.1
DMSO	32.1

Table 5.5 The enthalpy, entropy, and Gibb's free energy of reaction values for the ether hydrolysis of all lignin model compounds at 298 K as determined *via* DFT calculations performed using the software Gaussian 09.

Lignin Model Compound	ΔH_r^o, kcal/mol	ΔS_r^o, cal/mol-K	ΔG_r^o, kcal/mol
[P,P]	5.01	42.53	-7.66
[P,G]	4.78	46.97	-9.22
[P,S]	2.86	48.29	-11.53
[G,P]	-0.01	39.98	-11.93
[G,G]	0.66	44.46	-12.59
[G,S]	-2.02	44.23	-15.22
[S,P]	7.67	43.23	-5.21
[S,G]	6.24	44.93	-7.15
[S,S]	3.51	45.56	-10.06

References:

[1] G. W. Huber, S. Iborra, A. Corma, *Chem. Rev.* **2006**, *106*(9), 4044.
[2] T. Werpy, G. Petersen, A. Aden, J. Bozell, J. Holladay, J. White, A. Manheim, Report No. NREL/TP-510– 35523, *Top Value Added Chemicals from Biomass: Vol. 1—Results of Screening for Potential Candidates from Sugars and Synthesis Gas*, National Renewable Energy Laboratory, Golden, CO, **2004**.
[3] J. E. Holladay, J. F. White, J. J. Bozell, D. Johnson, Report No. PNNL-16983, *Top Value-Added Chemicals from Biomass-Volume II—Results of Screening for Potential Candidates from Biorefinery Lignin*, Pacific Northwest National Laboratory, Richland, WA, **2007**.
[4] a) S. E. Jacobsen, C. E. Wyman, *Appl. Biochem. Biotech.* **2000**, *84*(6), 81; b) B. C. Saha, *J. Ind. Microbiol. Biotech.* **2003**, *30*(5), 279; c) C. E. Wyman, S. R. Decker, M. E. Himmel, J. W. Brady, C. E. Skopec, L. Viikari, *Polysaccharides: Structural Diversity and Functional Versatility 2nd ed.* (Ed.: Severian Dumitriu), Marcel Dekker, New York, **2005**, pp. 995-1034.
[5] a) J. B. Binder, R. T. Raines, *J. Am. Chem. Soc.* **2009,** *131*(5), 1979; b) J. N. Chheda, Y. Roman-Leshkov, J. A. Dumesic, *Green Chem.* **2007**, *9*(4), 342; c) C. Sievers, I. Musin, T. Marzialetti, M. B. V. Olarte, P. K. Agrawal, C. W. Jones, *ChemSusChem* **2009**, *2*(7), 665.
[6] N. Yan, C. Zhao, P. J. Dyson, C. Wang, L. Liu, Y. Kou, *ChemSusChem* **2008**, *1*(7), 626.
[7] D. S. Argyropoulos, S. Menachem, *Adv. Biochem. Eng./Biotechnol.* **1997**, *57*, 127.
[8] M. Kleinert, T. Berth, *Energy Fuels* **2008**, *22*(2), 1371.
[9] a) R. Swatloski, S. Spear, J. Holbrey, R. Rogers, *J. Am. Chem. Soc.* **2002**, *124*, 4974; b) H. Olivier-Bourbigou, L. Magna, D. Morvan, *Appl. Catal., A* **2010**, *373*, 1.
[10] a) J. B. Binder, R. T. Raines, *Proc. Nat. Acad. Sci. U.S.A.* **2010**, *107*(10), 4516; b) L. Vanoye, M. Fanselow, J. D. Holbrey, M. P. Atkins, K. R. Seddon, *Green Chem*. **2009**, *11*(3), 390; c) S. J. Dee, A. T. Bell, *ChemSusChem* **2011**, *4*(8), 1166; d) K. R. Enslow, A. T. Bell, *RSC Adv.* **2012**, *2*(26), 10028.
[11] S. Li, K. Lundquist, M. Paulsson, *Acta Chem. Scand.* **1995**, *49*, 623.
[12] D. MacFarlane, S. Forsyth, *Ionic Liquids as Green Solvents: Progress and Prospects* (Eds.: R. D. Rogers, K. R. Seddon), ACS Symposium Series 856, Oxford University Press, Washington, D.C., **2003**, pp. 264-276.
[13] V. Kamavaram, R. G. Reddy, *Int. J. Therm. Sci.* **2008**, *47*(6), 773.
[14] a) J. G. Huddleston, A. E. Visser, W. M. Reichert, H. D. Willauer, G. A. Broker, R. D. Rogers, *Green Chem*. **2001**, *3*, 156; b) A. Kumar, S. S. Pawar, *Sci. China Chem.* **2012**, *55*(8), 1633.
[15] J. B. Binder, M. Gray, J. White, Z. Zhang, *Biomass Bioenergy* **2009**, *33*, 1122.
[16] J. Zakzeski, P. Bruijnincx, A. Jongerius, B. Weckhuysen, *Chem. Rev.* **2010**, *110*(6), 3552.